## Title

Restoring Lysosomal Acidification as a Therapeutic Strategy for Neurodegenerative Disorders



## ISBN

9798190900231

## Author

Garda, Virginia Grazia

## Publication Date

2026-09-03

Peer reviewed|Thesis/dissertation

# Restoring Lysosomal Acidification as a Therapeutic Strategy for Neurodegenerative Disorders

by
Virginia Garda

DISSERTATION
Submitted in partial satisfaction of the requirements for degree of
DOCTOR OF PHILOSOPHY

in

Chemistry and Chemical Biology

in the

GRADUATE DIVISION
of the
UNIVERSITY OF CALIFORNIA, SAN FRANCISCO

Approved:

DocuSigned by:
Aimee Kao
745CF57D40DB494...

Aimee Kao
Chair

DocuSigned by:
Michelle Arkin
Signed by:9658434...

Michelle Arkin

Jason Gestwicki
DocuSigned by:
E5...

Jason Gestwicki

Jason Sello
2F30A400EE504B5...

Jason Sello

Committee Members

# Dedication and Acknowledgements

I would not have been able to complete my PhD without the help of countless people throughout my time in graduate school. I would like to thank my advisors, Aimee Kao and Michelle Arkin, for their exceptional mentorship. Both have been incredibly supportive while also giving me the independence to take ownership of my project, allowing me to grow as a scientist over the past several years. The opportunity to learn from two mentors with distinct approaches to scientific thinking and laboratory leadership has also had a profound influence on my development.

The Kao and Arkin labs have been wonderful and supportive environments in which to work. In the Kao lab, I would especially like to thank Molly Hodul and Mac Welch for always being willing to discuss my work and provide thoughtful feedback. I am also grateful to two of Molly's mentees, Maya Debnath and Edwina Mambou, for carrying out key experiments for my project. Drea Argouarch has been an excellent lab manager, and her organizational skills helped me keep my own project on track. I would also like to thank Marcus Chin, from whom I inherited this project, for providing invaluable support when I first joined the two labs. From the SMDC, I would like to thank Zain Alam and Jez Lafuente for their essential assistance in carrying out my screen. In the Arkin lab, I am grateful to the members of my subgroup who provided helpful feedback during data presentations, including Andy Ambrose, Chad Altobelli, Lucy Luo, and Ziwen Ziang.

I benefited greatly from the guidance of my thesis committee members, Jason Gestwicki and Jason Sello, who provided thoughtful feedback at pivotal moments in my project. They also served on my qualifying exam committee alongside Aparna Lakkaraju and Deanna Kroetz, whose insights and feedback during the exam helped shape my work.

I was also fortunate to complete an internship at Eli Lilly during my fifth year of graduate school. I would especially like to thank Juanita Limas for organizing the internship and providing invaluable mentorship throughout my time there. Kevin Bruemmer patiently taught me proteomics,

and Kevin Burris offered helpful feedback throughout my project. Other scientists from whom I learned from during my time there include Ramy Malty Wendy Gough, and Jesus Guitierrez.

As an undergraduate student, I worked at the Molecular Foundry in LBNL for two years, which was a very collaborative environment. Ron Zuckermann was a great PI to work under as his enthusiasm for science was contagious. By entrusting me with my own project and giving me the independence to pursue it, he enabled me to learn and grow tremendously. I would especially like to thank Behzad Rad for being an outstanding mentor during that time. I also spent a summer in Caroline Ajo-Franklin's lab, and I am grateful to her for giving me that opportunity and to Frankie Manea for being such a wonderful and fun mentor.

My career path was also greatly influenced by the two years I spent at Mitokinin, where I was first introduced to neurodegenerative disease research. During that time, I learned not only a great deal of science but also how to think critically about scientific questions and approach research. I am grateful to everyone there, especially Nick Hertz, Dan DeRoulet, Dara Ditsworth, Rishi Rakhit, and Randall Chin.

I would also like to thank the friends who made my years in graduate school so enjoyable, including Leo Chen, José Montaño, Kaan Kumru, Berliza Soriano, Nick Lue, and Maureen Morla.

Finally, I am deeply grateful to my family for their support. Although I am the first scientist in my family, they have always taken a genuine interest in my career and regularly asked about the progress of my research. Unfortunately, my dad passed away shortly after I graduated from college and was therefore unable to see me begin graduate school, but he always encouraged me to pursue an advanced degree. My mom has been incredibly encouraging throughout my time in graduate school and has always tried to cheer me up when I've felt demotivated. I dedicate this thesis to my parents for all their care.

.

# Contributions

**Chapter 1:**

**Lysosomal pH Dysregulation as a Driver of Aging and Neurodegeneration**

**Authors**: Virginia G. Garda[1,2], Aimee W. Kao[1]

V. G.G. and A.W.K. outlined the paper, V.G.G. wrote the manuscript and made the figures, A.W.K. heavily edited it.

**Chapter 2:**

**WNK inhibitors acidify lysosomes and enhance lysosomal proteolytic activity**

**Authors**: Virginia G. Garda[1,2], Maya Debnath[1], Molly Hodul[1], Edwina A. Mambou[1], Kevin J. Bruemmer[3], Kevin D. Burris[3], Juanita C. Limas[3], Aimee W. Kao[1*], Michelle R. Arkin[2*]

Under review at *Cell Chemical Biology*.

Conceptualization of overarching project: V.G.G., M.R.A., A.W.K., K.D.B., and J.C.L. V.G.G. performed the majority of experiments. M.H. designed experiments involving *C. elegans* and wrote the corresponding methods section. E.A.M. and M.D. performed *C. elegans* experiments and analyzed corresponding data. K.J.B. and V.G.G. designed and performed proteomics experiments. V.G.G., M.R.A, and A.W.K. wrote the manuscript, all authors edited and approved of the manuscript.


1. Memory and Aging Center, Department of Neurology, University of California, San Francisco, California, California 94158, United States
2. Small Molecule Discovery Center, Department of Pharmaceutical Chemistry, University of California, San Francisco, California 94143, United States
3. Lilly Research Laboratories, Eli Lilly and Company, Indianapolis, Indiana 46285 United States

* Co-corresponding authors

# Restoring Lysosomal Acidification as a Therapeutic Strategy for Neurodegenerative Disorders

Virginia Garda

## Abstract

Lysosomes are membrane-bound organelles that maintain cellular homeostasis by degrading intracellular waste as the endpoint of autophagic pathways. Impaired lysosomal function contributes to the disruption of proteostasis that characterizes aging and neurodegenerative diseases, and a growing body of evidence indicates that lysosomal alkalinization is a common feature of these conditions. Because lysosomal hydrolases require an acidic luminal environment for optimal activity, dysregulation of lysosomal pH is increasingly recognized as an important contributor to disease pathogenesis. Chapter 1 of this thesis reviews current understanding of lysosomal pH dysregulation in aging and neurodegeneration, with emphasis on the mechanisms underlying lysosomal alkalinization and the effects of restoring lysosomal acidity. Chapter 2 describes a phenotypic high-throughput screen that ultimately identified two novel lysosomal acidification compounds, WNK463 and WNK-IN-11, that are inhibitors to the WNK family of kinases, which had not previously been linked to lysosomal pH regulation. Collectively, this work advances our understanding of lysosomal pH dysregulation and supports lysosomal acidification as a promising therapeutic strategy for aging and neurodegenerative diseases.

# Table of Contents

# List of Figures

# List of Tables

# Chapter 1: Lysosomal pH Dysregulation as a Driver of Aging and Neurodegeneration


## Abstract

As the final common pathway for autophagic processes, lysosomes are essential for maintaining proteostasis. Emerging evidence suggests that lysosomal pH is frequently dysregulated in both normal aging and neurodegeneration, with most models exhibiting lysosomal alkalinization, although hyper-acidification has also been reported in specific contexts. Because lysosomal hydrolases require an acidic luminal environment for optimal activity, altered lysosomal pH impairs degradative function and contributes to aging and disease-associated phenotypes. Importantly, restoration of lysosomal acidity rescues lysosomal dysfunction and ameliorates pathological features across numerous cellular and animal models, highlighting lysosomal pH as a potential therapeutic target. This review summarizes current understanding of lysosomal pH regulation, the mechanisms underlying its dysregulation during aging and neurodegeneration, and the consequences of altered lysosomal acidity for cellular homeostasis and disease progression.


## Introduction

Lysosomes are membrane-bound organelles that play a central role in cellular homeostasis by degrading and recycling intracellular material. Initially characterized as merely the “recycling bin” of cells, lysosomes are now recognized as dynamic organelles that integrate nutrient sensing, metabolic signaling, and cellular stress responses with their degradative functions.[1,2] Lysosomes contain a diverse repertoire of hydrolytic enzymes, including proteases,

lipases, glycosidases, and nucleases, which collectively enable the breakdown of a wide range of substrates. In chaperone-mediated autophagy (CMA), chaperone-bound cytosolic proteins are directly translocated across the lysosomal membrane through LAMP-2A, in contrast to endosomal microautophagy where mutivesicular bodies are utilized to digest material, or macroautophagy in which proteins, aggregates, and even entire organelles are delivered to lysosomes via autophagosomes.[3–5] Through these pathways, lysosomes maintain proteostasis and organelle quality control, functions that are particularly important in long-lived post-mitotic cells such as neurons.

A growing body of evidence implicates lysosomal dysfunction in neurodegeneration. Neuropathological studies have identified several hallmarks consistent with impaired lysosomal function in neurodegenerative diseases (NDs), including the accumulation of lysosomes and autophagic vesicles within affected neurons, and the presence of lysosomal lumen proteins in the cytoplasm indicative of lysosomal rupture.[6,7] Genetic studies have strengthened this connection, as mutations in numerous lysosome-associated genes are either causative or a risk factor for the development of neurodegenerative diseases.[8,9] In addition, some of these mutations result in lysosomal storage disorders when present in a homozygous state, which suggests that there is mechanistic overlap between the two disease types; importantly, NDs are strongly age-associated disorders, so it is possible that subtle lysosomal defects might accumulate over time and drive their progression.[10–12] Because neurons are highly dependent on lysosomal degradation to remove damaged proteins and organelles over a lifetime, they may be particularly vulnerable to even modest declines in lysosomal function.

One phenotype repeatedly observed in cellular models of neurodegeneration and animal models of aging is lysosomal alkalinization. pH reflects the concentration of protons within a solution and affects the protonation state and therefore the structure and function of biomolecules. Lysosomes normally maintain a highly acidic luminal environment with a pH of approximately 4.5–

5.0 for the optimal activity of its hydrolases.[13,14] Given the central role of luminal acidity in lysosomal function, the downstream consequences of lysosomal alkalinization are varied and profound (**Figure 1.1**). Understanding how lysosomal pH changes during aging and neurodegeneration may provide important insights into disease mechanisms and identify new therapeutic opportunities.

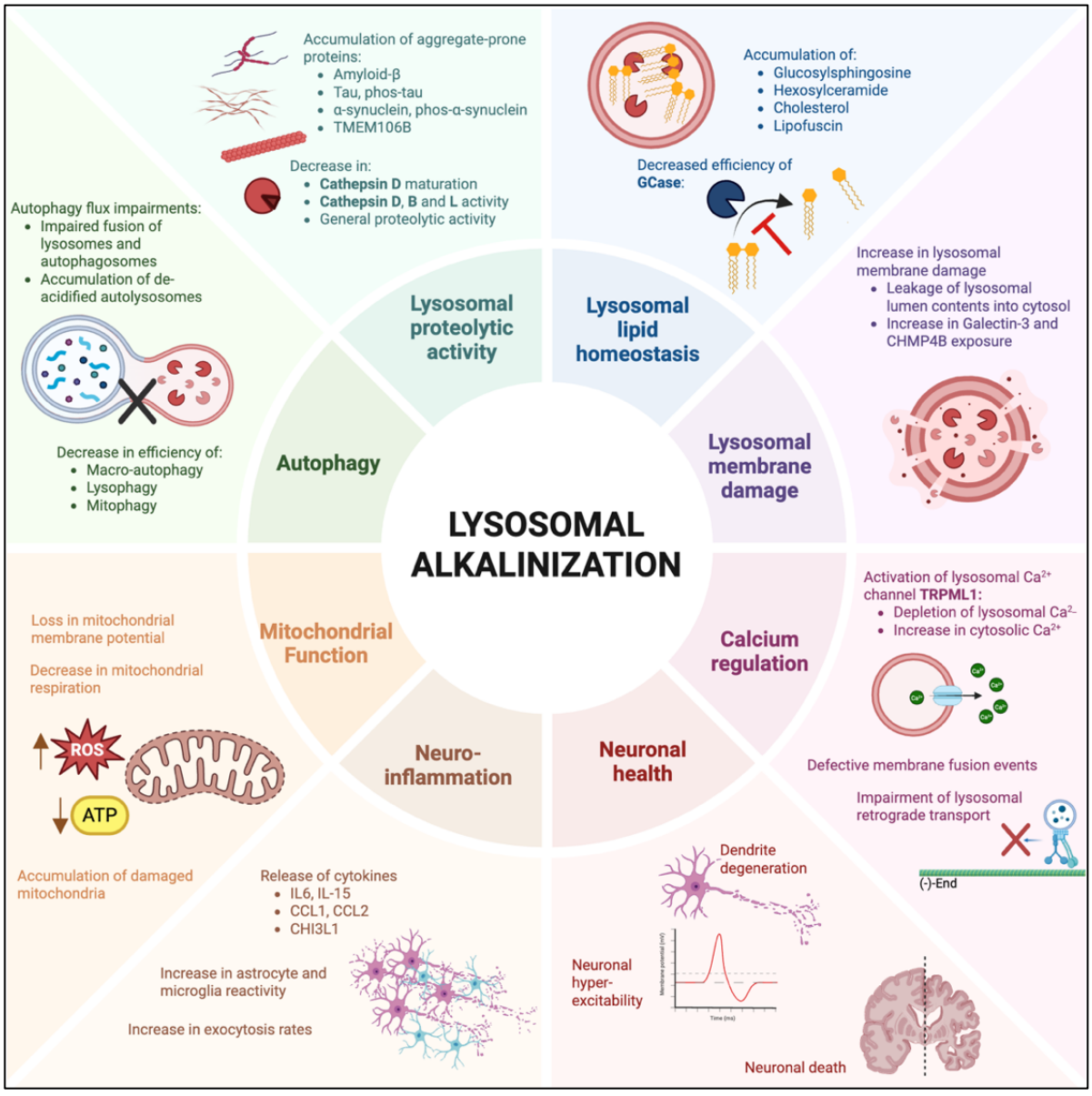


**Figure 1.1 - Downstream consequences of lysosomal alkalinization.**
An elevation of lysosomal pH causes dysfunctions in lysosomal proteolytic activity, autophagy, mitochondrial efficiency, neuroinflammation, neuronal health, calcium regulation and lysosomal lipid homeostasis. Figure generated with BioRender.

# Basic Biology of Lysosomes

## Overview of lysosomal proteases

Cathepsins are the largest family of lysosomal proteases and can be classified by the identity of their catalytic residues.[15,16] Cathepsins D and E are aspartic cathepsins, A and G are serine cathepsins, and the remaining eleven cathepsins, which include B and. L, are cysteine cathepsins.[15] Cathepsins B, D, F, A, L and Z are the most highly expressed in neuronal cells, although there are some variations in expression between brain regions.[16] Their pro-protein form is inactive since their amino-terminus consists of a pro-peptide that binds to the active site and blocks substrate binding.[17] Upon arrival at the lysosome, they are they are cleaved into their mature and active forms, either auto-catalytically or by other cathepsins, and thus their molecular weight and availability of their active site is often used as a proxy for enzyme activity.[17–19]

Lysosomal pH directly regulates the activity of lysosomal hydrolases, as an acidic pH is required for the removal of their inhibitory pro-peptide. The activity of individual proteases, however, differ in their pH dependence. The aspartyl protease cathepsin D exhibits maximal activity at approximately pH 4.[20,21] In contrast, the cysteine protease cathepsin L is more active at pH 5 than at pH 6 but becomes irreversibly inactivated under more acidic conditions around pH 4.[22,23] Cathepsin B displays even greater variability, with its pH optimum depending on substrate identity; for example, substituting the P2 residue adjacent to the cleavage site from glutamine to arginine shifts the optimal pH from 4.6 to 7.2.[24] More broadly, the catalytic efficiency of all cathepsins is influenced by substrate sequence; ND-associated mutations and phosphorylation sites in aggregate-prone proteins have been shown to decrease the rate at which they are degraded by lysosomes.[25,26] Indeed, the current phospho-tau biomarkers of Alzheimer's Disease are likely released protease-resistant fragments of tau release by lysosomes into the extracellular space.[26]

## Lysosomal pH sensors

Lysosomal pH sensors fall into three major categories: lysosomotropic dyes, dextran-conjugated probes, and genetically encoded sensors (**Table 1.1**).[27,28] Lysosomotropic dyes are weak bases that accumulate in acidic compartments following protonation.[27] Although convenient because of their short incubation times, they are the least specific, as they accumulate in multiple acidic organelles and can themselves elevate lysosomal pH.[29] Dextran-conjugated probes reach lysosomes through endocytosis, providing greater lysosomal specificity, but they label only lysosomes that receive endocytosed cargo; accordingly, a study utilizing electron microscopy showed that only approximately 70% of lysosomes in HeLa cells contained dextran-conjugated probes after uptake.[29–31] Genetically encoded sensors, which consist of fluorescent proteins fused to lysosomal membrane proteins, provide the highest specificity and permit cell type-specific pH measurements in vivo.[28,32] However, overexpression of lysosomal membrane proteins such as LAMP1 can cause plasma membrane mislocalization, making transient transfection and strong promoters unsuitable.[33] Consequently, lysosomal localization should be validated by co-localization with established lysosomal markers.

Independent of sensor type, several factors influence measurement accuracy. The sensor's pH-sensitive fluorophore should ideally have a pKa close to the lysosomal pH of 4.5–5.0 for optimal sensitivity.[27] Single-fluorophore probes estimate lysosomal pH from fluorescence intensity alone, which can be confounded by differences in lysosome abundance and size.[29] Consequently, ratiometric probes incorporating a second pH-insensitive fluorophore provide more reliable measurements by normalizing for lysosomal volume and probe abundance.

**Table 1.1 - Categories of sensor to measure lysosomal pH**

| Sensor Type | Advantages | Disadvantages | Name | Change with increasing acidity | pKa |
|---|---|---|---|---|---|
| Lysosomotropic Dyes | Fast labeling time; high signal to noise; | Low specificity to lysosomes; not viable for most model organisms; likely raises lysosomal pH | LysoSensor Yellow/Blue DND-160 | Shift: blue at high pH to yellow at low pH | 4.2[34] |
| | | | LysoSensor Blue DND-167 | Activated | 5.1[34] |
| | | | LysoSensor Green DND-189 | Activated | 5.2[34] |
| | | | Acridine Orange | Shift: green when present as a monomer in cytosol to orange/red when it dimerizes in lysosome[35] | |
| Dextran-based dyes | Specific localization into lysosomes; relatively fast labeling time | May not localize to lysosomes if endocytosis is compromised in model system; mainly limited to cellular models | LysoSensor Yellow/Blue-Dextran | Shift: blue at high pH to yellow at low pH | 3.9[34] |
| | | | Oregon Green-Dextran | Quenched | 4.7[36] |
| | | | FITC-Dextran | Quenched | 5.9[37] |
| | | | pHrodo Green/Red-Dextran | Activated | 6.5[38] |
| Genetically encoded sensors | High localization specificity to lysosomes; compatible with animal models; can be specifically expressed in specific tissues and cell types | Inconvenient for expedient experiments because it requires stable expression; may need to adjust promoter to avoid localization to cell membrane | FIRE-pHLy | mTFP1 is Quenched | 4.3[39] |
| | | | pHLARE | sGFP is Quenched | 5.9[40] |
| | | | RpH-LAMP1-3xFLAG | pHluorin is quenched | 6.5[41] |

# Mechanisms of lysosomal acidification

The luminal acidity of lysosomes is primarily established by the vacuolar ATPase (v-ATPase), a multi-subunit motor protein that uses energy derived from ATP hydrolysis to pump protons into the lysosomal lumen. It is composed of a membrane-bound $V_0$ domain and a cytosolic $V_1$ domain, which can readily associate or disassociate with each other to regulate lysosomal pH in response to various stimuli. For example, amino acid starvation stimulates $V_1$-$V_0$ assembly,

while glucose and serum deprivation reduce it.[42–44] This is partially controlled by the activity of mTOR complex 1, which inhibits v-ATPase assembly when active at the lysosomal membrane.[45] Because proton transport generates a transmembrane voltage gradient that opposes further acidification, lysosomes rely on counter-ion fluxes—including $Na^+$ and $K^+$ efflux and $Cl^-$ influx through the ClC-7 antiporter—to dissipate this electrical potential and sustain v-ATPase activity.[46]

Lysosomal acidification is also influenced by mitochondrial function. Inhibition of the mitochondrial electron transport chain elevates lysosomal pH, likely because proton pumping across the mitochondrial inner membrane supplies protons to the v-ATPase through mitochondria–lysosome contact sites.[47,48] Although mitochondria are also the primary source of ATP required for v-ATPase activity, moderate changes in ATP availability are unlikely to limit lysosomal acidification because intracellular ATP concentrations are several orders of magnitude greater than the Michaelis constant for v-ATPase ATP hydrolysis.[49] Consistent with this model, inhibition of mitochondrial ATP synthase with oligomycin does not alter lysosomal pH, suggesting that mitochondrial regulation of lysosomal acidification depends primarily on proton availability rather than ATP production.[48]

Lysosomal pH also varies according to subcellular localization. Perinuclear lysosomes are more acidic than peripheral lysosomes, although the mechanisms underlying this spatial heterogeneity are not yet fully understood.[50] Measurements of lysosomal re-acidification following dissipation of the proton gradient with carbonyl cyanide m-chlorophenyl hydrazone (CCCP) suggest that peripheral lysosomes exhibit lower proton pump activity and greater proton leakage.[50] In addition, enhanced acidification of perinuclear lysosomes has been proposed to result from increased assembly of the v-ATPase, with greater association of the $V_1$ and $V_0$ domains observed in this lysosomal population.[52]

## Methods for modifying lysosomal pH

A variety of genetic, pharmacological, and nanomaterial-based approaches have been developed to experimentally manipulate lysosomal pH. These tools have been instrumental in establishing causal relationships between lysosomal acidification and cellular function, while also evaluating the therapeutic potential of lysosomal re-acidification in aging and NDs.

The most commonly used methods for inducing lysosomal alkalinization are bafilomycin A1 (BaF) and chloroquine. BaF directly inhibits the v-ATPase, thereby preventing proton pumping into the lysosomal lumen.[51] In contrast, chloroquine is a weak base that accumulates in acidic compartments, where it buffers luminal protons and elevates lysosomal pH.[53] These compounds are frequently used to model lysosomal alkalinization, although they have also been used to rescue cellular models that exhibit lysosomal hyper-acidification.[54,55]

Several approaches have been developed to restore lysosomal acidity. One is overexpression of v-ATPase subunits through transient transfection or stable viral transduction, which successfully re-acidifies lysosomes in both yeast and mammalian cells.[56–58] Another involves acidic nanoparticles, which are typically composed of biodegradable polymers such as poly(lactic-co-glycolic acid) (PLGA).[59,60] These particles enter cells through endocytosis and accumulate within lysosomes, where degradation of the polymer releases weakly acidic functional groups that lower lysosomal pH. Although acidic nanoparticles have poor penetration across the blood-brain barrier, intracerebral injection successfully delivers them to lysosomes in the mouse brain.[61]

Small molecules represent the largest and most diverse class of lysosomal acidification strategies and are attractive because of their experimental simplicity and therapeutic potential. More than 30 lysosomal acidification compounds have now been identified (**Table 1.2**). These compounds act through diverse mechanisms, including direct activation of the v-ATPase, ATP-competitive inhibition of mTOR and other kinases, modulation of lysosomal ion channels, or, in

the case of several natural products, through mechanisms that remain unknown. Collectively, these compounds rescue numerous disease-associated phenotypes, including impaired cathepsin activity, defective lysosomal proteolysis, protein aggregation, and autophagic dysfunction (**Table 1.2**). Future studies evaluating their long-term efficacy, safety, and pharmacokinetic properties will determine whether lysosomal acidification can be translated into therapies for neurodegenerative and other age-associated diseases.

**Table 1.2 - Small molecule lysosomal acidifiers**

| Small molecule | Description | Lysosomal pH sensor | Cellular or Animal Model | Effects likely downstream of lysosomal acidification |
|---|---|---|---|---|
| EN6 | v-ATPase covalent binder, blocks v-ATPase-Ragulator interaction | LysoSensor Yellow/Blue DND-160 | HEK293 cells | Activates autophagy.[62] |
| Schisandrol A | Covalent binder of v-ATPase V0d1 subunit, increases v-ATPase activity | LysoSensor Yellow/Blue DND-160 | Rat adrenal pheochromocytoma cells (PC12) | Increases cell viability and portion of polarized mitochondria in cells treated with advanced glycation end-products.[63] |
| C381 | Localizes to lysosomes, possibly interacts with v-ATPase | LysoSensor Green DND-189 | K562 cells, human dermal fibroblasts, MPTP-treated mice | Enhances basal and stress-induced lysophagy in fibroblasts. Reduces phos-α-syn accumulation in MPTP-treated mice.[64] |
| Anacardic acid | Aurora Kinase A activator | LysoSensor Yellow/Blue DND-160 | Primary rat cortical neurons, SH-SY5Y cells | Reduces Aβ1-40 and Aβ1-42 accumulation in SH-SY5Y cells over-expressing AβPP695, the major neuronal AβPP isoform in humans.[65] |
| Torin1, AZD8055 | ATP-competitive mTOR inhibitors | LysoSensor Yellow/Blue DND-160 | Mouse embryonic fibroblasts | Enhance general lysosomal proteolysis, including cathepsin B and L activity.[45] |
| PP242, OSI-027 | | FIRE-pHLy | SH-SY5Y cells | Enhances maturation of cathepsin D.[66] |
| Imatinib | ATP-competitive Abl kinase inhibitor | LysoSensor Green DND-189 | Human macrophages | Enhances maturation of cathepsin D.[67] |
| AZD0530 | ATP-competitive inhibitor of Tyrosine Kinases | LysoSensor Yellow/Blue-Dextran | Down Syndrome Patient-derived fibroblasts | Enhances v-ATPase activity, reduces lysosomal membrane permeability.[68] |
| L803-mts | ATP-competitive GSK-3 Inhibitor | LysoTracker Red | SH-SY5Y cells; 5xFAD mouse model | Enhance maturation of cathepsin D in cells; reduced Aβ deposits and ameliorated cognitive deficits in mic.[69] |

| Small molecule | Description | Lysosomal pH sensor | Cellular or Animal Model | Effects likely downstream of lysosomal acidification |
|---|---|---|---|---|
| AS1842856 | Small molecule that reduces GSK3a/b protein levels | LysoSensor Green DND-189 | Neuro2a cells; APP/PS1 mice | Enhances lysosomal membrane integrity in cells; reduced hippocampal Aβ plaque area and ameliorated cognitive deficits in mice.[70] |
| Mli-2 | LRRK2 inhibitor | LysoSensor Yellow/Blue DND-160 | GBA1 heterozygous null iPSC-derived neurons | Enhanced cathepsin L activity levels.[71] |
| Apilimod | PIKfyve inhibitor | Oregon Green-Dextran | HEK293T, U2OS cells | No other phenotypes were measured.[72] |
| KU-60019 | ATP-competitive inhibitor of ATM serine/threonine kinase | Oregon Green-Dextran | Human telangiectasia fibroblasts | Reduced etoposide-induced senescence, increased mitochondrial respiration and reduced ROS levels.[73] |
| WNK463 | ATP-competitive inhibitor of WNK family of kinases | FIRE-pHLy, Dojindo Lysosomal pH dyes | SH-SY5Y cells, Neuro2a cells | Increased cathepsin D maturation, enhanced cathepsin B, L and overall lysosomal proteolytic activity, upregulated autophagy and mitophagy.[76] |
| WNK-IN-11 | Allosteric inhibitor of WNK1 and WNK3 | FIRE-pHLy, Dojindo Lysosomal pH dyes | SH-SY5Y cells, Neuro2a cells | Increased cathepsin D maturation, enhanced cathepsin B and overall lysosomal proteolytic activity, and upregulated autophagy.[76] |
| Valproic Acid | HDAC6 inhibitor | LysoSensor Yellow/Blue DND-160 | APPswe SH-SY5Y cells; APP/PS1 mice | Enhanced autophagic flux and cathepsin B maturation in cells; reduction of Aβ burden in the brain and ameliorated spatial learning in mice.[74] |
| Hyaluronic acid | Glycosaminoglycan polymer, substrate of Hyaluronidase | pHLARE | Primary hippocampal neurons | Rescues dendritic spine density and enhances lysosomal proteolytic activity in Aβ-treated hippocampal neurons.[58] |
| ML-SA1 | TRPML1 agonist | LysoSensor Yellow/Blue DND-160 | Rat primary neurons | Reduces Aβ1-40 and Aβ1-42 accumulation.[75] |
| Tetrandrine | TPC2 inhibitor | LysoSensor Yellow/Blue-Dextran | PSEN1-mutant SH-SY5Y cells; 5xFAD mice | Enhances autophagy flux in cells; ameliorates memory of mice.[77] |
| isoproterenol | Beta-adrenergic agonist | LysoSensor Yellow /Blue-Dextran | PSEN1 KO blastocysts | Enhances maturation of cathepsin D and activity levels of cathepsin B, and rescues impaired autophagic flux.[78] |
| Capsaicin | TRPV1 agonist | LysoSensor Yellow/Blue DND-160 | Neuro2a cells treated with Aβ1-42 peptide; 3xTg-AD mice | Reduced accumulation of lipid droplets in cells; reduced hippocampal Aβ and phos-Tau levels and improved spatial memory in mice.[79] |

| Small molecule | Description | Lysosomal pH sensor | Cellular or Animal Model | Effects likely downstream of lysosomal acidification |
|---|---|---|---|---|
| Clioquinol | Zinc ionophore, increases lysosomal zinc levels | LysoSensor Green DND-189 | Rat cortical primary neurons overexpressing LRRK2 R1441C | Rescues impaired autophagic flux and increases lysosomal proteolytic activity.[80] |
| Rimeporide | Inhibitor of proton leak channel NHE | Oregon Green-Dextran | HAP1 cells | Enhances GCase activity levels.[81] |
| ABO | ANXA7, increases protein levels, calcium-dependent phospho-lipid binding protein | Acridine Orange | Bone Marrow Stromal Cells (BMSCs) | Reduces senescence induced by high passage number.[82] |
| Cyclic adenosine monophosphate (cAMP) | ATP derivative, messenger molecule | LysoSensor Yellow/Blue DND-160 | Fibroblasts with familial AD mutation PS1 A246E | Enhances cathepsin D maturation, rescues blockage of autophagic flux.[83] |
| NKH-477 | Activator of adenylyl cyclase, increases cAMP levels | LysoSensor Yellow /Blue-Dextran | Primary oligodendrocytes treated with psychosine; Twitcher Mice | Enhance cathepsin B and D activity in cells; life-span extension in mice.[84] |
| Clofoctol | Antibiotic against gram-positive bacteria | LysoSensor Yellow /Blue-Dextran | Primary oligodendrocytes treated with psychosine | Enhance cathepsin B and D activity.[84] |
| Insulin-like growth factor 1 | Hormone | LysoSensor Yellow /Blue-Dextran | Primary oligodendrocytes treated with psychosine | Enhance cathepsin B and D activity.[84] |
| Pseudoginsenoside-F11 | Natural Product, modulator of AMPK and TFEB signaling pathways | LysoSensor Green DND-189 | Microglia | Enhanced degradation of oligomeric Aβ, enhancement of autophagic flux.[85] |
| DNLA | Natural product | LysoTracker Red | PC12 cells; APP/PS1 mice | Enhances vATPase subunit V1a and V0a1 protein levels and cathepsin D maturation in cells; reduced Aβ1-42 levels, enhanced autophagic flux and ameliorated memory of mice.[86,87] |
| Rifampicin | Natural product, antimicrobial | LysoSensor Yellow/Blue DND-160 | Immortalized human microglial cells treated with rotenone | Ameliorates rotenone-induced inflammation, enhances autophagic flux.[88] |
| SGJ | Blue fluorescent molecule that localizes to lysosomes | LS Green DND-189 and Acridine Orange | HEK293T, BMSCs | Reduction of senescence marker SA-β-gal in BMSCs.[89] |

# Lysosomal pH in aging

Age-associated lysosomal alkalinization has been reported across a wide range of experimental systems, including cellular models of senescence and aging, yeast, *Caenorhabditis elegans*, and mammalian tissues. The consistency of this phenotype across these models suggests that impaired lysosomal acidification is a fundamental feature of aging. Mechanisms that have been identified to lead to this dysregulation of lysosomal pH include dysregulation of v-ATPase subunit expression and function, decreased mitochondrial-to-lysosome contact sites, and dysfunction of lysosomal membrane channels (**Figure 1.2**).

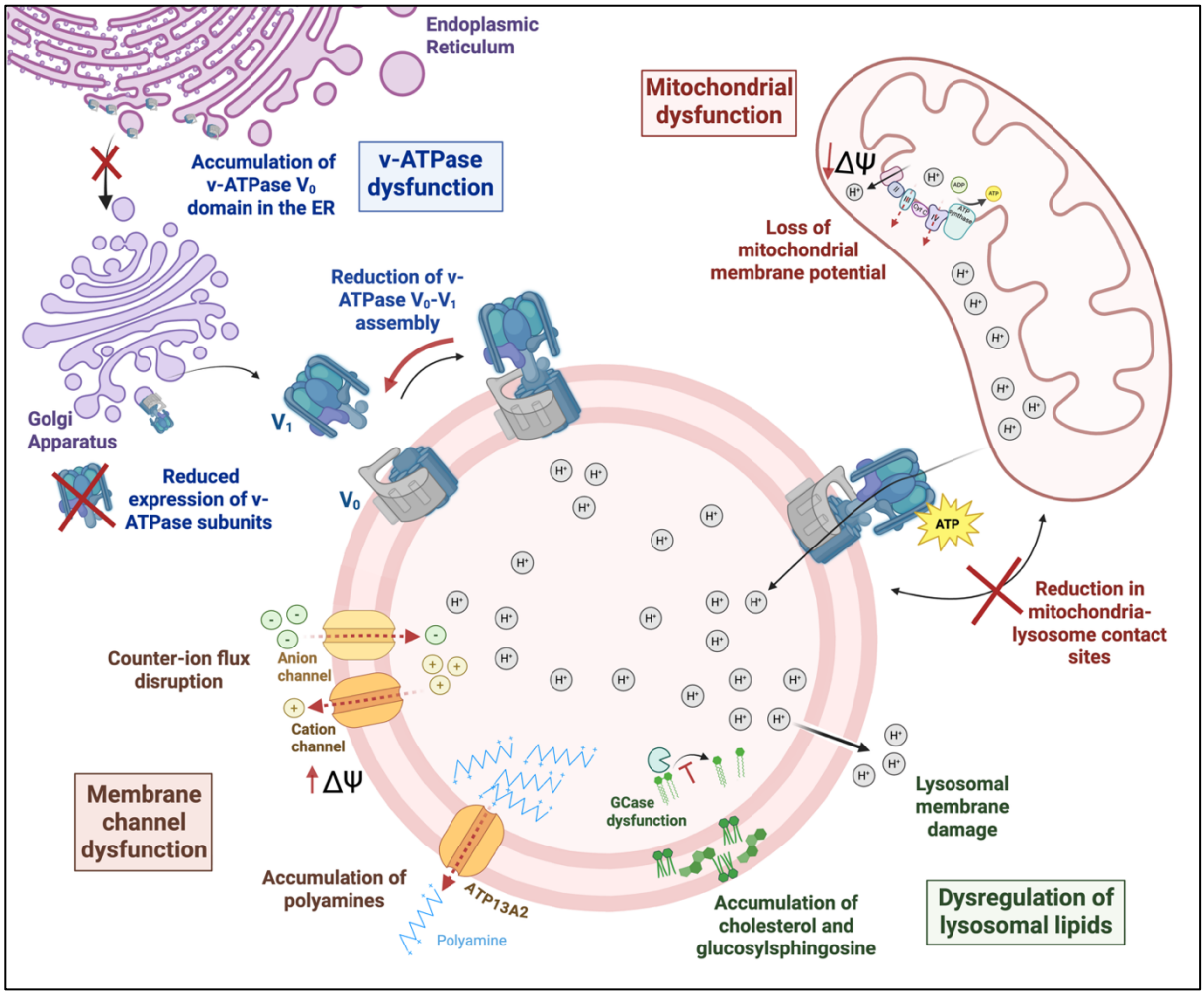


**Figure 1.2 - Mechanisms of lysosomal alkalinization in aging and neurodegeneration**
Identified mechanisms that lead to the alkalinization of lysosomes in aging and neurodegeneration include the dysfunction of the v-ATPase, mitochondria and lysosomal membrane channels as well as the dysregulation of lysosomal lipids. Figure generated with BioRender.

## Cellular Models of Aging

Cellular senescence is a widely used model for studying aging-related cellular changes, given that the accumulation of senescent cells has been strongly associated with organismal aging and numerous age-related diseases.[90] Senescence is defined as a permanent loss of replicative capacity in cells that have not undergone terminal differentiation. Elevation of lysosomal pH has been observed following multiple methods of senescence induction, including ultraviolet and ionizing irradiation, treatment with senescence-inducing compounds, and multiple rounds of replication.[48,73,82,91–93] Interestingly, senescent cells also exhibit an increase in the number of lysosomes per cell due to an increase in TFEB-dependent lysosomal biogenesis.[94] Consequently, overall lysosomal proteolytic activity at the cellular level remains relatively preserved despite reduced degradative efficiency within individual lysosomes, which suggests that senescent cells partially compensate for impaired lysosomal acidification by increasing lysosome abundance.

Mechanistically, lysosomal alkalinization appears to result, at least in part, from reduced expression of v-ATPase components upon senescence induction. Transcriptomic analyses have shown downregulation of several v-ATPase genes in senescent cells, including *ATP6AP2* and *ATP6V1C2*, suggesting that impaired v-ATPase activity contributes directly to the increase in lysosomal pH.[92,93] In addition, lysosome-to-mitochondria contact sites, which have been demonstrated to be a source of protons for the v-ATPase, decline in senescent cells.[48] This is likely due to a decrease in mitochondrial mass in senescent cells, which coupled to the increase in lysosomal mass, reduces possible contact sites between the two organelles.

Several studies have shown that restoring lysosomal acidity reverses key senescence-associated phenotypes. In a chemical screen, KU-60019 emerged as the strongest senescence-rescuing compound and was subsequently shown to acidify lysosomes by inhibiting ATM kinase, which suppresses v-ATPase assembly through phosphorylation of the V1g subunit.[73] ATM

inhibition in etoposide-treated fibroblasts also increased mitochondrial respiration and reduced reactive oxygen species production. Similarly, restoration of lysosome–mitochondria contact sites acidified lysosomes, rescued autophagic flux, and abolished senescence-associated transcriptomic signatures in lung fibroblasts subjected to ionizing radiation.[48] Overall, these findings suggest that cellular senescence is highly tied to lysosomal acidity and function.

As terminally differentiated cells, neurons cannot undergo replicative senescence and thus might not exhibit the same lysosomal changes as senescent cells. Primary embryonic cortical neurons aged in culture for 28 days exhibit many hallmarks of aging including the accumulation of lipofuscin.[95] Neurons were also found to lose lysosomal acidity with extended culturing times, and this was accompanied by reduced lysosomal proteolytic activity, accumulation of cathepsin D, and synapse loss.[96] Importantly, treatment with ML-SA1, a TRPML1 agonist that promotes lysosomal $Ca^{2+}$ efflux and lysosomal acidification, restored lysosomal degradative capacity, reduced lipofuscin accumulation, and rescued synaptic deficits in aged neurons.[96] These findings suggest that lysosomal alkalinization is not merely a consequence of cellular aging but contributes directly to age-associated cellular dysfunction.

One promising approach for modeling neuronal aging is direct transdifferentiation, in which somatic cells are converted directly into neurons. Unlike induced pluripotent stem cells (iPSCs), transdifferentiated neurons retain age-associated epigenetic markers, enabling the study of aging phenotypes in human neurons.[97] Unfortunately, data regarding lysosomal pH changes in transdifferentiated neurons remains limited. In one study, no significant difference in lysosomal pH was observed between neurons generated from young and aged donors.[98] However, lysosomal pH was measured using FITC-dextran, a probe with a relatively high pKa of approximately 6 that may lack sensitivity for detecting subtle increases within the physiological lysosomal pH range.[37] Interestingly, treatment of transdifferentiated neurons from aged patients with C381, a lysosomal acidifier, reduced $A\beta_{42}$ accumulation and increased cathepsin B activity,

which suggests that lysosomal acidification remains therapeutically beneficial even when measurable pH differences are difficult to detect.[64,98] Future studies applying more sensitive lysosomal pH sensors in transdifferentiated neurons may clarify whether aged neurons exhibit lysosomal alkalinization.

## Lysosomal pH and aging in model organisms

### *Yeast*

Budding yeast (*Saccharomyces cerevisiae*) have proven to be a useful aging model due to their short lifespans, thoroughly mapped genome, and conserved pathways with mammals. They divide asymmetrically into easily distinguished “mother” and “daughter” cells, and their replicative lifespan is used as a proxy for age.[99] Yeast vacuoles perform analogous degradative functions and share similar acidification mechanisms as lysosomes. Aged mother cells consistently exhibit less acidic vacuoles than young cells, along with hallmarks of aging that include accumulation of aggregate-prone proteins such as α-synuclein, mitochondrial membrane de-polarization, and elevated production of reactive oxygen species.[56,100,101]

Multiple mechanisms have been proposed to explain age-dependent vacuolar alkalinization. One involves HCM1, a transcription factor that regulates v-ATPase gene expression.[100] Age-dependent loss of HCM1’s nuclear localization reduces v-ATPase expression, and HCM1 deletion similarly induces vacuolar alkalinization and shortens lifespan, both of which are rescued by v-ATPase overexpression. Age-dependent defects in v-ATPase assembly have also been identified, with reduced association between the $V_0$ and $V_1$ domains resulting from an age-associated decline in the RAVE complex component Rav2.[102] Consistent with a role for RAVE in facilitating v-ATPase assembly, deletion of its subunit Rav1 induces an elevation of vacuolar pH and shortens replicative lifespan. Another mechanism involves the plasma membrane proton ATPase (Pma1), which exports protons from the cytoplasm.[103] Age-dependent accumulation of

Pma1 reduces proton availability for vacuolar acidification, whereas the hypomorphic *pma1-105* allele preserves vacuolar acidity and extends lifespan. Lastly, there is a loss of mitochondria-vacuole contact sites with aging, which deprives the v-ATPase from readily-accessible protons.[48] Expressing a nanobody-based mitochondria and vacuole linker prevented vacuolar alkalinization with aging and extended replicative lifespan.

Other interventions that preserve vacuolar acidity have also been found to increase replicative lifespan, including the overexpression of the v-ATPase subunit vma-1, caloric restriction, and methionine restriction.[56,101,102] Overall, these findings show that vacuolar acidity is an important factor in determining the longevity of yeast.

## *Caenorhabditis elegans*

*Caenorhabditis elegans* is a popular animal model for aging research due to its multicellular nature, short life-span, transparency to light microscopy and genetic tractability.[104] Intestinal lysosomes can be readily labeled with pH-sensitive dyes, facilitating the measure of lysosomal pH of this cell type.[105] Using this approach, multiple groups independently demonstrated that intestinal lysosomes become progressively less acidic with age.[105–108] Importantly, this age-associated lysosomal alkalinization is not an inevitable consequence of aging; long-lived mutant strains, including *daf-2*, *eat-2*, and *isp-1* worms, retain lysosomal acidity during aging, suggesting that maintenance of lysosomal pH is associated with longevity-promoting pathways.[107] Future work probing lysosomal pH in other tissues—enabled by the development of genetically encoded lysosomal pH sensors—will reveal whether other types of cells, such as neurons, also lose lysosomal acidity with age.

Several interventions that preserve or restore lysosomal acidity extend lifespan in worms. Overexpression of transcription factors DAF-16 and XBP-1 has been shown to acidify intestinal lysosomes and extend lifespan.[106,109] Similarly, inducing lysosomal acidification through

alternative day fasting extends lifespan and reduces accumulation of aggregation-prone proteins in aged worms.[108] However, because these interventions affect multiple cellular pathways, whether their beneficial effects are mediated directly by lysosomal re-acidification remains unclear. Direct manipulation of lysosomal pH will be needed to establish its causal role in longevity.

### *Mammalian Models*

Some evidence for lysosomal loss with aging has also been reported with murine models. A study utilizing LysoSensor Green DND-189 reported that lysosomal pH is elevated in the femoral heads isolated from 60-week-old mice compared with those from 8-week-old mice.[110] Similarly, measurements carried out with LysoSensor Yellow/Blue DND-160 revealed that isolated urothelial cells from aged rats had less acidic lysosomes than those from young ones, which was accompanied by a loss in cathepsin B activity.[111] There are no reports of lysosomal pH changes in murine neural cells with age, likely because lysosomotropic dyes and dextran-based lysosomal pH sensors are not compatible with complex tissues. Future work utilizing genetically encoded lysosomal pH sensors in murine models could reveal whether the age-associated lysosomal alkalinization also occurs in the mammalian brain.

## Lysosomal pH in neurodegenerative diseases

Neurodegenerative diseases arise from diverse genetic and environmental risk factors, yet dysregulation of lysosomal pH has emerged as a common feature across these disorders (**Figure 1.3**). Depending on the disease mechanism, altered lysosomal pH may represent a primary pathogenic event, such as when mutations directly affect the acidification machinery, or arise secondary to broader defects in lysosomal homeostasis, including disrupted lipid metabolism, mitochondrial, dysfunction, accumulation of aggregated proteins, and aberrant

signaling pathways (**Figure 1.2**). Most neurodegenerative disease models exhibit lysosomal alkalinization, consistent with observations in aging. However, several studies have reported lysosomal hyper-acidification, suggesting that deviations from basal lysosomal pH impair hydrolase function regardless of directionality of the change.

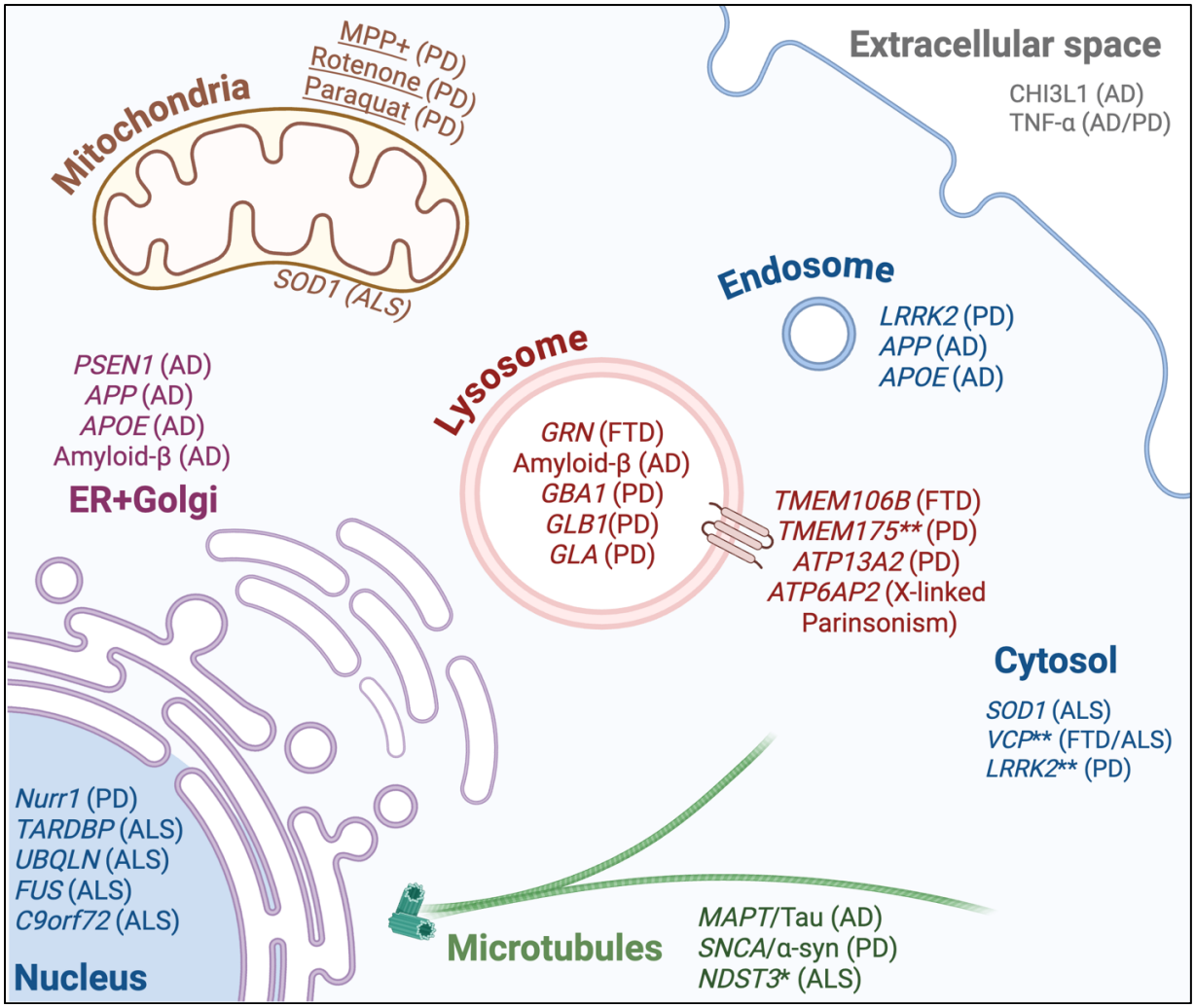


**Figure 1.3 - Genetic and environmental insults associated with NDs impacting the maintenance of lysosomal pH**

Genes and toxins that have been reported to affect lysosomal pH depicted in their typical subcellular localization. Most are associated with lysosomal alkalinization, which no asterisk indicates, while * indicates that they are associated with hyper-acidification and ** indicates that there are reports on both elevation and decrease in lysosomal pH. *Genes* are italicized, while environmental toxins are underlined. Disease associated with each gene or environmental toxin in parenthesis: AD: Alzheimer's disease, PD: Parkinson's disease, FTD: Frontotemporal dementia; ALS: amyotrophic lateral sclerosis.

Figure generated with BioRender.

## Alzheimer's Disease

A growing body of evidence suggests that lysosomal alkalinization is a common feature of Alzheimer's disease (AD) and may represent a convergent mechanism linking diverse risk factors to neuronal dysfunction. Importantly, this is supported by direct observations from patient-derived cells: lysosomal pH measurements using the DNA-based ratiometric probe *CalipHluor* demonstrated that monocytes isolated from patients with early-onset AD possess more alkaline lysosomes than those from age-matched healthy controls.[74,112] Impaired lysosomal acidification has also been reported in several cellular AD models, including those expressing *PSEN1* mutations and *APOE4*, the major genetic causes of familial and sporadic AD, respectively (**Table 1.3**).[29,32,113,114]

Reduced v-ATPase expression and activity are recurring features of both human AD and animal models. Transcriptomic analyses of postmortem AD brain tissue identified downregulation of *ATP6V1A* in cortical neurons, a finding subsequently confirmed across multiple brain regions and at the protein level.[115–117] In addition, the pseudo-kinase *STK11P* is upregulated in AD brain tissue and has been shown to inhibit v-ATPase assembly.[118] Similarly, 5xFAD and APP/PS1 mice models exhibit decreased abundance or maturation of the v-ATPase V0a1 subunit.[69,86] Most strikingly, conditional deletion of *ATP6V0A1* in the mouse forebrain is sufficient to induce memory impairment, neuronal hyperexcitability, and hippocampal neurodegeneration resembling AD pathology.[119] Together, these findings suggest that impaired lysosomal acidification may lie upstream of several hallmark features of AD pathogenesis.

**Table 1.3 - Cellular models of AD that exhibit elevated lysosomal pH**

| Gene | Associated Disease | Model Cell line | Genotype / Genetic manipulation | Lysosomal pH sensor |
|---|---|---|---|---|
| APOE3/4 | AD | Astrocytes | Human ApoE3 or ApoE4 expression | pHrodo Green-Dextran[113] |
| | | Neuro-2a (mouse neuroblastoma cells) | Human ApoE3 or ApoE4 expression | Oregon Green-Dextran[114] |

| Gene | Associated Disease | Model Cell line | Genotype / Genetic manipulation | Lysosomal pH sensor |
|---|---|---|---|---|
| PSEN1 | AD | Patient-derived fibroblasts | PSEN1 A246E mutation | LysoSensor Yellow/Blue DND-160[120] |
| | | Patient-derived fibroblasts | PSEN1 M233T mutation | LysoSensor Yellow/Blue-Dextran[78] |
| APP | Down Syndrome / AD | Patient-derived fibroblasts | Down syndrome patients (3 copies of APP) | LysoSensor Yellow/Blue-Dextran[121] |
| | | Primary cortical neurons | TS2 mice model (3 copies of APP) | LysoSensor Yellow/Blue-Dextran[121] |
| | | SHSY-5Y (undifferentiated) | APP695 | LysoSensor Yellow/Blue DND-160[122] |
| | | HT22 (mouse hippocampal cell line) | APP695 overexpression | LysoSensor Yellow/Blue DND-160[123] |
| Aβ | AD | Neuro-2a (mouse neuroblastoma cells) | Treatment with Aβ1-42 peptide | LysoSensor Yellow/Blue DND-160[79] |
| | | Neuro-2a (mouse neuroblastoma cells) | Treatment with Aβ oligomers | LysoSensor Green DND-189[70] |
| Tau | AD | SHSY-5Y (undifferentiated) | Tau P301L | LysoSensor Yellow/Blue DND-160[124] |
| | | HEK293 | Tau overexpression | LysoSensor Yellow/Blue DND-160[125] |
| | | HT22 (mouse hippocampal cell line) | Tau overexpression | pHLARE[58] |
| | | Astrocytes | Treatment with 4R tau fibrils | pHLARE[126] |
| | | Primary microglia | Treatment with sarkosyl-insoluble tau P301L fractions | LysoSensor Yellow/Blue DND-160[124] |
| CHI3L1 | AD | iPSC-derived astrocytes | Treatment with recombinant CHI3L1 | LysoSensor Yellow/Blue DND-160[127] |
| TNF-α | AD/PD | PC12 (rat neuroblastoma cells) | Treatment with recombinant TNF-α | LysoSensor Yellow/Blue-Dextran[128] |
| IL-1 + TNF-α + C1q | AD/PD/ALS | iPSC-derived astrocytes | Treatment with recombinant TNF-α, IL-1 and C1q | FIRE-pHLy[129] |

## *Presenilin 1*

Although presenilin 1 (PSEN1) is best known as the catalytic component of the γ-secretase complex, studies of PSEN1-mutant and knockout models have revealed an additional role in regulating lysosomal acidification (**Table 1.3**). Mechanistically, PSEN1 has been proposed to function as an endoplasmic reticulum (ER) chaperone that facilitates the proper maturation and trafficking of lysosomal membrane proteins.[78,130,131] PSEN1-knockout blastocysts exhibit incomplete glycosylation of V0a1, leading to its retention within the endoplasmic reticulum and reduced lysosomal localization.[130,131] Consistent with this model, knockdown of this V0a1 or expression of a nonglycosylatable V0a1 R447L mutant similarly impaired lysosomal acidification[131]. *PSEN1*-knockout cells also exhibit mislocalization of the $Cl^-/H^+$ antiporter ClC-7, with decreased lysosomal levels due to accumulation in the ER.[78] Because ClC-7 facilitates v-ATPase activity by lowering membrane potential, its mislocalization contributes to the elevation of lysosomal pH.[46] Elevated lysosomal pH subsequently activates the lysosomal $Ca^{2+}$ channel TRPML1, promoting $Ca^{2+}$ efflux and subsequent depletion of lysosomal calcium stores.[131]

Restoration of lysosomal acidity rescues several AD-associated defects in cellular models. Notably, treatment of *PSEN1*-knockout murine blastocysts with acidic nanoparticles restored lysosomal acidification, increased cathepsin D maturation, normalized autophagic flux, and restored lysosomal $Ca^{2+}$ levels through normalization of TRPML1 activity.[131]

## *Aggregated protein models*

Amyloid-β (Aβ) plaques and hyperphosphorylated tau-containing neurofibrillary tangles, the defining pathological hallmarks of AD, also directly impair lysosomal acidification. Elevated lysosomal pH has been reported in multiple tau and Aβ models, including tau overexpression, fibrillar tau exposure, Aβ treatment, and Down syndrome models of increased APP expression (**Table 1.3**).

Several mechanisms have been proposed to explain how Aβ and tau impair lysosomal acidification. Phosphorylated tau and $A\beta_{1-42}$ directly interact with v-ATPase subunits V1b2 and V0c, respectively, and reduce the rate of v-ATPase activity as measured via ATP hydrolysis.[58] APP-derived βCTF similarly impairs v-ATPase assembly through direct interaction with the V0a1 subunit, an interaction that is strengthened by pathogenic phosphorylation of APP at Tyr682.[68] AD-associated protein aggregates may also elevate lysosomal pH by compromising lysosomal membrane integrity; following endocytosis, tau fibrils accumulate within neuronal lysosomes and trigger CHMP4B-positive membrane damage, likely promoting proton leakage.[126]

Restoring lysosomal acidity ameliorates several downstream pathological phenotypes in aggregated protein models. Treatment of APP/PS1 mice with DNLA, a natural product that has been shown to promote lysosomal acidification in cellular models, rescued impaired autophagic flux, reduced $A\beta_{1-42}$ accumulation, and improved memory, supporting a causal role for lysosomal alkalinization in AD pathology.[86,87]

## *Neuroinflammation*

Neuroinflammation is increasingly recognized as an important contributor to AD pathogenesis that may be closely linked to lysosomal acidification. Plasma concentrations of TNF-α are elevated in patients with AD, and treatment of rat neuroblastoma cells with TNF-α increases lysosomal pH while disrupting autophagic flux and promoting α-synuclein accumulation.[128,132,133] These phenotypes are rescued by treatment with PP242, an mTOR inhibitor that also acidifies lysosomes.[39,128] Similarly, the pro-inflammatory mediators CHI3L1, which is elevated in the cerebrospinal fluid of AD patients, and the cytokine combination IL-1α, TNF-α, and C1q both elevate lysosomal pH in iPSC-derived astrocytes.[127,129,134] The cytokine cocktail also activated mTORC1 and mTORC2 signaling, suggesting that the observed lysosomal alkalinization may occur downstream of mTOR activation.[129]

Restoring lysosomal acidification also attenuates neuroinflammatory phenotypes in patient-derived AD models. Transdifferentiated neurons generated from fibroblasts of patients with sporadic or *PSEN1*-associated AD exhibit elevated levels of inflammatory cytokines along with an elevation of lysosomal pH.[98] Treatment with C381, a lysosomal acidifier, reduced the abundance of these cytokines. These findings suggest a bidirectional relationship between impaired lysosomal acidification and neuroinflammation in AD.

## Parkinson's Disease

There is also extensive research showing that lysosomal pH is dysregulated in Parkinson's Disease (PD). Lysosomal alkalinization has been observed in various cellular models, including those expressing disease-associated variants of *GBA1*, the most common cause of familial PD (**Table 1.4**). Notably, splice variants in *ATP6AP2* cause X-linked parkinsonism with spasticity.[135] This gene encodes an accessory subunit of the v-ATPase complex and iPSC-derived neurons expressing disease variants exhibit elevated lysosomal pH, along with decreased $V_0$-$V_1$ v-ATPase assembly.[136] Defects in mitophagy, the selective autophagic degradation of dysfunctional mitochondria, are a major driver of PD.[137] Because mitophagy depends on functional lysosomes, impaired lysosomal acidification likely contributes to mitochondrial dysfunction and thus is another key contributor to PD pathogenesis. Despite the strong evidence linking lysosomal alkalinization to PD, studies of PD-associated LRRK2 and TMEM175 variants have produced conflicting effects on lysosomal pH, and whether these discrepancies arise from biological heterogeneity or methodological differences remains to be determined.

**Table 1.4 - Cellular models of PD that exhibit aberrant lysosomal pH**

| Gene / Toxin | Effect on lyso pH | ND | Model Cell line | Genotype / Genetic manipulation / Treatment | Lysosomal pH sensor |
|---|---|---|---|---|---|
| α-syn | Alkalinization | PD | SHSY-5Y (undifferentiated) | α-syn WT and A30P and A53T overexpression | LysoSensor Green DND-189[138] |

| Gene / Toxin | Effect on lyso pH | ND | Model Cell line | Genotype / Genetic manipulation / Treatment | Lysosomal pH sensor |
|---|---|---|---|---|---|
| | | | SHSY-5Y (undifferentiated) | α-syn A30P overexpression | LysoSensor Yellow/Blue DND-160[139] |
| | | | BE-M17 cells (undifferentiated) | α-syn overexpression | LysoSensor Yellow/Blue-Dextran[140] |
| | | | Primary microglia | Treatment with α-synuclein preformed fibrils | LysoSensor Yellow/Blue DND-160 ; Dojindo pHLys Red + LysoPrime Green[141] |
| GBA1 | | | iPSC-derived neurons | GBA1 heterozygous null | LysoSensor Yellow/Blue DND-160[71] |
| | | | Mouse astrocytes | GBA1 D409V (het and homozygous) | LysoSensor Yellow/Blue DND-160[142] |
| | | | BE-M17 cells (differentiated into dopaminergic neurons) | GBA1 N370S and L444P | LysoSensor Yellow/Blue DND-160[143] |
| | | | iPSC-derived dopaminergic neurons | GBA1 E326K and N370S | LysoSensor Yellow/Blue DND-160[143] |
| GLB1 | | | Patient-derived fibroblasts | GLB1 R419Q | LysoSensor Green DND-189[144] |
| GLA | | | Patient-derived fibroblasts | GLA D313Y | LysoSensor Green DND-189[144] |
| ATP13A2 | | | Patient-derived fibroblasts | ATP13A2 L3202 and L6025 | LysoSensor Yellow/Blue-Dextran[57] |
| | | | M17 (neuroblastoma cells) | ATP13A2 L3292 | LysoSensor Yellow/Blue-Dextran[61] |
| | | | iPSC-derived neurons | ATP13A2 KO | Oregon Green-Dextran[81] |
| NURR1 | | | Neuro2a (mouse neuroblastoma cells) | NURR1 KD via shRNA | LysoSensor Green DND-189[145] |
| ATP6AP2 | | X-linked PD | iPSC-derived neurons | ATP6AP2 splice variant | LysoSensor Yellow/Blue DND-160[136] |
| | | | HeLa cells | ATP6AP2 KD vi siRNA | LysoSensor Yellow/Blue DND-160[136] |
| MPP+ | | PD | M17 (neuroblastoma cells) | Treatment with MPP+ | LysoSensor Yellow/Blue-Dextran[61] |
| | | | PC-12 (Rat neuroblastoma cells) | Treatment with MPP+ | LysoSensor Yellow/Blue DND-160[146] |
| Paraquat | | | Differentiated SHSY-5Y cells and primary astrocytes | Treatment with Paraquat | LysoSensor Yellow/Blue DND-160[147] |

| Gene / Toxin | Effect on lyso pH | ND | Model Cell line | Genotype / Genetic manipulation / Treatment | Lysosomal pH sensor |
|---|---|---|---|---|---|
| Rotenone | | | Immortalized microglial cells | Treatment with Rotenone | LysoSensor Yellow/Blue DND-160[88] |
| LRRK2 | Alkalinization | | Primary mouse cortical neurons | LRRK2 G2019S mutation | LysoSensor Yellow/Blue DND-160[148] |
| | | | Primary rat cortical neurons | LRRK2 R1441C mutation | LysoSensor Green DND-189[80] |
| | | | iPSC-derived astrocytes originating from patients | LRRK2 I1371V mutation | LysoSensor Yellow/Blue DND-160[149] |
| | Hyper-acidification | | Primary astrocytes | LRRK2 G2019S | LysoSensor Yellow/Blue DND-160[150] |
| | | | A549 cells (epithelial lung cell line) | LRRK2 R1441G | Oregon Green-dextran[151] |
| TMEM175 | Alkalinization | | Primary neurons | TMEM175 KO (under media lacking growth factors) | LysoSensor Yellow/Blue DND-160[152] |
| | | | Primary neurons, macrophages | TMEM175 KO (under media lacking growth factors) | Oregon Green-Dextran[72] |
| | Hyper-acidification | | SHSY-5Y (undifferentiated) | TMEM175 M393T | Oregon Green-dextran[153] |
| | | | Primary neurons | TMEM175 knockout | Oregon Green-dextran[55] |

## *α-Synuclein overexpression and fibril models*

Aggregation of α-synuclein (α-syn) into Lewy bodies is a pathological hallmark of PD, and increasing evidence indicates that α-syn directly impairs lysosomal acidification (**Table 1.4**). Overexpression of wild-type or mutant α-syn consistently elevates lysosomal pH in neuronal cell models, while exposure of primary microglia to preformed α-syn fibrils produces a similar phenotype.[138–140]

Mechanistically, α-syn appears to disrupt v-ATPase function. In microglia, α-syn fibrils reduce V0c abundance and $V_1$-$V_0$ assembly, and α-syn directly interacts with the V0c subunit, suggesting that it destabilizes the v-ATPase complex.[141] α-Syn-containing exosomes from PD patients similarly reduce abundance of the v-ATPase subunit V1g1.[154] In parallel, α-syn overexpression induces lysosomal membrane damage, providing an additional mechanism for

lysosomal alkalinization through proton leakage.[140] Finally, given that α-syn triplication and quadruplication are associated with PD, overly abundant protein may simply overwhelm the degradative capacity of the lysosome.[155,156]

Restoring lysosomal acidity rescues multiple disease phenotypes in α-syn disease models. Overexpression of the V0c subunit re-acidifies lysosomes, reduces α-syn pathology, improves cell viability, and ameliorates motor deficits and dopaminergic neuron loss in α-syn PFF mice.[141] Likewise, acidic nanoparticles restore lysosomal function while reducing α-syn accumulation by enhancing both macroautophagy and chaperone-mediated autophagy in α-syn-overexpressing neuroblastoma cells.[139,140]

## *Toxin-based PD models*

The herbicide paraquat and the insecticide rotenone are well-established environmental risk factors for PD.[157] Both compounds share structural similarity with MPP+, the active metabolite of the PD-linked neurotoxin MPTP.[158] Exposure to each has been shown to elevate lysosomal pH in cellular models (**Table 1.4**). Because all three toxins inhibit the mitochondrial electron transport chain and reduce mitochondrial membrane potential, one possible explanation for their shared effect on lysosomal pH is that mitochondrial dysfunction decreases proton availability at mitochondria–lysosome contact sites, thereby limiting proton pumping by the v-ATPase.[159]

Restoring lysosomal acidity rescues many of the downstream consequences of toxin exposure. Acidic nanoparticle treatment increases mitochondrial activity and autophagic flux in MPP+-treated PC-12 cells.[146] This rescue suggests that restoring lysosomal acidity may improve mitochondrial health by enhancing mitophagy and maintaining a healthier mitochondrial pool. In MPTP-treated mice, acidic nanoparticles rescue the number of TH-positive cells in the substantia nigra, and treatment with the lysosomal acidifier C381 reduces phosphorylated α-synuclein levels.[61,64]

## *ATP13A2*

*ATP13A2* encodes a lysosomal cation transporter and is an established genetic risk factor for PD. PD-associated mutations result in reduced expression of the ATP13A2 protein, and thus expression of disease associated variants and ATP13A2 knockout in cellular models both result in an elevation of lysosomal pH (**Table 1.4**).[57]

Recent work suggests that this phenotype arises through dysregulation of lysosomal polyamine homeostasis. ATP13A2 normally exports polyamines from the lysosomal lumen, and as a consequence, ATP13A2 deficiency results in their accumulation.[160] Because polyamines are polybasic molecules, they buffer luminal protons while increasing lysosomal membrane potential, thereby reducing v-ATPase activity. Restoration of lysosomal acidity in ATP13A2-mutant neuroblastoma cells with acidic nanoparticles alleviates a blockage of autophagic flux and enhances cathepsin D maturation and activity, demonstrating that impaired acidification contributes directly to lysosomal dysfunction.[61]

## *GBA1*

*GBA1* encodes β-glucocerebrosidase (GCase), a lysosomal hydrolase that catalyzes the conversion of glucosylceramide (GlcCer) to glucose and ceramide. Mutations in GBA1, one of the strongest genetic risk factors for PD, consistently impair lysosomal acidification (**Table 1.4**). Several mechanisms appear to contribute to this phenotype. GBA1-mutant neurons exhibit increased mTORC1 activity together with reduced $V_1$-$V_0$ assembly, consistent with previous work demonstrating that activated mTORC1 inhibits v-ATPase assembly.[45,161] In parallel, mutant neurons accumulate glucosylsphingosine and cholesterol, both of which independently have been reported to increase lysosomal pH.[84,143,162] Because GCase activity itself declines as lysosomal pH increases, lysosomal alkalinization likely establishes a positive feedback loop that further reduces substrate clearance.[81,163]

Restoring lysosomal acidity improves several downstream defects in GBA1 models. Treatment with acidic nanoparticles re-acidified lysosomes in GBA1-mutant iPSC-derived dopaminergic neurons while increasing GCase activity, mitophagy, and mitochondrial membrane potential.[161] Likewise, acidic nanoparticles partially restored lysosomal acidity in GBA1-mutant fibroblasts, resulting in increased cathepsin D maturation and reduced LC3B-II levels, consistent with restoration of stalled autophagic flux.[61] Together, these findings suggest that impaired lysosomal acidification is an important downstream consequence of GBA1 mutations and that restoring lysosomal pH can improve both lysosomal and mitochondrial function.

## *LRRK2*

LRRK2 mutations are among the strongest genetic risk factors for PD and have been reported to alter lysosomal pH (**Table 1.4**). Some studies have found that pathogenic LRRK2 variants elevate lysosomal pH in neuronal models, including primary neurons and patient-derived iPSC astrocytes.[80,148,149] One proposed mechanism is that wild-type LRRK2 interacts with the v-ATPase V0A1 subunit, whereas the R1441C mutation disrupts this interaction, reducing V0A1 expression and lysosomal localization.[80] Re-acidifying lysosomes by treating primary LRRK2 R1441C neurons with the zinc ionophore clioquinol enhances lysosomal proteolysis, rescues stalled autophagic flux, and restores lysosomal calcium levels.[80,164]

However, not all LRRK2 models exhibit lysosomal alkalinization. Primary astrocytes expressing LRRK2's G2019S mutation and A549 cells carrying the R1441G mutation instead exhibit lysosomal hyper-acidification despite reduced cathepsin D activity and impaired lysosomal proteolysis.[150,151] This could be an indirect effect of the *LRRK2* mutation, representing a compensatory hyper-acidification. Consistent with this idea, increased ATP13A2 expression has been proposed as an explanation for this phenotype.[150] Alternatively, the conflicting lysosomal pH observations may reflect either cell type-specific effects, with lysosomal alkalinization primarily

reported in neurons and hyper-acidification in astrocytes and epithelial cells, or technical differences, as studies reporting lysosomal alkalinization relied exclusively on lysosomotropic dyes.

## *TMEM175*

TMEM175 is a lysosomal ion channel whose physiological function remains controversial. Although it can conduct both protons and $K^+$ depending on experimental conditions, it is unclear which activity predominates *in vivo.*[55,72].Consequently, studies examining the effects of TMEM175 deficiency have reported both lysosomal hyper-acidification and alkalinization (**Table 1.4**).

One model proposes that TMEM175 functions primarily as a proton leak channel. Consistent with this hypothesis, TMEM175 knockout or expression of catalytically inactive mutants results in lysosomal hyper-acidification.[55,165,166] Consistently, activation of TMEM175 with arachidonic acid elevates lysosomal pH by promoting proton efflux.[55] Notably, partial neutralization of these hyper-acidic lysosomes with BaF restores cathepsin D maturation and cathepsin B activity, suggesting that excessive acidification can impair lysosomal proteolysis.[51,55]

An alternative model proposes that TMEM175 primarily conducts $K^+$ under physiological conditions. In this model, TMEM175 dissipates lysosomal membrane potential to support continued v-ATPase activity, particularly during cellular stress.[72] Accordingly, TMEM175 knockout neurons exhibit lysosomal alkalinization, although only under growth factor-deprived conditions.[72,152] Supporting this model, inhibition of the v-ATPase alkalinizes lysosomal pH at similar rates in wild-type and TMEM175-deficient neurons, arguing against TMEM175 functioning primarily as a proton leak channel.[72] Regardless of the direction of the pH change, TMEM175 deficiency consistently reduces cathepsin D maturation and promotes α-syn accumulation.[152] Future studies will be required to determine whether the conflicting effects on lysosomal pH reflect differences in physiological context or distinct ion-conducting functions of TMEM175.

# Frontotemporal dementia and amyotrophic lateral sclerosis

Frontotemporal dementia (FTD) and amyotrophic lateral sclerosis (ALS) are increasingly recognized as a disease spectrum that shares overlapping genetic causes and pathological mechanisms.[167] Compared with AD and PD, relatively few studies have directly examined lysosomal pH in FTD/ALS models. Nevertheless, the available evidence suggests that impaired lysosomal acidification is a recurring feature across multiple disease-associated genes (**Table 1.5**).

**Table 1.5 - Cellular models of FTD/ALS that exhibit aberrant lysosomal pH**

| Gene | Effect on lysosomal pH | ND | Model Cell line | Genotype / Genetic manipulation | Lysosomal pH sensor |
|---|---|---|---|---|---|
| GRN | Alkalinization | FTD | Mouse bone-marrow derived macrophages | GRN KO | LysoSensor Yellow/Blue DND-160[168] |
| | | | iPSC-derived neurons | GRN KO | Oregon Green-Dextran[169] |
| TMEM106B | | FTD | HeLa | TMEM106B overexpression | LysoSensor Green DND-189[170] |
| | | | Primary mouse neurons | TMEM106B overexpression | LysoTracker / LAMP1[171] |
| FUS | | ALS | Cos7 cells (fibroblasts) | FUS P525L and R495X | Oregon Green-Dextran[172] |
| | | | Cos7 cells (fibroblasts) | Hypomethylation variants | Oregon Green-Dextran[172] |
| TARDBP /TDP-43 | | ALS | Pateint-derived fibroblasts | TDP-43 G376D | LysoSensor Yellow/Blue DND-160[173] |
| SOD1 | | ALS | Rat primary fibroblasts | SOD1 G93A | Acridine Orange[174] |
| VCP | Alkalinization | ALS | iPSC-derived motor neurons | VCP R155H | LysoSensor Yellow/Blue DND-160[175] |
| | Hyper-acidification | ALS/ FTD | iPSC-derived microglia | VCP R155C and R191Q | LysoSensor Green DND-189[176] |
| NDST3 | Hyper-acidification | ALS | RPE cells | NDST3 KO in C9orf72 repeat expansion cells | LysoSensor Yellow/Blue Dextran[54] |

## *Progranulin*

Loss-of-function mutations in *GRN*, which cause progranulin haploinsufficiency, are among the most common genetic causes of FTD.[177,178] Multiple studies have demonstrated that

progranulin deficiency elevates lysosomal pH, whereas restoration of progranulin re-acidifies lysosomes (**Table 1.5**). Elevated lysosomal pH has been reported in *GRN* knockout bone marrow-derived macrophages and iPSC-derived neurons, while progranulin overexpression or treatment with recombinant progranulin lowers lysosomal pH in multiple cellular models.[168,169,179,180]

Several mechanisms have been proposed to explain how progranulin regulates lysosomal acidification. Recent work demonstrated that lysosomal progranulin enhances v-ATPase recruitment and ATP hydrolysis, resulting in lysosomal hyper-acidification when overexpressed, whereas *GRN* knockout reduces both total and lysosomal V0a3 abundance.[181] In parallel, progranulin deficiency alters lysosomal lipid composition, including reduced bis(monoacylglycero)phosphate (BMP) and elevated glucosylsphingosine.[168] Although the effect of BMP depletion on lysosomal pH has not been tested directly, increasing BMP levels through phosphatidylglycerol supplementation acidifies lysosomes, suggesting that reduced BMP may contribute to lysosomal alkalinization.[182] Likewise, glucosylsphingosine has been shown to elevate lysosomal pH.[84] Together, these findings suggest that lipid dysregulation contributes to impaired lysosomal acidification in progranulin-deficient models.

## *TMEM106B*

Variants in TMEM106B are associated with FTLD-TDP and modify disease risk in progranulin-associated FTD, with certain alleles conferring protection in GRN mutation carriers.[183] Overexpression of TMEM106B increases lysosomal pH, although these findings were obtained using relatively indirect measures of lysosomal acidity (**Table 1.5**).[170,171] Mechanistically, TMEM106B physically interacts with the v-ATPase and reduces abundance of the $V_0$ domain, thereby impairing lysosomal acidification.[184] More recently, accumulation of the TMEM106B C-terminal fragment has been shown to form lysosomal fibrils that eventually puncture the lysosomal

membrane, suggesting that they might lead to lysosomal membrane damage that results in a leakage of protons.[183]

### *ALS-associated genes*

Evidence linking lysosomal pH to ALS is more limited and, in some cases, conflicting (**Table 1.5**). Disease-associated FUS variants elevate lysosomal pH, while mutations in VCP increase lysosomal pH in iPSC-derived motor neurons and impair lysophagy, the specialized type of autophagy that targets damaged lysosomes.[172,175,185] These defects were rescued by the VCP inhibitor CB-5083.[175] In contrast, ALS-associated VCP mutations produce lysosomal hyper-acidification in iPSC-derived microglia together with increased cathepsin D activity, suggesting cell type-specific regulation of lysosomal pH.[176] Similarly, knockout of NDST3, which is downregulated in tissues from patients carrying C9orf72 repeat expansions, results in lysosomal hyper-acidification combined with reduced cathepsin B maturation, activity, and overall lysosomal proteolysis.[54] Partial neutralization of lysosomal pH with BaF rescues these proteolytic defects, demonstrating that excessive acidification, like lysosomal alkalinization, can impair lysosomal function.

Overall, compared with AD and PD, considerably less is known about lysosomal pH regulation in FTD/ALS. Most studies have focused on characterizing lysosomal pH changes rather than testing whether restoring physiological lysosomal acidity improves disease-associated phenotypes. Establishing the therapeutic potential of lysosomal pH correction therefore remains an important priority for future research in FTD and ALS.

## Conclusions and Future Perspectives

Growing evidence indicates that dysregulation of lysosomal pH is a conserved feature of both normal aging and neurodegenerative diseases. Across cellular models, model organisms,

and mammalian systems, lysosomes generally become more alkaline with age, and similar defects are observed in multiple models of NDs. An emerging theme is that lysosomal pH is both a regulator and a target of numerous processes disrupted during aging and neurodegeneration. Elevated lysosomal pH impairs many aspects of lysosomal biology, including hydrolase activity, autophagic flux, lysosomal membrane integrity, mitochondrial quality control, lipid homeostasis, ion flux, and inflammatory signaling. Conversely, many of these same processes—including mitochondrial dysfunction, lipid dysregulation, protein aggregation, and neuroinflammation—can themselves disrupt lysosomal acidification (**Figure 1.4**). These reciprocal interactions likely establish feedforward mechanisms that progressively amplify cellular dysfunction during aging and disease.

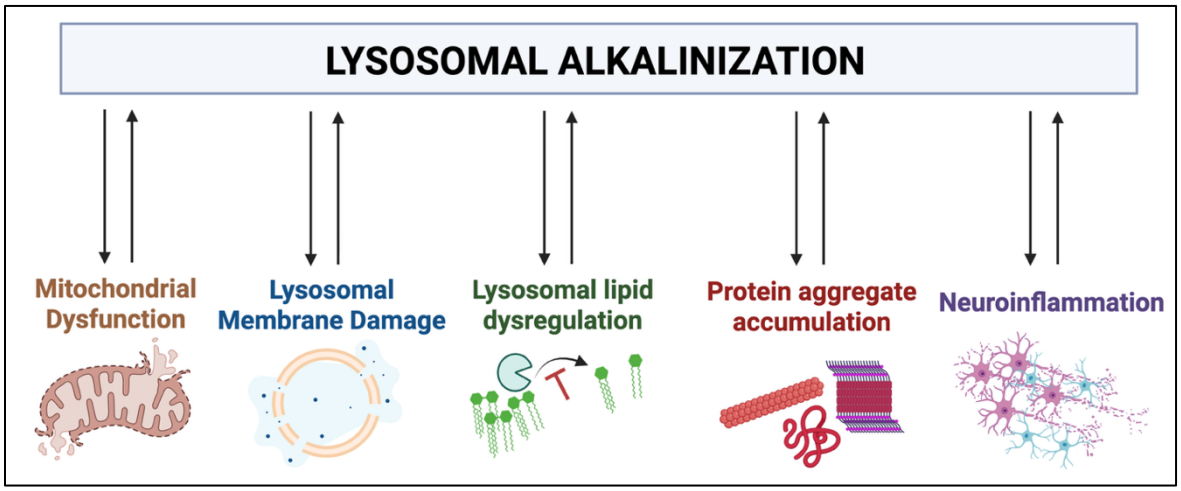


**Figure 1.4 - Bidirectional relationship between lysosomal alkalinization and other cellular defects in NDs.**
Lysosomal alkalinization has a bidirectional relationship with mitochondrial dysfunction, lysosomal membrane damage, lipid dysregulation, protein aggregate accumulation and neuroinflammation. Figure generated with BioRender.

Despite substantial progress, important questions remain. Human neuronal aging remains underexplored, and direct transdifferentiation provides a promising platform for determining whether lysosomal alkalinization occurs in aged human neurons while preserving age-associated epigenetic signatures. Likewise, the development and application of genetically encoded lysosomal pH sensors in mammalian models will enable longitudinal, cell type-specific

measurements of lysosomal acidity *in vivo*. Finally, although several studies have demonstrated the benefits of lysosomal re-acidification in cellular and murine models, whether these strategies can be translated into therapies for neurodegenerative and other age-associated diseases remains to be determined.

# Chapter 2: WNK inhibitors acidify lysosomes and enhance lysosomal proteolytic activity

## Significance

Lysosomes play a critical role in cellular proteostasis with their functional and genetic defects linked to neurodegenerative diseases. A loss of normal lysosomal acidity has been observed in several cellular models of neurodegeneration and animal models of aging. Lysosomal re-acidification is a potential strategy for the prevention and treatment of neurodegenerative diseases, but few compounds are known to have such activity. Through a phenotypic screen and follow-up studies, we identified two novel lysosomal acidification compounds, WNK463 and WNK-IN-11. Both compounds inhibit WNKs, a family of kinases that sense osmolarity to regulate ion channel activity, that have no reported connection with lysosomal pH. WNK inhibition led to an increase in the lysosomal levels of subunits of the vacuolar ATPase, the molecular motor that pumps protons into organelles. We thus uncovered a novel pathway of lysosomal pH regulation. In addition, WNK463 and WNK-IN-11 increased lysosomal activity in an Alzheimer's Disease cell model, demonstrating their use as tool compounds for lysosomal re-acidification in neurodegeneration models.

## Summary

Loss of lysosomal acidity with aging likely contributes to neurodegenerative disease progression. To identify compounds that reverse this phenotype, we conducted an imaging-based screen for small molecules that acidify lysosomes. WNK463, an ATP-competitive inhibitor of the WNK family of kinases, emerged as the top hit. Treatment with an allosteric WNK inhibitor, WNK-

IN-11, and genetic knock-down of the WNK orthologue of *Caenorhabditis elegans* also led to lysosomal acidification. The hit compounds induced autophagy, but blocking autophagy initiation did not block acidification by the two compounds. Sub-components of the vacuolar-ATPase (v-ATPase), the molecular motor that acidifies lysosomes, were enriched in the lysosomes of cells that had been treated with WNK463 and WNK-IN-11, which is likely contributing to lysosomal acidification. WNK inhibitors also increased lysosomal proteolytic activity in a cell line expressing ApoE4, a variant linked to Alzheimer's disease. We propose that lysosomal re-acidification may be a beneficial treatment for neurodegenerative diseases.

# Introduction

One of the main features of neurodegenerative diseases (NDs) is the accumulation of protein aggregates, such as amyloids and neurofibrillary tangles in Alzheimer's Disease (AD) and Lewy bodies in Parkinson's Disease (PD), in affected areas of the brain.[186] The strong association between their appearance and ND progression suggests that defects in protein homeostasis networks are an important driver of these diseases.[187,188] Lysosomes play a crucial role in homeostasis by degrading a diversity of cellular waste products, from specific proteins through chaperone-mediated autophagy, to larger cargo – including entire organelles – through macro-autophagy.[189,190] Several phenotypes observed in the post-mortem brains of affected individuals implicate lysosomal defects in disease progression; phenotypes include an accumulation of lysosomes and autophagic vesicles, an increase of lysosomal lumen proteins in the cytoplasm of neurons, and the presence of multiple lysosomal proteins in amyloid plaques and Lewy bodies.[6,7]

Genetic predisposition also provides evidence for the link between lysosomal dysfunction and NDs. Mutations in genes encoding lysosomal proteins are causative for both familial early onset NDs and a risk factor for sporadic late-onset forms of these diseases.[190] In addition, some mutations that cause lysosomal storage disorders when present in a homozygous state are risk

factors for NDs in a heterozygous one.[10] Subtle lysosomal damage may lead to NDs over time because the post-mitotic status of neurons makes them unable to dispose of cytosolic waste through cell division and thus vulnerable to proteostatic stress.[12,190]

Loss of lysosomal acidity is observed in multiple cellular models of NDs. For example, a mouse neuroblastoma line expressing human *APOE4*, the most common genetic risk for sporadic AD, exhibits a loss of lysosomal acidity when compared to a line expressing *APOE3.*[114] Similar results have also been shown in cell lines expressing disease-associated mutants of *PSEN1*, *LRRK2* and *ATP13A2.*[29,57,80,131] Lysosomal pH alkalinization has also been observed in eukaryotic models of aging; studies have found that the lysosomal pH of intestinal cells and neurons of *C. elegans* increases with age.[109,191,192] This observation is relevant because aging is the greatest risk factor for NDs, implicating aging defects as critical for their progression.[193]

Lysosomes are the most acidic compartments in cells due to the proton-pumping activity of the vacuolar ATPase (v-ATPase), and their pH is critical to their proteolytic function.[194–196] Cathepsins, a family of lysosomal proteases, tend to be most active near basal lysosomal pH.[25] Autolysosomes have been observed to be deacidified in the brains of several AD mouse models and this change appears to occur prior to the accumulation of amyloids.[197] Thus, the loss of lysosomal acidity may occur early in NDs and be a major driver of their progression.

Re-acidifying lysosomes could thus be beneficial to treat NDs, but only a limited number of compounds are known to do so. Previously, our labs conducted a phenotypic high throughput screen to find small molecules that lower lysosomal pH.[66] The screen found that two compounds with similar structures, OSI-027 and PP242, acidified lysosomes and increased Cathepsin D activity. These compounds both inhibit mTOR, a known pathway in lysosomal pH regulation.[45,62] Identification of compounds that acidify lysosomes via previously unrecognized mechanisms would provide new tools that could deepen understanding of the basic biology of lysosomal pH regulation and be adapted for the treatment of NDs. With that goal, we conducted another high-

throughput screen with a larger library of bioactive small molecules and identified WNK kinases as new targets for lysosomal pH regulation.

# Results

## High-content imaging screen identifies WNK463 as a lysosomal acidification compound

Modest modifications were made to the parameters of our prior high-content imaging screen for novel lysosomal acidification compounds[66]. To measure changes in lysosomal pH, we again used FIRE-pHLy, a genetically encoded lysosomal pH sensor.[198] FIRE-pHLy is targeted to the lysosome by LAMP1, which is fused to two fluorescent proteins: mTFP1 faces the lysosomal lumen where its fluorescent signal gets quenched at a low pH (pKa ~4.3), while mCherry faces the cytosol where its fluorescent signal remains constant. Lysosomal pH can thus be reported through the ratio of mTFP1 to mCherry signal (subsequently referred to as FIRE-pHLy ratio), with more acidic pH resulting in a lower ratio.

We used the same FIRE-pHLy expressing cell line as the previous study, SH-SY5Y, which is a neuroblastoma line that can be terminally differentiated into neuronal-like cells.[199] Testing the hits from the previous screen revealed that the FIRE-pHLy assay had a higher dynamic range in undifferentiated SH-SY5Y cells than in differentiated ones.[66] Thus, to maximize the number of potential hits, we utilized undifferentiated SH-SY5Y cells in this screen. In addition, it facilitated assay scale-up, allowing the screening of a larger library with 7372-bioactive compounds.[66] Each compound was tested on a single well at a 10 μM dose and 6-hour time point. Screening controls included an acidifying compound (OXA-01) and an alkalinizing molecule (Bafilomycin-A; BaF) that inhibits the v-ATPase.[200] OXA-01, an analog of OSI-027, was chosen as the acidifying control in

the screen because it led to a slightly greater decrease in FIRE-pHLy ratio (lysosomal acidification) than OSI-027 or PP242 (**Figure 2.1.A**).[201]

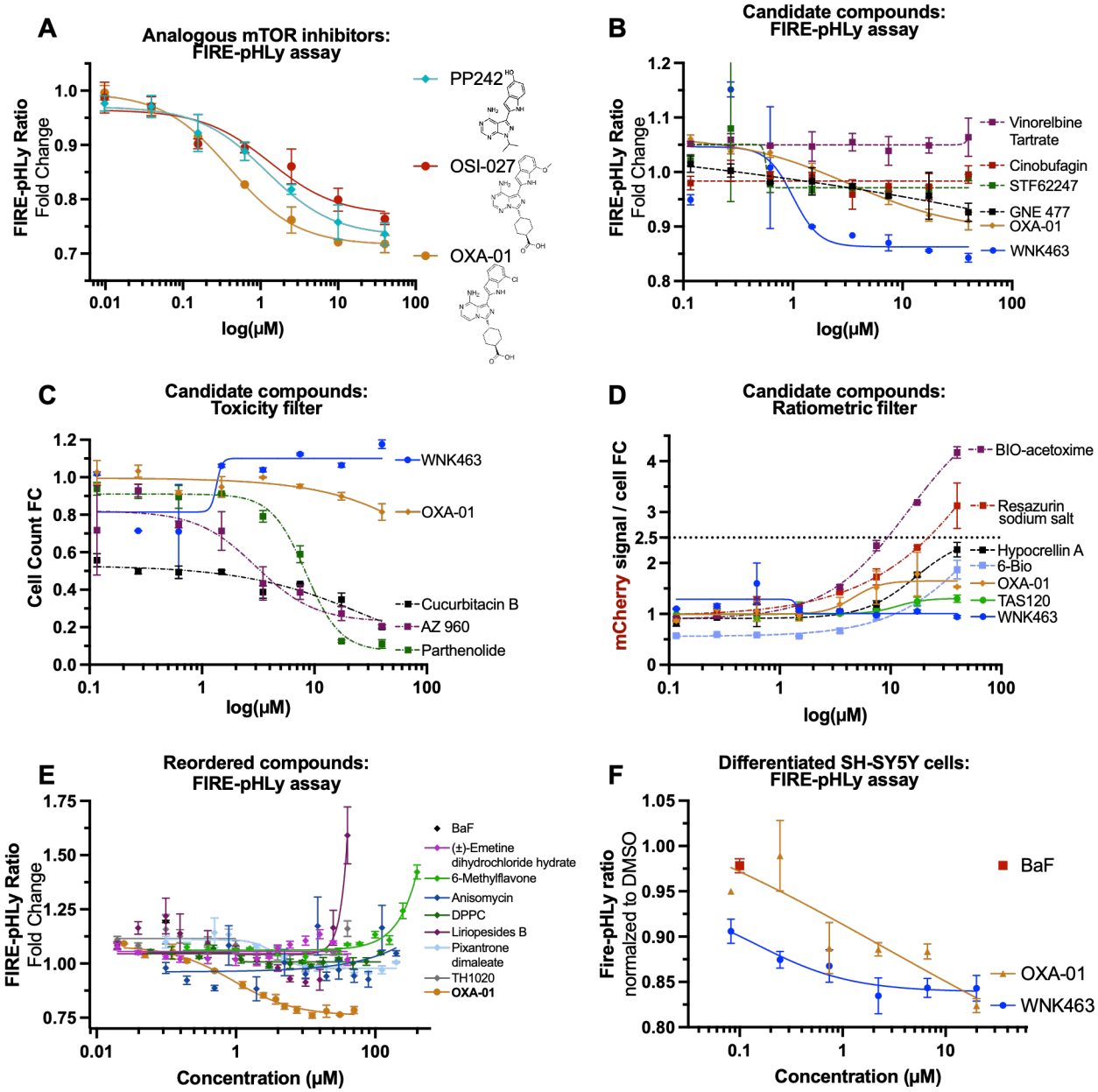


**Figure 2.1- Dose response curves related to TargetMol compound screen**
(A) FIRE-pHLy ratio of SH-SY5Y cells treated with mTOR inhibitors (4 h, *n*=3).
(B-C) Example compounds from screen of 190 candidate compounds. Compounds with dotted lines were eliminated based on different filters (6 h, *n*=2).
(B) Candidate compound screen filter based on dose-dependent decrease in FIRE-pHLy ratio.
(C) Candidate compound screen filter based on a large decrease in cell count fold change as a proxy for compound toxicity.
(D) Candidate compound screen ratiometric filter. Compounds with an mCherry signal per cell fold-change curve top plateau of 2.5 (black dotted line) or greater were eliminated.
(E) FIRE-pHLy ratio fold change curves of re-ordered compounds that did not acidify cells (6 h, *n*=3).
(F) FIRE-pHLy ratio of differentiated SH-SY5Y cells treated with pH-modulating compounds (4 h, *n*=3).
Represented as mean ± SEM, fitted to 4PL curves. Normalized to DMSO-treated wells.

To select hits, the FIRE-pHLy ratio was normalized to OXA-01-treated wells (100%) and DMSO-treated wells (0%; **Figure 2.2.A**). A relatively modest threshold of 30% FIRE-pHLy ratio relative effect was chosen because the compounds could lead to a greater degree of acidification at higher concentrations, and because even mild lysosomal acidifiers could also be useful hits. We then considered fluorescence artifacts; a compound that increased mCherry fluorescence could have decreased the FIRE-pHLy ratio without affecting lysosomal pH, so compounds that increased the mCherry signal per cell more than 2.5-fold were removed from further analysis as a ratiometric control filter (**Figure 2.2.B**). The remaining compounds were then ranked by FIRE-pHLy ratio b-score to consider row and column effects within each plate (**Figure 2.2.C**). The top 190 compounds were advanced for further testing.

The 190 candidate compounds were tested at a 6-hour time point in a dose response ranging from 0.1 to 40 μM. The fold-change in FIRE-pHLy ratio, mCherry signal per cell, and nuclear count was quantified for each compound. We selected active compounds based on the following properties: dose-dependent decrease in FIRE-pHLy ratio, low toxicity (changes in cell count were used as a proxy), and no large increase in the mCherry signal per cell (**Figures 2.1.B-D**). Eleven compounds passed all filters and were repurchased from commercial vendors.

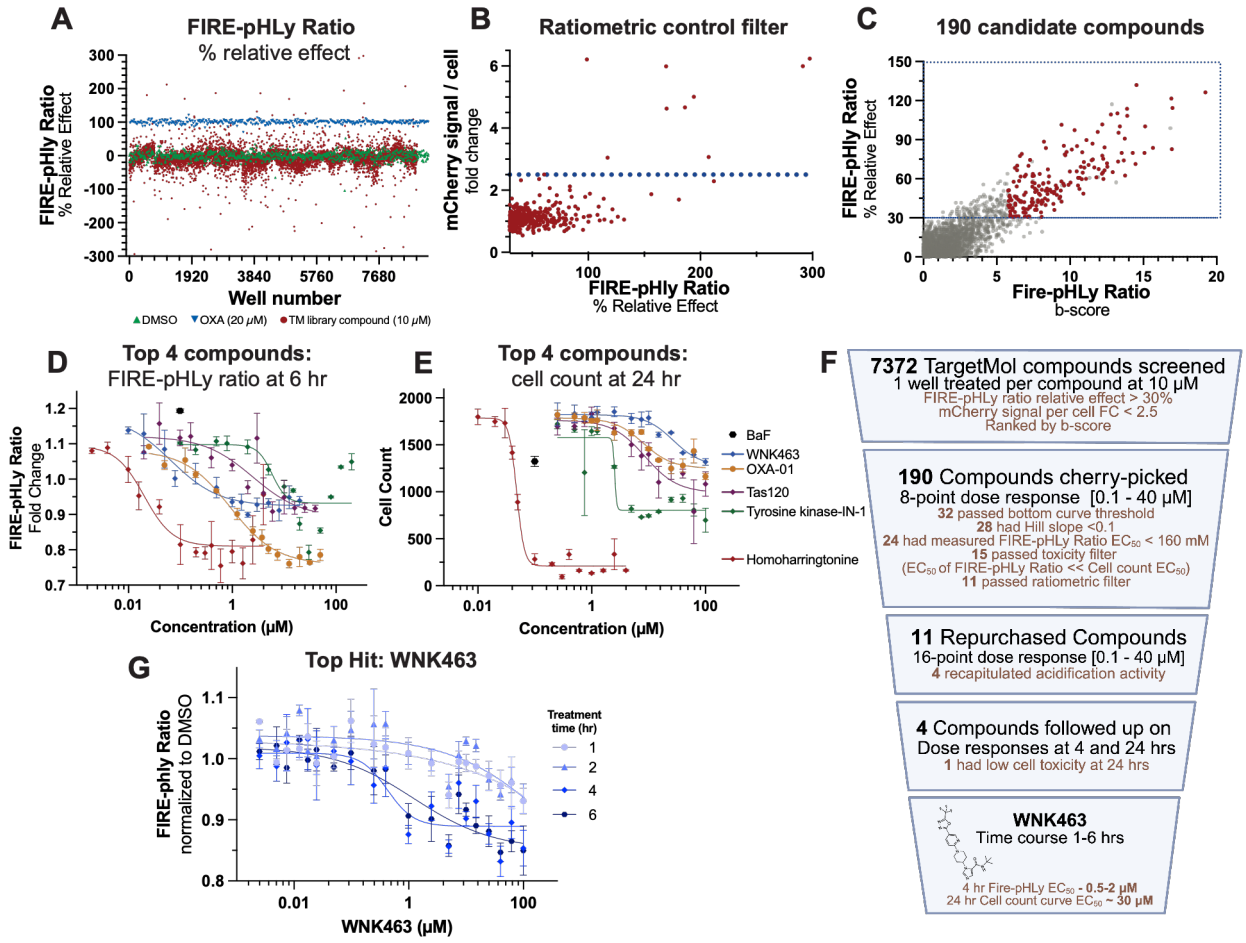


**Figure 2.2 - High-content imaging screen for lysosomal acidifiers**

(A) Scatterplot of the mTFP1 to mCherry ratio (FIRE-pHLy ratio) relative effect scores from the primary screen of the TargetMol (TM) compound library. FIRE-pHLy ratio was normalized to OXA-01 treated wells (100%) and DMSO-treated wells (0%; 10 μM, 6 h, n = 1).
(B) Ratiometric filter based on mCherry signal per cell in primary screen. Compounds with an mCherry signal per cell score over 2.5-fold change (blue dashed line) were removed from further analysis (10 μM, 6 h, n = 1).
(C) Top 190 compounds from primary screen that were selected as candidates for further testing. The blue dashed line depicts the cutoff for the minimum FIRE-pHLy ratio percent relative decrease, 30%. Remaining compounds were then ranked by their FIRE-pHLy ratio b-score (10 μM, 6 h, n = 1).
(D) FIRE-pHLy ratio dose-response curves of top four re-ordered compounds at 6 hours of treatment. Normalized to DMSO-treated wells (n=2).
(E) Cell count dose-response fold-change curves of top four re-ordered compounds treatment (24h, n=3).
(F) Workflow of screen that resulted in WNK463 emerging as the top hit.
(G) Time course of WNK463 treatment's effect on FIRE-pHLy ratio. Normalized to DMSO-treated wells (1-6 h, n=3).
(D,E,G) Represented as mean ± standard error of measurement (SEM). Data fitted to four-parameter logistic (4PL) curves.

The top eleven compounds were re-tested at 6 hours with 14 doses **(Figures 2.2.D-E**).

Only the following four compounds acidified lysosomes in a dose-responsive manner: WNK463,

Homoharringtonine, TAS-120, and XL999 (**Table 2.1**).[202–205] The four compounds were re-tested at 24 hours; WNK463 was the only compound that did not induce a drastic reduction in nuclear count, and it thus emerged as the screen's top hit (**Figures 2.2.E-F and Table 2.1**). A time course from 1-6 hours was performed with this compound, showing lysosomal acidification reaching its maximum level within a 4-hour treatment (**Figure 2.2.G**). Terminally differentiated FIRE-pHLy-expressing SH-SY5Y cells were treated with WNK463, which resulted in a decrease in FIRE-pHLy ratio (**Figure 2.1.F**). This result confirmed that WNK463's lysosomal acidification activity is not limited to cycling cells since it is active in neuronal-like cells.

WNK463 is an ATP-competitive inhibitor of with-no-lysine kinases (WNKs), which are characterized by the idiosyncratic location of their catalytic lysine.[202] The WNKs are sensors of osmotic pressure and regulate ion homeostasis by modulating the activity of cation-chloride cotransporters.[206] There are four WNK isoforms found in mammals and they are nearly ubiquitously expressed across tissues.[207] Connections between WNK defects and nervous system disorders have already been established; *WNK1* mutations cause hereditary sensory and autonomic neuropathy type II, a degenerative peripheral nervous system disease, and *WNK3* mutations lead to a rare form of X-linked intellectual disability.[208,209] However, there is no reported connection between WNK activity and lysosomal pH regulation.

**Table 2.1 - Summary of top 4 compounds from TargetMol screen**

| | | | Fire-pHLy Ratio at 6 hours | | Cell Count Curve at 24 hours | |
|---|---|---|---|---|---|---|
| **Compound** | **Target** | **Description** | **$EC_{50}$ (μM)** | **Bottom Plateau** % relative to OXA's | **$EC_{50}$ (μM)** | **Bottom Plateau** % fold change from DMSO's |
| **WNK463** 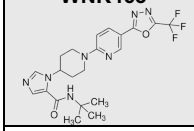 | WNKs | ATP-competitive inhibitor of WNK kinase family.[202] | 0.1 | 0.92 | 27 | 70% |
| **Tas-120** 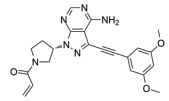 | FGFR1-4 | Highly selective, and irreversible FGFR inhibitor.[204] | 2.5 | 0.89 | 8.7 | 40% |
| **Homoharringtonine** 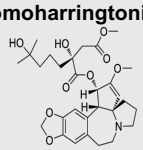 | Ribosome | Inhibits protein synthesis by binding to the A-site of the ribosome.[205] | 0.020 | 0.81 | 0.048 | 10% |
| **XL999** 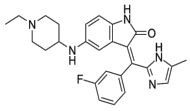 | VEGFR, PDGFR | Promiscuous tyrosine kinase inhibitor. Potent against KDR, Flt-1, FGFR1 and PDGFRα.[203] | 5.8 | 0.93 | 2.5 | 55% |

# Validation of WNK463 as a lysosomal acidifier due to its WNK inhibition activity

ATP-competitive kinase inhibitors often have off-target activities, so two approaches were taken to determine whether WNK463 acidifies lysosomes through WNK inhibition.[210] First, two additional commercially available WNK inhibitors, WNK-IN-11 and WNK1-IN-1, were tested for lysosomal acidification activity in the FIRE-pHLy assay.[211,212] WNK-IN-11 acidified lysosomal pH, while WNK1-IN-1 had no effect (**Figures 2.3.A-B**). The WNK inhibition activity of these compounds was confirmed by measuring the phosphorylation levels of SPAK (phos-SPAK), one of the main WNK substrates, via immuno-blotting. One and four hours of WNK463 and WNK-IN-11 treatment led to a significant decrease in the ratio of phos-SPAK to full-length SPAK at doses that led to lysosomal acidification (**Figure 2.3.C**). Meanwhile, WNK1-IN-1 had no significant effect on SPAK phosphorylation levels, indicating that it was a poor inhibitor of the WNKs in the tested SH-SY5Y cell line, correlating with its inability to acidify lysosomes in this assay.

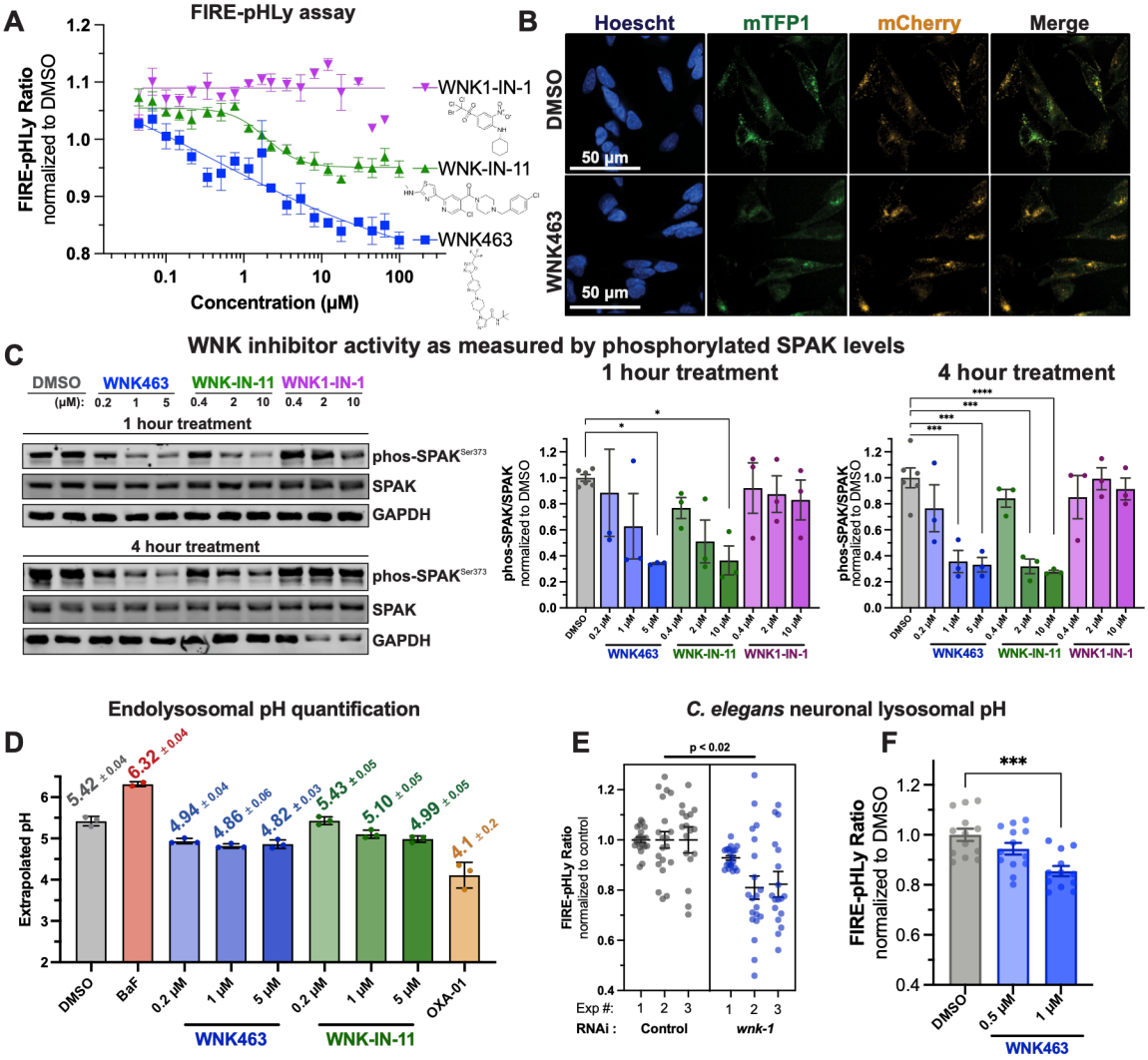


**Figure 2.3 - Validation of WNK463 as a lysosomal acidifier through WNK inhibition**

(A) Dose response curves of FIRE-pHLy ratio normalized to DMSO of SH-SY5Y cells treated for four hours with WNK inhibitors. Represented as mean ± SEM, curves fitted to 4PL curves (*n*=3).

(B) Representative images of FIRE-pHLy-expressing SH-SY5Y cells treated with DMSO or WNK463 (5 μM) for four hours (scale bar = 50 μm).

(C) Western blot analysis of phosphorylation levels of WNK substrate SPAK at Serine 373 in SH-SY5Y cells after WNK inhibitor treatment. Representative images (Left). Bar plots with quantification at one (middle) and four (left) hours of treatment (*n*=3). Statistical test: ordinary one-way (OOW) ANOVA, Dunnett's multiple comparisons (DMC).

(D) Bar plot of the estimated endolysosomal pH of SH-SY5Y cells treated for four hours with DMSO, BaF (100 nM), WNK463, WNK-IN-11, or OXA-01 (20 μM). Measured with Dojindo lysosomal pH dye kit. Represented as mean ± SEM (*n*=3).

(E) Dot plot of FIRE-pHLy ratio relative to control in response to genetic knockdown of *wnk-1* via RNAi in *C. elegans* strain expressing FIRE-pHLy in neurons. Each data point represents one animal. Statistical test: nested t-test (3 replicates with *n*=20).

(F) Bar plot of FIRE-pHLy ratio relative to control of *C. elegans* strain expressing FIRE-pHLy in neurons treated with DMSO or WNK463 for 24 hours. Each point represents one animal. Statistical test: OOW ANOVA, DMC (*n*=12).

(C, E-F) Represented as mean ± SEM. Significance labels: $*p<0.05$, $**p<0.01$, $***p<0.001$, $****p<0.0001$.

The identification of two WNK inhibitors as lysosomal acidification compounds supports a role for WNK activity in regulating lysosomal pH. WNK463 and WNK-IN-11 are structurally and mechanistically dissimilar, and thus unlikely to have the same off-target activity (**Table 2.2**). Moreover, both compounds appear to have similar $EC_{50}$'s in the SPAK phosphorylation and FIRE-pHLy assays. These results are consistent with existing literature, since published KINOMEscan data shows that both compounds have very little activity against other kinases.[96,213]

WNK463 leads to a greater decrease in FIRE-pHLy ratio than WNK-IN-11, which might be due to differences in their mechanism of action; WNK463 is a competitive inhibitor and has a similar activity against all four human WNKs, while WNK-IN-11 is allosteric and is selective towards WNK1 and WNK3 (**Table 2.2**). If more than one WNK isoform is involved in lysosomal pH regulation, then inhibiting all of them may lead to greater changes in lysosomal pH (**Figure 2.3.A**).[214]

**Table 2.2 - Inhibition and lysosomal acidification activity of 3 WNK inhibitors**

| | 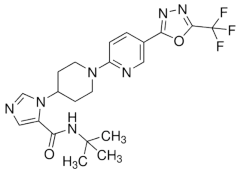 | 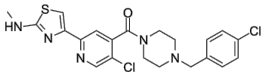 | 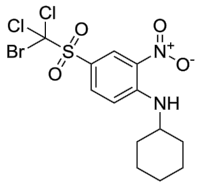 |
|---|---|---|---|
| | **WNK463** | **WNK-IN-11** | **WNK1-IN-1** |
| **Mode of inhibition** | ATP-competitive | Allosteric | Allosteric |
| **Reported Target** | WNK1,2,3,4[202] | WNK1,3[211] | WNK1 > WNK3[212] |
| **FIRE-pHLy assay ($EC_{50}$) at 4hr** | 0.5-2 μM | 1-2 μM | N/A |
| **Active concentrations of SPAK inhibition at 4 hr** | 1 and 5 μM | 2 and 10 μM | None at concentrations tested |

To provide an orthogonal measure of the effects of WNK463 and WNK-IN-11 on lysosomal pH, we used a dye-based lysosomal pH quantification kit. The kit consists of two dyes that selectively label lysosomes, pHLys Red (pRed) and LysoPrime Green (LP-Green). The fluorescence intensity of pRed increases with decreasing lysosomal pH, while that of LP-Green

remains constant. Thus, the ratio of pRed to LP-Green signal is negatively correlated with lysosomal pH, with higher ratios representing more acidic compartments. The kit can also be used to estimate absolute lysosomal pH by treating stained cells with buffers of different pH's and ionophores that equilibrate intracellular and extracellular pH. Using this method, we measured the absolute pH of lysosomes from SH-SY5Y cells treated with lysosomal pH-modulating compounds. To validate the assay, we first tested BaF and OXA-01 as alkalinizing and acidifying controls, respectively (**Figure 2.3.D**). Interestingly, the estimated pH of DMSO-treated wells was 5.4, which is higher than the reported average lysosomal pH of 4.5 to 5.[198,215] Thus, the Dojindo kit dyes may be labeling cellular compartments other than lysosomes, such as endosomes. Nevertheless, the assay appears to serve as a useful orthogonal measure of what may be endolysosomal pH. WNK463 and WNK-IN-11 were confirmed as lysosomal acidifiers with this assay, with the highest tested concentrations lowering pH by approximately 0.55 and 0.4 pH units, respectively.

Lastly, we sought to determine if genetic WNK knockdown also led to lysosomal acidification. We assessed that knockdown of WNKs would be difficult to achieve in human cells because they express four WNKs, and knockdown of one can affect the concentration levels of the rest.[216] Alternatively, *C. elegans* only has one WNK orthologue, *wnk-1*[217]. *C. elegans' wnk-1* was knocked down via RNA interference (RNAi) in a strain with stable expression of FIRE-pHLy in neurons. Animals with *wnk-1* RNAi knockdown exhibited a lower FIRE-pHLy ratio than control animals (**Figure 2.3.E**). The same effect was induced with WNK463 treatment of FIRE-pHLy worms (**Figure 2.3.F**). These results further support the role of WNK activity in modulating lysosomal pH.

## WNK inhibitors upregulate autophagy

Next, we wanted to understand the mechanism by which WNK inhibition leads to lysosomal acidification. In their best-characterized pathway, the WNKs phosphorylate and

activate two structurally similar kinases, SPAK and OXSR1, which in turn regulate the activity of several ion channels.[207,218] To determine whether lysosomal acidification was occurring through this canonical pathway, we treated SH-SY5Y cells expressing FIRE-pHLy with an allosteric SPAK/OXSR1 inhibitor, ZT-1a.[219] The inhibitory activity of this compound was confirmed by detecting a decrease in the phosphorylation level of NKCC1, one of the substrates of SPAK, via immuno-blotting (**Figures 2.4.A-C**). Treatment with the same dose of ZT-1a increased FIRE-pHLy ratio, corresponding to an alkalinization rather than acidification of lysosomal pH (**Figure 2.5.A**). This is the opposite effect we would expect if the WNKs regulated lysosomal pH via SPAK and OXSR1 activation. Therefore, the WNKs are likely lowering lysosomal pH via alternative pathways, potentially involving one or more of the dozens of WNK substrates that have been reported.[213,220]

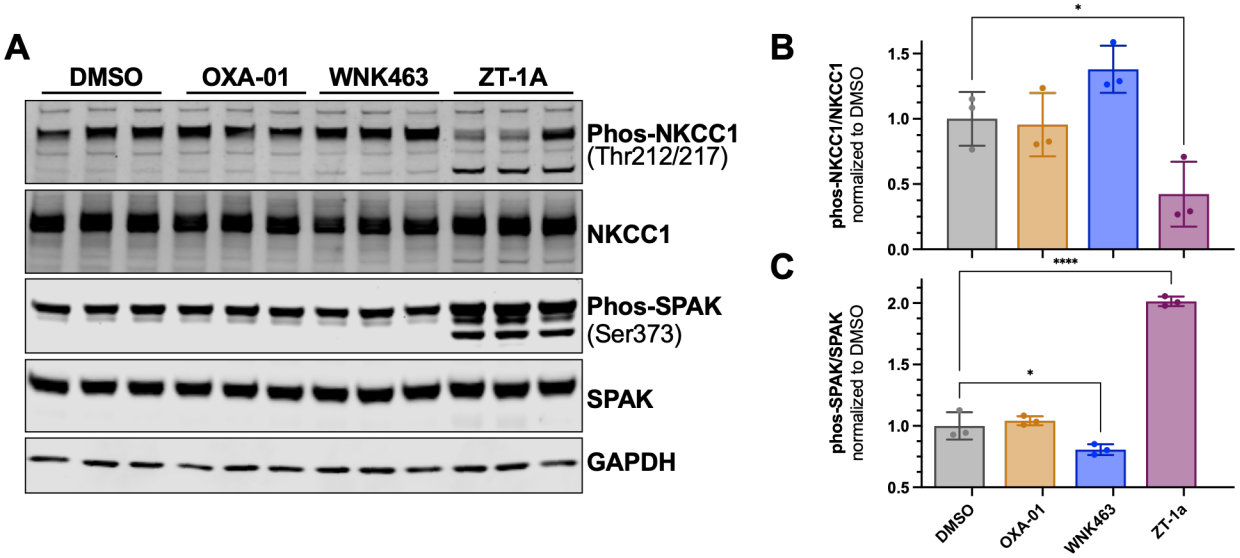


**Figure 2.4 - ZT-1a is active as a SPAK/OXSR-1 inhibitor**
(A-C) Western blot analysis of the effect of ZT-1a on the SPAK/OXSR-1 activity of SH-SY5Y cells, as measured by phosphorylation levels of SPAK and its substrate NKCC1 (4 h, n=3).
(A) Images of Western blots used to quantify relative levels of phosphorylated SPAK (Ser373), SPAK, phosphorylated NKCC1 (Thr212/217), NKCC1, NKCC1 and GAPDH.
(B) Quantification of SPAK phosphorylation levels at Ser373 over full-length SPAK, normalized to DMSO-treated samples.
(C)Quantification of NKCC1 phosphorylation levels at Thr212 and Thr217 over full-length NKCC1, normalized to DMSO-treated samples.
(B, C) Represented as mean ± SEM. Statistical test: OOW ANOVA, DMC. Significance labels: $*p<0.05$, $**p<0.01$, $***p<0.001$, $****p<0.0001$.

Although literature on the connection between WNKs and lysosomes is limited, two studies report WNK involvement in autophagy induction.[218,221] They demonstrate that chemical inhibition of the WNKs and genetic knockdown of *wnk1*, *oxsr1* and *spak* leads to an upregulation of autophagy.[218,221] To determine whether WNK463 and WNK-IN-11 induce autophagy, autophagy flux changes were measured with two probes, DAPRed and DALGreen.[222] Both bind to autophagosomes, but the fluorescence signal of DAPRed is insensitive to pH while DALGreen only fluoresces at a low pH; hence, the probes can be used to detect autophagosome and autolysosome formation, respectively. SH-SY5Y cells were incubated with these dyes and subsequently treated with lysosomal pH-modulating compounds (**Figures 2.5.B-D**). OXA-01 increased the fraction of the cell area covered by DAPRed and DALGreen, which was expected because mTOR complex 1 inhibition is known to induce autophagy.[201] WNK463, WNK-IN-11 and ZT-1a had the same effect as OXA-01 on DAPRed and DALGreen, corroborating the reports that WNK inhibition leads to an upregulation of autophagy.

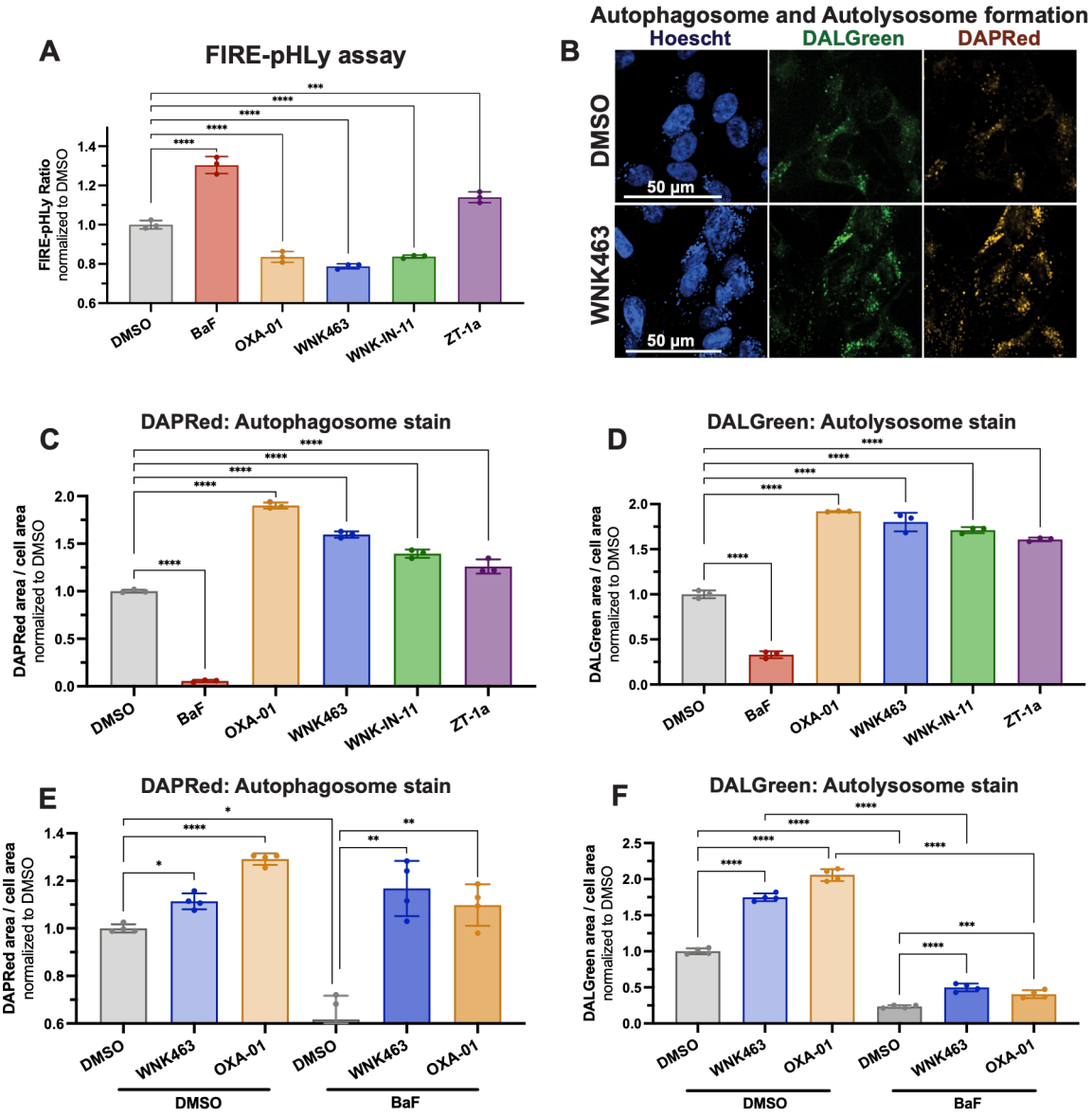


**Figure 2.5 - WNK inhibitors upregulate autophagy by increasing autophagy initiation**
(A) FIRE-pHLy ratio of SH-SY5Y cells treated with DMSO, BaF (100 nM), OXA-01 (20 µM), WNK463 (5 µM), WNK-IN-11 (5 µM), or SPAK/OSR-1 inhibitor ZT-1a (20 µM) for four hours.
(B-G) Assays monitoring autophagy in SH-SY5Y cells by staining autophagosomes with DAPRed stain and autolysosomes with DALGreen stain.
(B) Representative images of SH-SY5Y cells treated with DMSO or WNK463 (5 µM) for six hours (scale bar = 50 µm).
(C-D) SH-SHSY cells were treated with DMSO, BaF (100nM), OXA-01 (µM), WNK463 (5 µM), WNK-IN-11(5 µM), or ZT-1a (20 µM) for six hours. Fractional cell area stained by DAPRed (C). Fractional cell area stained by DALGreen (D).
(E-F) Cells were co-treated with DMSO or BaF (100nM) and DMSO, WNK463 (5 µM) or OXA-01 (20 µM) for four hours. Fractional cell area stained by DAPRed (E). Fractional cell area stained by DALGreen (F).
(A, C-F) Normalized to DMSO-treated wells. Statistical test: OOW ANOVA, DMC. Represented as mean ± SEM (n=3). Significance labels: ∗p<0.05, ∗∗p<0.01, ∗∗∗p<0.001, ∗∗∗∗p<0.0001.

The effect of WNK463 upon markers of autophagy was also measured and were compared to that of mTOR inhibitor OXA-01. Phosphorylated mTOR Ser2448 is correlated with

mTOR complex 1 inhibition and autophagy upregulation.[223] A 6-hr treatment with WNK463 led to a decrease in mTOR phospho-Ser2448 (**Figures 2.6.A-B**). Phosphorylation of mTOR complex 1 substrates p70 S6 kinase and S6 ribosomal protein also decreased with WNK463 treatment (**Figures 2.6.A, C-D**).[224] The effect of WNK463 on these readouts was more modest than that induced by OXA-01, which is a direct inhibitor of mTOR.[201] However, phosphorylation levels of Akt, a substrate of mTOR complex 2, increased with WNK463 treatment; this is often observed in response to mTOR complex 1 inhibition and is thought to act as a negative regulator of its activity (**Figures 2.6.A,E**).[225] Surprisingly, phosphorylation levels of Ulk1 and 4E-BP1, two other substrates of mTOR complex 1, did not change upon WNK463 treatment (**Figures 2.6.A, F-G**).[224]

Overall, these data demonstrate that WNK inhibition upregulates autophagy, albeit in a manner distinct from direct mTOR inhibition.

To confirm that the observed changes in autophagy were due to increased autophagy induction rather than a block in autophagic flux, WNK463 treatment was combined with BaF or VPS34-IN1, compounds that block autophagosome-lysosome fusion and autophagosome formation, respectively.[200,226,227] Co-treatment with BaF reduced the autolysosome fraction area per cell relative to WNK463-only but had no effect on WNK463-mediated increase in autophagosomes (**Figures 2.5.E-F**). Co-treatment with VPS34-IN1, an inhibitor of the autophagy initiation complex protein VPS34, reduced the fractional area per cell of both autolysosomes and autophagosomes compared to WNK463 alone (**Figures 2.6.H-I**).[226,227] Interestingly, WNK463 partially reversed the autophagy-blocking effects of VPS34-IN1. Together, these data showed that the increased levels of autophagosomes and autolysosomes induced by WNK463 treatment resulted from increased autophagosome formation. In addition, the lysosomal pH of VPS34-IN1-treated cells was still reduced with WNK463 treatment, indicating that WNK inhibition still induces lysosomal acidification when autophagosome formation is blocked (**Figure 2.6.J**). This result

suggests that WNK inhibition leads to both autophagy upregulation and lysosomal acidification but potentially through distinct molecular pathways.

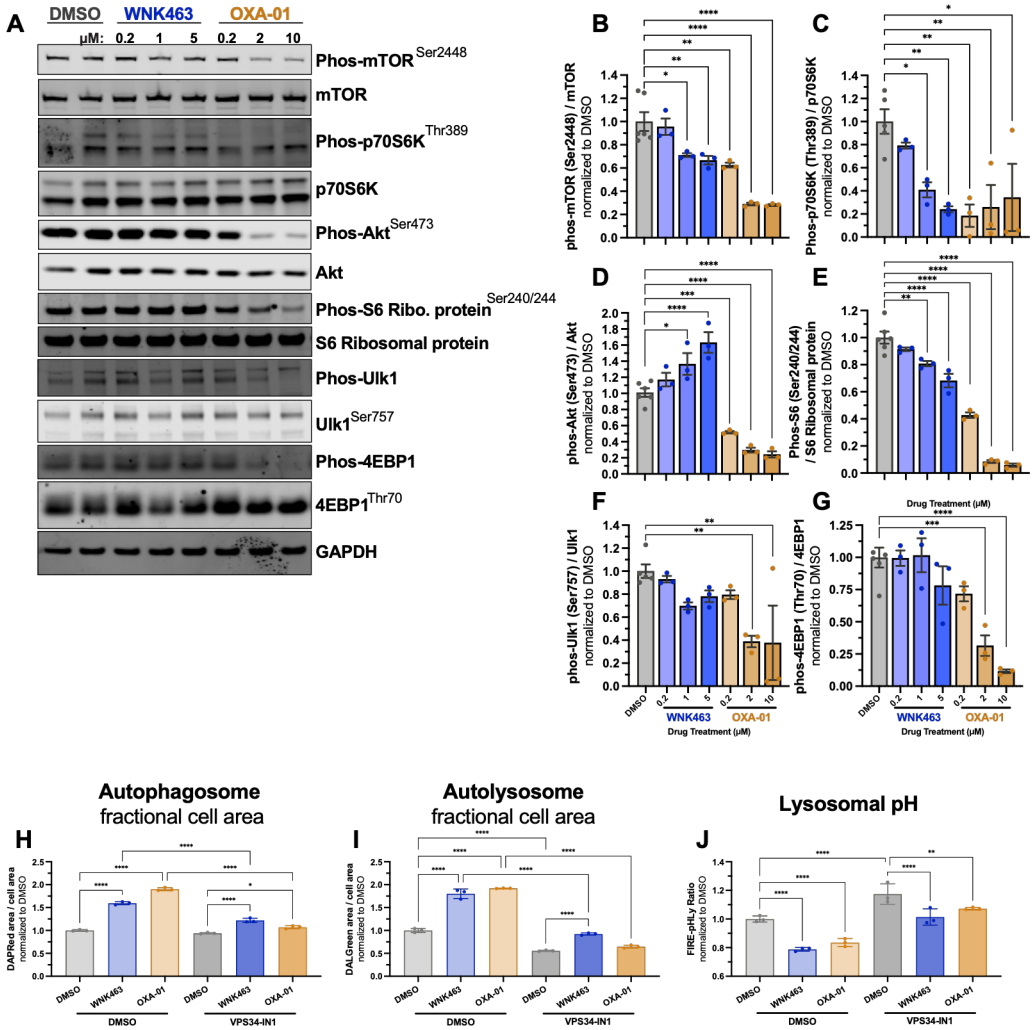


**Figure 2.6 - WNK463 is inducing autophagy by increasing autophagosome formation**
(A-G) Western blot analysis of the effect of WNK463 and OXA-01 on the phosphorylation status of mTOR and some of its substrates. SH-SY5Y cells were treated with pH-modulating compounds (6h).
(A) Representative western blots.
(B) Quantification of phos-mTOR (Ser2448) over full-length mTOR.
(C) Quantification of phos-p70S6 kinase (Thr389) over full-length p70S6 kinase.
(D) Quantification of phos-S6 ribosomal protein (Ser240/244) over full-length S6 ribosomal protein.
(E) Quantification of phos-Akt (Ser473) over full-length Akt.
(F) Quantification of phos-Ulk1 (Ser757) over full-length Ulk1.
(G) Quantification of phos-4EBP1 (Thr70) over full-length 4EBP1.
(H-J) Co-treatment of autophagy blocker VPS34-IN-1 and pH-modulating compounds. SH-SY5Y cells were co-treated with DMSO or VPS34-IN1 (5 μM) and DMSO, WNK463 (5 μM) or OXA-01 (20 μM) for four hours.
(H) Autophagosome area per cell area of SH-SY5Y cells stained with DAPRed fluorescent dye.
(I) Autolysosome area stained per cell area of SH-SY5Y cells stained with DALGreen fluorescent dye.
(J) FIRE-pHLy ratio of SH-SY5Y cells.
(B-J) Normalized to DMSO-treated cells. Represented as mean ± SEM ($n$=3). Statistical test: OOW ANOVA, DMC. Significance labels: $*p<0.05$, $**p<0.01$, $***p<0.001$, $****p<0.0001$.

## WNK inhibitors enhance lysosomal v-ATPase levels

To gain insight into the molecular mechanisms underlying lysosomal acidification by WNK inhibition, we performed quantitative proteomics of isolated lysosomes. SH-SY5Y cells expressing an HA-tagged TMEM192—a lysosomal membrane protein—were immunoprecipitated with anti-HA antibody beads in a process known as Lyso-IP.[228] Purified lysosome fractions and whole cell lysate were then analyzed via LC-MS/MS. Comparing lysosomal protein abundance between the lysosome and whole cell fractions of DMSO-treated cells revealed that the Lyso-IP method was successful in enriching for lysosomal proteins (**Figures 2.7.A-B**).

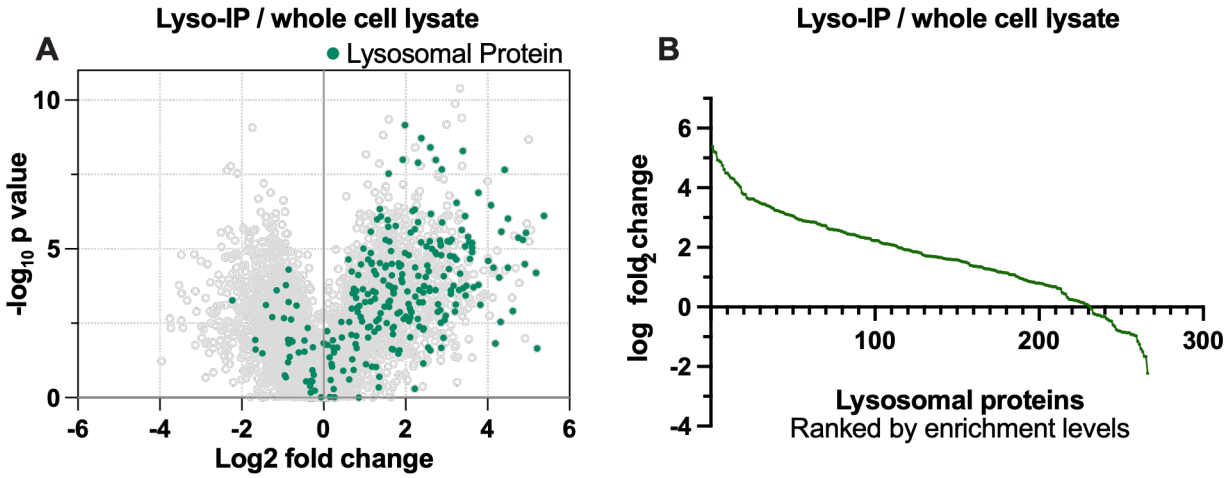


**Figure 2.7 - Lyso-IP method successfully enriches lysosomal proteins**
SH-SY5Y TMEM192-3xHA cells were treated with DMSO for four hours, then lysosomes were isolated via Lyso-IP method. Proteins that have GO cellular component annotations containing “lysosome” or “lysosomal” were classified as lysosomal proteins.
(A) Volcano plot comparing protein abundance in samples isolated through the Lyso-IP method and those obtained from whole cell lysates. Lysosomal proteins in green, rest of proteins in gray.
(B) $Log_2$ fold change of abundance of lysosomal proteins in Lyso-IP fraction compared to whole cell lysates. Lysosomal proteins were ranked from most to least enriched.
Represented as mean of replicates ($n$ = 3).

Next, we compared the Lyso-IP fraction from WNK463-treated cells with that from DMSO-treated ones. Notably, WNK463 significantly increased the lysosomal levels of almost all subunits of the v-ATPase, the molecular motor responsible for acidifying lysosomes.[194] Both the membrane-bound $V_0$ and the cytosolic $V_1$ subunits were enriched in the Lyso-IP fraction (**Table**

**2.3, Figure 2.8.A**). This enrichment was unlikely to be caused by increased protein expression, since there was no significant difference in v-ATPase subunit abundance between the whole cell fractions (**Figure 2.8.B**). WNK-IN-11 treatment also led to an enrichment of lysosomal v-ATPase subcomponents without affecting their cellular levels (**Figures 2.9.A-B**). Conversely, WNK1-IN-1 did not increase lysosomal v-ATPase levels, which was consistent with the fact that it did not induce lysosomal acidification according to the FIRE-pHLy assay.

**Table 2.3 - – WNK463 enhances lysosomal levels of v-ATPase subunits**

| Gene | vATPase complex | Fold Change | % increase | P-value | -log10, p value |
|---|---|---|---|---|---|
| ATP6V1C1 | V1 | 2.35 | 135 | 0.003 | 2.52 |
| ATP6V1H | V1 | 2.19 | 119 | 0.0010 | 3.02 |
| ATP6V1A | V1 | 2.17 | 117 | 0.000005 | 5.29 |
| ATP6V0C | V1 | 1.93 | 93 | 0.002 | 2.79 |
| ATP6V1B2 | V1 | 1.92 | 92 | 0.00008 | 4.10 |
| ATP6V1F | V1 | 1.65 | 65 | 0.01 | 2.01 |
| ATP6V1D | V1 | 1.57 | 57 | 0.006 | 2.22 |
| ATP6V1E1 | V1 | 1.56 | 56 | 0.22 | 0.65 |
| ATP6V1E2 | V1 | 1.52 | 52 | 0.05 | 1.29 |
| ATP6V1G1 | V1 | 1.39 | 39 | 0.02 | 1.63 |
| ATP6V0A1 | V0 | 2.15 | 115 | 0.003 | 2.47 |
| ATP6V0C | V0 | 1.93 | 93 | 0.002 | 2.79 |
| ATP6V0D1 | V0 | 1.55 | 55 | 0.002 | 2.69 |
| ATP6AP1 | V0 | 1.50 | 50 | 0.02 | 1.61 |
| ATP6V0A2 | V0 | 1.26 | 26 | 0.01 | 1.98 |

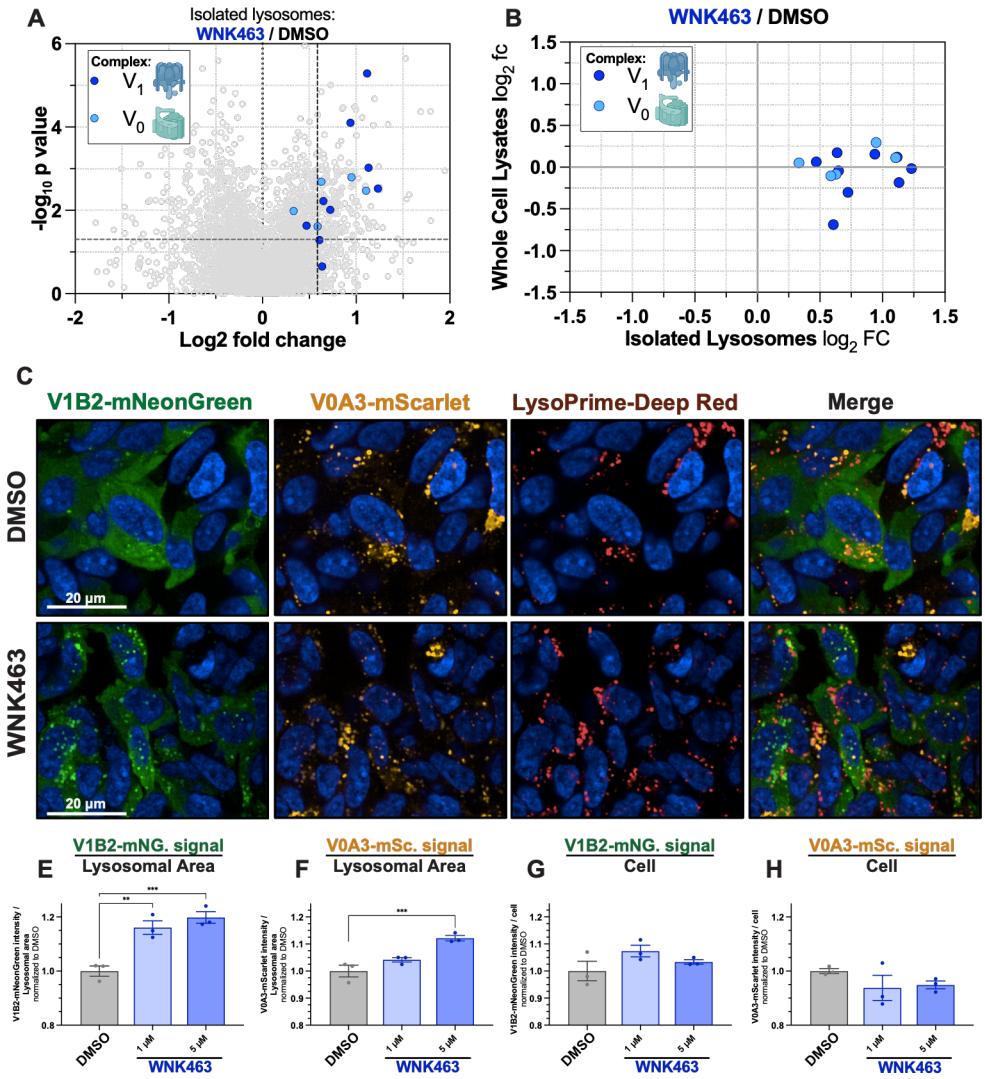


**Figure 2.8 - WNK463 enhances lysosomal v-ATPase levels**
(A-B) Proteomic analysis of whole cell lysates and isolated lysosomes from SH-SY5Y TMEM192-3xHA cells treated with DMSO or WNK463 (5 µM) for four hours. V-ATPase complex $V_0$ and $V_1$ subunits represented by teal and dark blue dots, respectively. Represented as mean of replicates (*n*=3).
(A) Volcano plot comparing abundance of proteins in isolated lysosomes from WNK463-treated cells to those from DMSO-treated cells. Dotted lines represent significant enrichment thresholds, set at a p value of 0.05, and fold change in abundance of 1.5.
(B) Comparison of abundance of v-ATPase subunits in whole cell lysates (y-axis) and isolated lysosomes (x-axis) between WNK463 and DMSO-treated cells.
(C-G) SH-SY5Y cells expressing V1B2-mNeonGreen and V0A3-mScarlet stained with lysosomal dye, LysoPrime Deep Red, and treated with DMSO or 5 µM of WNK463 for four hours.
(C) Representative images (scale bar = 20 µm).
(D-E) Total signal of V1B2-mNeonGreen (D) and V0A3-mScarlet (E) per area in segmented LysoPrime Deep Red-stained lysosomes. (F-G) Signal of V1B2-mNeonGreen (F) and V0A3-mScarlet (G) per cell.
(D-G) Represented as mean ± SEM (*n*=3). Statistical test: OOW ANOVA, DMC. Significance labels: $*p<0.05$, $**p<0.01$, $***p<0.001$, $****p< 0.0001$.

To confirm this finding, we stably expressed two v-ATPase subcomponents conjugated to fluorescent proteins, V1B2-mNeonGreen and V0A3-mScarlet, in SH-SY5Y cells and treated them

with WNK463. The signal of V1B2-mNeonGreen in DMSO-treated cells was diffuse throughout the cell because the $V_1$ complex alternates between the cytosol and binding to the membrane-bound $V_0$ domain. WNK463 treatment resulted in a visible increase in the number of observable V1B2-mNeonGreen puncta and an increase in the intensity of mNeonGreen signal within segmented V0A3-mScarlet puncta; suggesting an increase in $V_1$ complexes bound to $V_0$ (**Figures 2.8.C and 2.9.C**). To confirm that this corresponded to greater co-localization with lysosomes, the cells were stained with the lysosomal dye LysoPrime Deep Red (**Figure 2.8.C**). In segmented lysosomes, the integrated intensity per area of both V1B2-mNeonGreen and V0A3-mScarlet increased with WNK463 treatment (**Figures 2.8.D-E**). In V0A3-mScarlet puncta, the intensity of LysoPrime Deep Red dye signal per area also increased, indicating greater co-localization between the two (**Figure 2.9.D**). Simultaneously, the intensity of V0A3-mScarlet and V1B2-mNeonGreen per cell was not altered (**Figures 2.8.F-G**). This supported the proteomic data that vATPase subcomponents were being enriched in lysosomes with WNK463 treatment, while their overall cellular abundance remained constant.

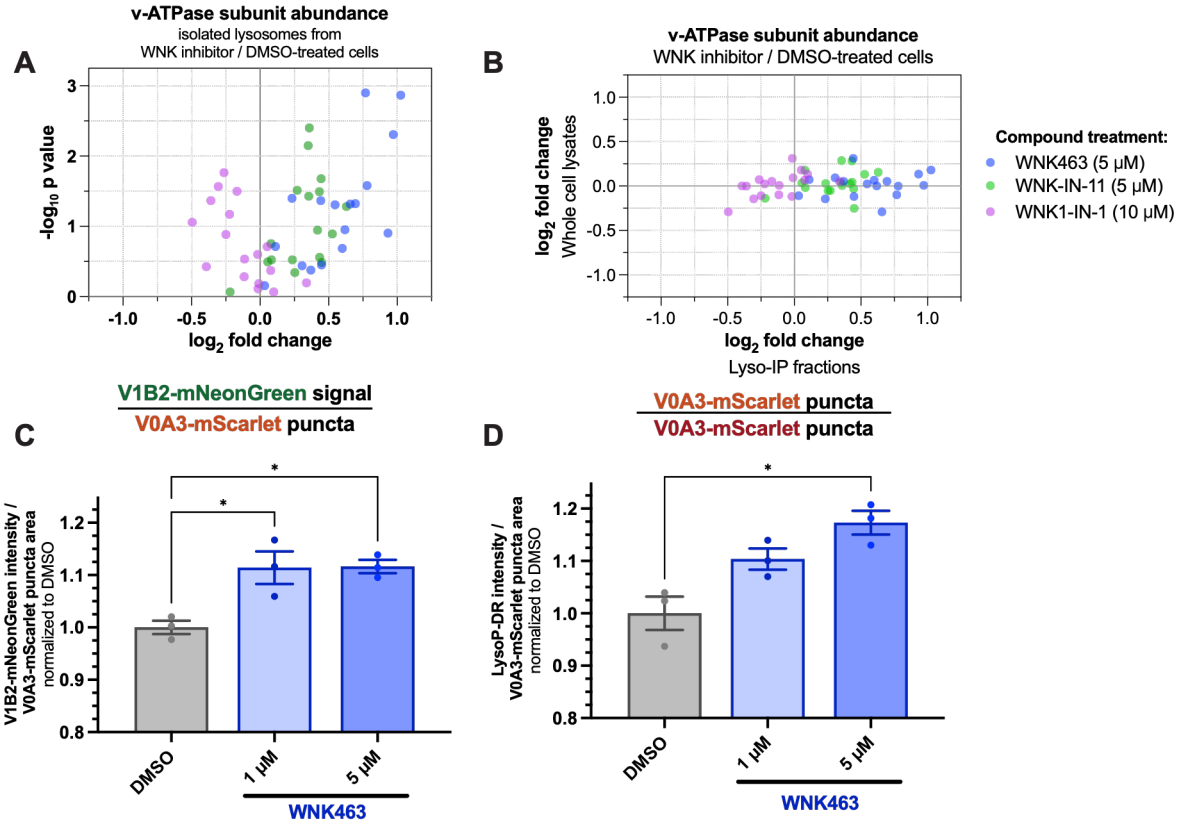


**Figure 2.9 - WNK463 and WNK-IN-11 enhance lysosomal v-ATPase levels**
(A-B) SH-SY5Y TMEM192-3xHA cells were treated with DMSO or WNK inhibitors for four hours, then lysosomes were isolated via Lyso-IP method. Data represented as mean of replicates ($n$ = 3).
(A) Volcano plot comparing protein abundance in isolated lysosomes from cells treated with WNK inhibitors to those from cells treated with DMSO.
(B) Comparison of abundance of v-ATPase subunits in whole cell lysates (y-axis) and isolated lysosomes (x-axis) between WNK463 and DMSO-treated cells.
(C-D) SH-SY5Y cells expressing V1B2-mNeonGreen and V0A3-mScarlet stained with lysosomal dye, LysoPrime Deep Red, and treated with DMSO or WNK463 (1 or 5 μM) for four hours.
(C) Total signal of V1B2-mNeonGreen per area in V0A3-mScarlet segmented puncta.
(D) Total signal of LysoPrime Deep Red per area in V0A3-mScarlet segmented puncta.
Represented as mean ± SEM ($n$=3). Statistical test: OOW ANOVA, DMC. Significance labels: $*p<0.05$

Given that WNK inhibitor treatment did not appear to alter cellular v-ATPase subunit expression, the observed lysosomal enhancement is likely to have been due to changes in their subcellular distribution. Gene enrichment analysis of the lysosomal proteomics data revealed that Rab GTPases, the master regulators of intracellular vesicle trafficking, were also enriched in lysosomes upon WNK463 treatment (**Figure 2.10.A**).[229] Gene enrichment analysis of the Lyso-IP data also revealed that WNK463 treatment increased the levels of ER membrane proteins found in lysosomes and—to a much lesser extent—that of endosomal membrane and late endosome

proteins (**Figure 2.10.B**). This finding suggested that the enriched vATPase subunits may have originated from these compartments.[215]

An increased number of assembled v-ATPase complexes on lysosomes would promote proton pumping into the lysosomal lumen and is therefore likely to be the main driver of lysosomal acidification that occurs with WNK inhibition.

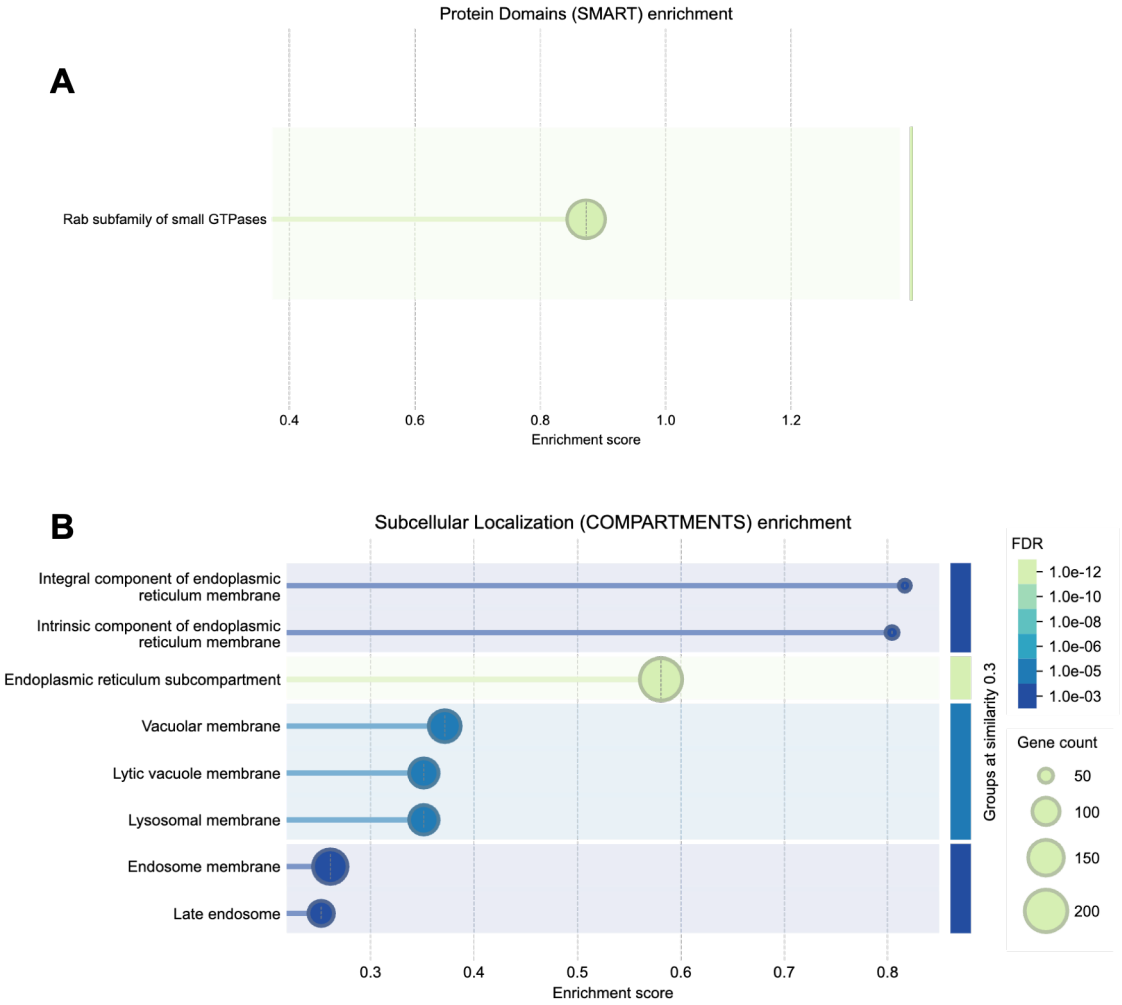


**Figure 2.10 - WNK463 enhances lysosomal abundance of Rabs and ER proteins**
Gene enrichment analysis of lysosomal fractions of SH-SY5Y TMEM192-3xHA cells treated with DMSO or WNK463 (5 μM) for four hours. Lysosomes were isolated via Lyso-IP method.
(A) Enrichment analysis of protein domains according to SMART database.
(B) Gene ontology enrichment analysis of subcellular localization.

## WNK inhibitor treatment increases lysosomal proteolytic activity in cellular models

WNK463 and WNK-IN-11 were tested in lysosomal activity assays to determine whether the increased acidification correlates with enhanced proteolysis. First, their effect on the activity of individual cathepsins was assessed. BODIPY-pepstatin A is a probe for active cathepsin D as pepstatin A binds to the catalytic site of cathepsin D that is only accessible in the active form of the enzyme.[19] SH-SY5Y cells treated with WNK463 and WNK-IN-11 exhibited a significantly greater BODIPY-pepstatin A signal per cell, which was comparable to the effect induced by OXA-01 (**Figure 2.11.A**). This finding suggested that treatment with WNK inhibitors promoted cathepsin D activity.

Magic Red substrates (MgRS) are conjugated peptides used to probe the activity of individual cathepsins.[230] The substrate peptide sequence is designed for specific cleavage by its target cathepsin, resulting in the dequenching of the conjugated fluorophore. WNK463 and WNK-IN-11 treatment led to a significant increase in cathepsin B MgRS signal per cell, but only WNK463 increased cathepsin L MgRS signal per cell (**Figures 2.11.B-C**). However, this increase in signal was lower than that induced by OXA-01. This suggests that WNK463 treatment leads to a modest increase in the activity level of cathepsins B and L, which are among the most abundant cathepsins.[231]

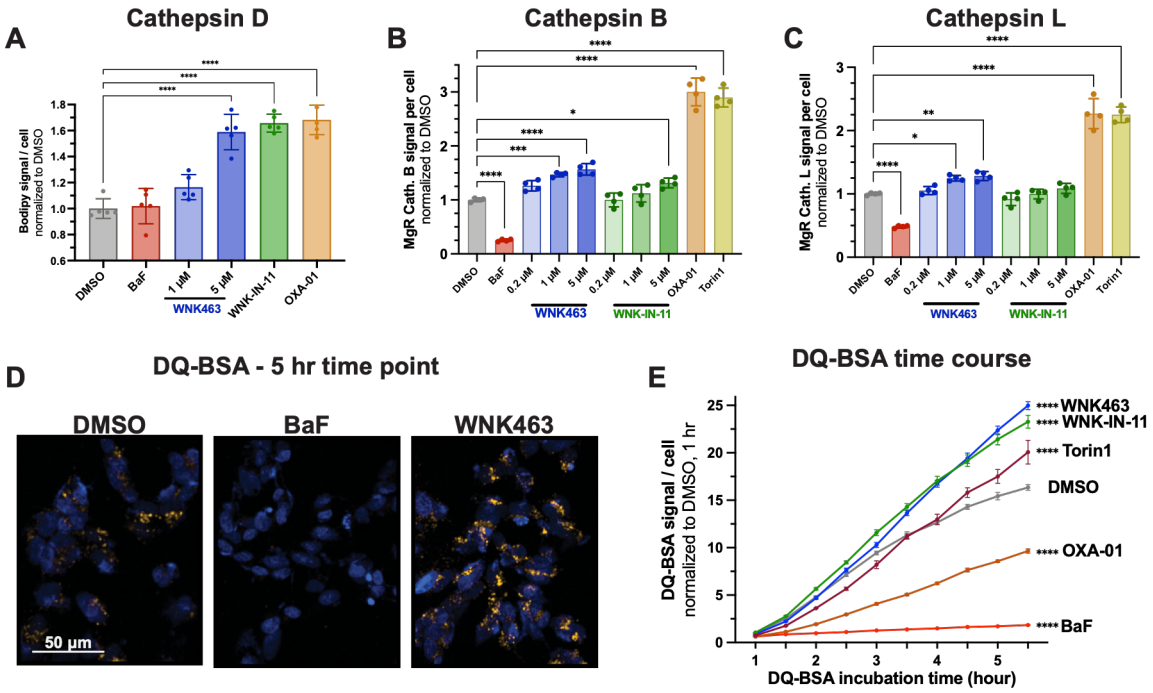


**Figure 2.11 - WNK463 enhances lysosomal v-ATPase levels**
(A-B) Proteomic analysis of whole cell lysates and isolated lysosomes from SH-SY5Y TMEM192-3xHA cells treated with DMSO or WNK463 (5 μM) for four hours. Lysosomes were isolated via Lyso-IP method. V-ATPase complex V0 and V1 subunits represented by teal and dark blue dots, respectively. Represented as mean of replicates (n=3).
(A) Volcano plot comparing abundance of proteins in isolated lysosomes from WNK463-treated cells to those from DMSO-treated cells. Dotted lines represent significant enrichment thresholds, set at a p value of 0.05, and fold change in abundance of 1.5.
(B) Comparison of abundance of v-ATPase subunits in whole cell lysates (y-axis) and isolated lysosomes (x-axis) between WNK463 and DMSO-treated cells.
(C-G) SH-SY5Y cells expressing V1B2-mNeonGreen and V0A3-mScarlet stained with lysosomal dye, LysoPrime Deep Red, and treated with DMSO or 5 μM of WNK463 for four hours.
(C) Representative images (scale bar = 20 μm).
(D-E) Total signal of V1B2-mNeonGreen (D) and V0A3-mScarlet (E) per area in segmented LysoPrime Deep Red-stained lysosomes.
(F-G) Total signal of V1B2-mNeonGreen (F) and V0A3-mScarlet (G) per cell.
(D-G) Represented as mean ± SEM (n=3). Statistical test: OOW ANOVA, DMC. Significance labels: *p<0.05, **p<0.01, ***p<0.001, ****p< 0.0001.

Next, we tested the WNK inhibitors in a lysosomal proteolytic activity assay that measures the signal of DQ-BSA.[232] This reagent consists of BSA molecules conjugated to an excess of fluorescent dyes that self-quench. DQ-BSA molecules are transported to lysosomes via endocytosis, where their cleavage leads to de-quenching of the conjugated dyes. SH-SY5Y cells were pre-treated with various pH-modulating compounds for three hours, DQ-BSA was added,

and its signal was monitored for 5.5 hours. WNK463 and WNK-IN-11 both led to a significant increase in DQ-BSA signal per cell, which was greater than that induced by Torin1, another ATP-competitive mTOR inhibitor (**Figures 2.11.D-E**). These results showed that lysosomal acidification induced by WNK inhibitors could increase lysosomal proteolytic activity, which is often impaired in ND models.[233] Surprisingly, OXA-01 treated cells exhibited lower DQ-BSA signal than DMSO-treated cells, even though the compound increased cathepsin D, B and L activity according to the previous assays. This may be due to decreased DQ-BSA endocytosis in OXA-01 treated cells.

In the previous assays, WNK463 and WNK-IN-11 were tested in models exhibiting basal lysosomal pH, whereas many aging and ND models exhibit an elevated lysosomal pH. We wanted to test these compounds in a neurodegenerative disease-associated model with alkaline lysosomes to determine whether WNK inhibition could re-acidify this compartment and rescue downstream defects. We obtained Neuro2a (N2a) cells, murine neuroblastoma lines, expressing human ApoE3 or AD-linked ApoE4 (subsequently referred to as hAPOE3 and hAPOE4, respectively). Published work has shown that compared to the hAPOE3-expresing line, the hAPOE4-expressing line exhibits more alkaline lysosomes, lower cathepsin B proteolytic levels, and reduced basal and stress-induced mitochondrial autophagy (mitophagy).[114] The latter is significant because mitochondrial defects, including an accumulation of damaged mitochondria due to a downregulation of mitophagy, have been shown to be early cellular changes in AD.[234]

We first used the Dojindo lysosomal pH kit to confirm the pH-modulating activities of various compounds in both N2a lines. Treatment with OXA-01, WNK463 and WNK-IN-11 increased the ratiometric signal of the kit's dyes in both hAPOE3- and hAPOE4-expressing cells, indicating that they acidified lysosomes in both lines (**Figure 2.12.A**). Next, we probed lysosomal proteolytic activity with DQ-BSA and cathepsin B MgRS. We found that hAPOE4-expressing cells exhibited lower cathepsin B MgRS and DQ-BSA signal per cell, both of which were increased

through treatment with WNK inhibitors to levels comparable to those of hAPOE3-expressing cells (**Figures 2.12.B-C**).

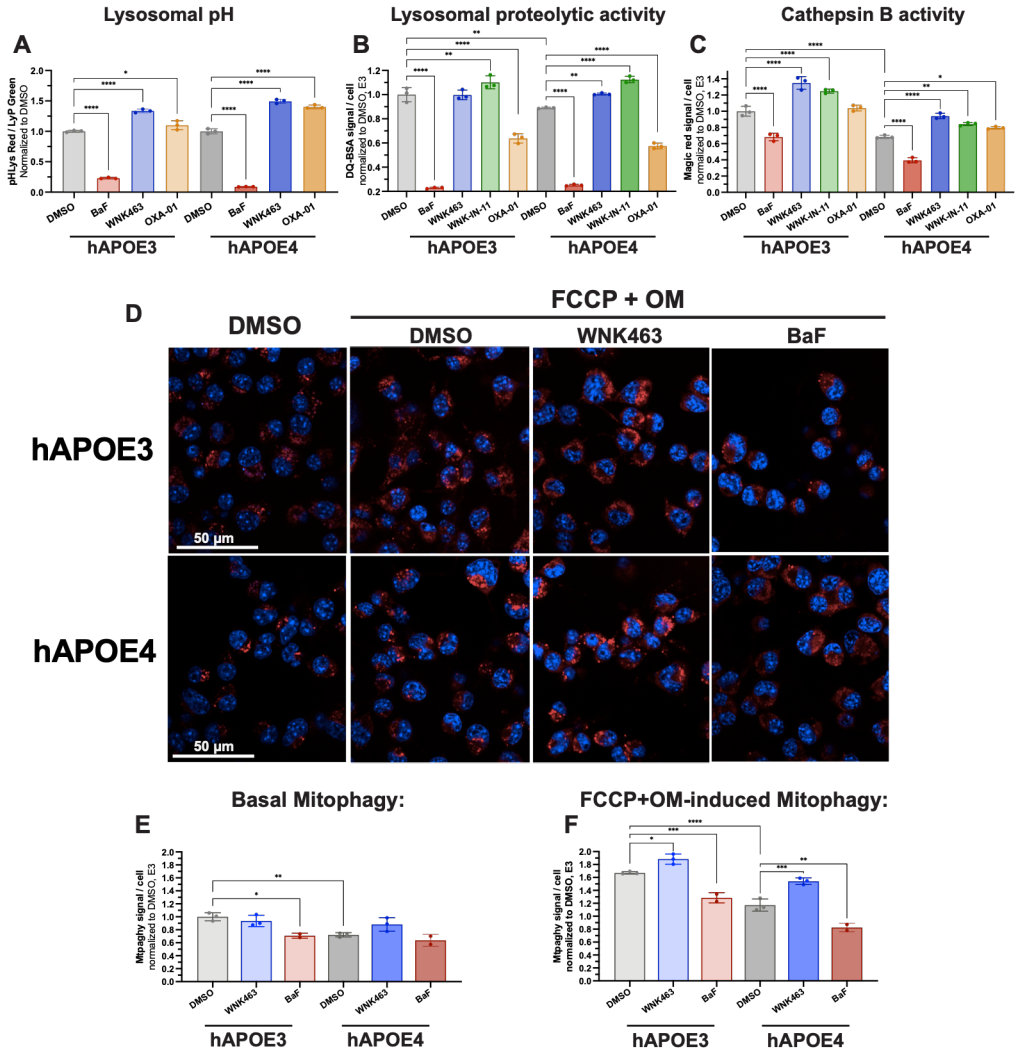


**Figure 2.12 - WNK inhibitors rescue lysosomal defects of hAPOE4-expressing Neuro-2a cells**
(A) Relative lysosomal pH of N2a cells expressing human hApoE3 or human hAPOE4 and treated with pH-modifying compounds for four hours. Measured by the ratiometric signal of lysosomal dyes pHLys Red and LysoPrime Green. Data normalized to DMSO-treated cells of corresponding cell line.
(B-C) Probe signal per cell of N2a lines treated with lysosomal pH-modifying compounds for four hours and DQ-BSA for three hours (B) or magic red substrate for cathepsin B for one hour (C). Data normalized to the signal per cell of DMSO-treated hAPOE3 cells.
(D-E) Monitoring of mitophagy in N2a lines. Cells were stained with Mtphagy dye, then treated with DMSO, WNK463 (5 µM), or BaF (100 nM) for four hours and subsequently treated with either DMSO or FCCP and oligomycin (FCCP/OM, 10 µM) for 1.5 hours.
(D) Representative images: Mtphagy dye signal in red and Hoescht-stained nuclei in blue (scale bar = 50 µm).
(E-F) Mtphagy dye signal per cell. Basal mitophagy (E) and stress-induced mitophagy via treatment with FCCP and oligomycin (F). Data normalized to the signal per cell of DMSO-treated hAPOE3 cells experiencing basal mitophagy.
(A-C, E, F) Statistical test: OOW ANOVA, DMC. Represented as mean ± SEM ($n$=3). Significance labels: $*p<0.05$, $**p<0.01$, $***p<0.001$, $****p<0.0001$.

Mitophagy levels were measured with Dojindo's Mtphagy probe. This dye localizes to mitochondria and exhibits fluorescence at a low pH, so its signal correlates with the fusion of mitochondria and autolysosomes, a key step in the mitophagy pathway.[235] Mitophagy was upregulated via co-treatment with FCCP, which de-polarized mitochondrial membranes, and oligomycin, an inhibitor of the mitochondrial H+-ATP-synthase.[236,237] This mitochondrial stress increased Mtphagy signal levels per cell in both hAPOE3- and hAPOE4-expressing cells and was lowered with BaF-treatment, which validates the mitophagy assay (**Figures 2.12.D-F**). The hAPOE4-expressing cell line exhibited lower levels of both basal and stress-induced mitophagy, as previously reported.[114] Treatment with WNK463 alone did not affect basal levels of Mtphagy signal intensity of either line but increased it in both cell lines when mitochondrial damage was induced via FCCP and oligomycin treatment (**Figures 2.12.E-F**). This result demonstrated that WNK463 did not affect basal mitophagy but increases stress-induced mitophagy levels. Defects in stress-induced mitophagy are correlated with AD progression; hence, lysosomal acidification via WNK inhibitors could be a beneficial treatment in these diseases.[114,234]

# Discussion

The major advance of this study was the identification of WNK463 as a novel lysosomal acidification compound, which uncovers a connection between WNK activity and lysosomal pH regulation and in addition, provides a tool molecule to study the effects of lysosomal acidification in ND and aging models (**Figure 2.13**). WNK inhibition was confirmed to lead to lysosomal acidification pharmacologically and genetically, because the allosteric inhibitor WNK-IN-11 and knock-down of the *C. elegans* WNK orthologue both phenocopied the effect of WNK463 on lysosomal pH.

Inhibition of the WNKs and their downstream kinases, SPAK/OXSR1, has been demonstrated to lead to an upregulation of autophagy.[218,221] We confirmed that our two WNK

inhibitors and an inhibitor of SPAK/OXSR1 upregulate autophagy initiation by observing an accumulation of autophagosomes and autolysosomes after WNK463 and WNK-IN-11 treatment. Interestingly, the SPAK/OXSR1 inhibitor alkalinized lysosomes and thus had the opposite effect that would be expected if lysosomal acidification were downstream of the canonical WNK-SPAK/OXSR pathway. In addition, inhibiting autophagy initiation through a VPS34 inhibitor blocked most of the upregulation of autophagy of WNK463 but did not block its lysosomal acidification effects. These findings suggest that the WNKs regulate autophagy initiation and lysosomal pH through distinct molecular pathways.

We demonstrated that WNK463 treatment leads to an enhancement of fully assembled v-ATPases in lysosomes, which is likely the main mechanism of lysosomal acidification through WNK inhibition (**Figure 2.13**). This increase is likely due to changes in the subcellular localization of the v-ATPase complexes, since no changes in abundance of their subunits was observed in the whole cell lysates. The $V_0$ and $V_1$ domains are assembled in the endoplasmic reticulum (ER) and cytosol, respectively, and bind together in the Golgi and endosomes; making these compartments the likeliest sources of the enriched v-ATPases.[215] WNK463 treatment was also shown to lead to an increase in ER proteins found in lysosomes, which suggests that the enriched $V_0$ subunits originate from the ER, and it is plausible that they are in turn recruiting $V_1$ domains from the cytosol.[215] The WNKs have been reported to regulate the subcellular localization of several membrane proteins, making it likely that they could also affect that of v-ATPases.[213,238–241] Further work measuring changes in the abundance of v-ATPase subcomponents in different cellular compartments is required to determine the source of enriched vATPases in response to WNK inhibition.

A possible mechanism of WNK involvement in v-ATPase holoprotein assembly is direct phosphorylation of one of the subcomponents. A plant orthologue of the WNKs, AtWNK8, was shown to be able to bind and phosphorylate vATPase domain V1c1.[242] However, other WNK

isoforms of the same species did not have the effect and this result has not been reproduced in other organisms, making this mechanism less likely in the mammalian cell lines used in our work. Nevertheless, phosphorylation changes in v-ATPase domains, perhaps through intermediatory kinases, may be involved in this pathway. A recent study reports that calcium/calmodulin-dependent protein kinase type 2 delta (CAMK2D) phosphorylates V0a1, and elevated phosphorylation levels of this subunit inhibit the trafficking of the $V_0$ complex from the ER to lysosomes.[243] Rab14 suppresses CAMK2D activity, and the Rabs were also found to be enriched in lysosomes upon WNK inhibition, so it is possible that a Rab is involved in v-ATPase regulation by the WNKs. Measuring v-ATPase phosphorylation levels in response to WNK inhibition might reveal a new phosphorylation site involved in v-ATPase complex assembly and trafficking.

The discovery of WNK463 and WNK-IN-11 as lysosomal acidifiers makes them useful tool molecules. An endolysosomal pH assay was used to quantify the absolute pH changes induced by different lysosomal acidification compounds, showing that WNK463 and WNK-IN-11 treatment led to a decrease of 0.56 and 0.43 pH units, respectively, which was more modest than the 1.3 pH unit decrease induced by OXA-01 treatment. This subtlety was not particularly concerning to us, because the mild decrease in lysosomal pH nonetheless boosted proteolytic activity, and too drastic of a pH reduction might even reduce it by falling outside the optimal pH range of lysosomal hydrolases. Indeed, WNK463 and WNK-IN-11 treatment induced cathepsin D maturation, increased cathepsin B and L activity levels, and enhanced lysosomal proteolysis in SH-SY5Y cells (**Figure 2.13**). More importantly, the two WNK inhibitors enhanced cathepsin B activity, lysosomal proteolysis, and stress-induced mitophagy in human apoE4-expressing Neuro2a cells that exhibit an elevated lysosomal pH, demonstrating that they can rescue phenotypes associated with lysosomal deacidification in ND-models. In addition, WNK463 was shown to acidify neuronal

lysosomes in *C. elegans* and could thus also be useful to study lysosomal acidification in animal models.

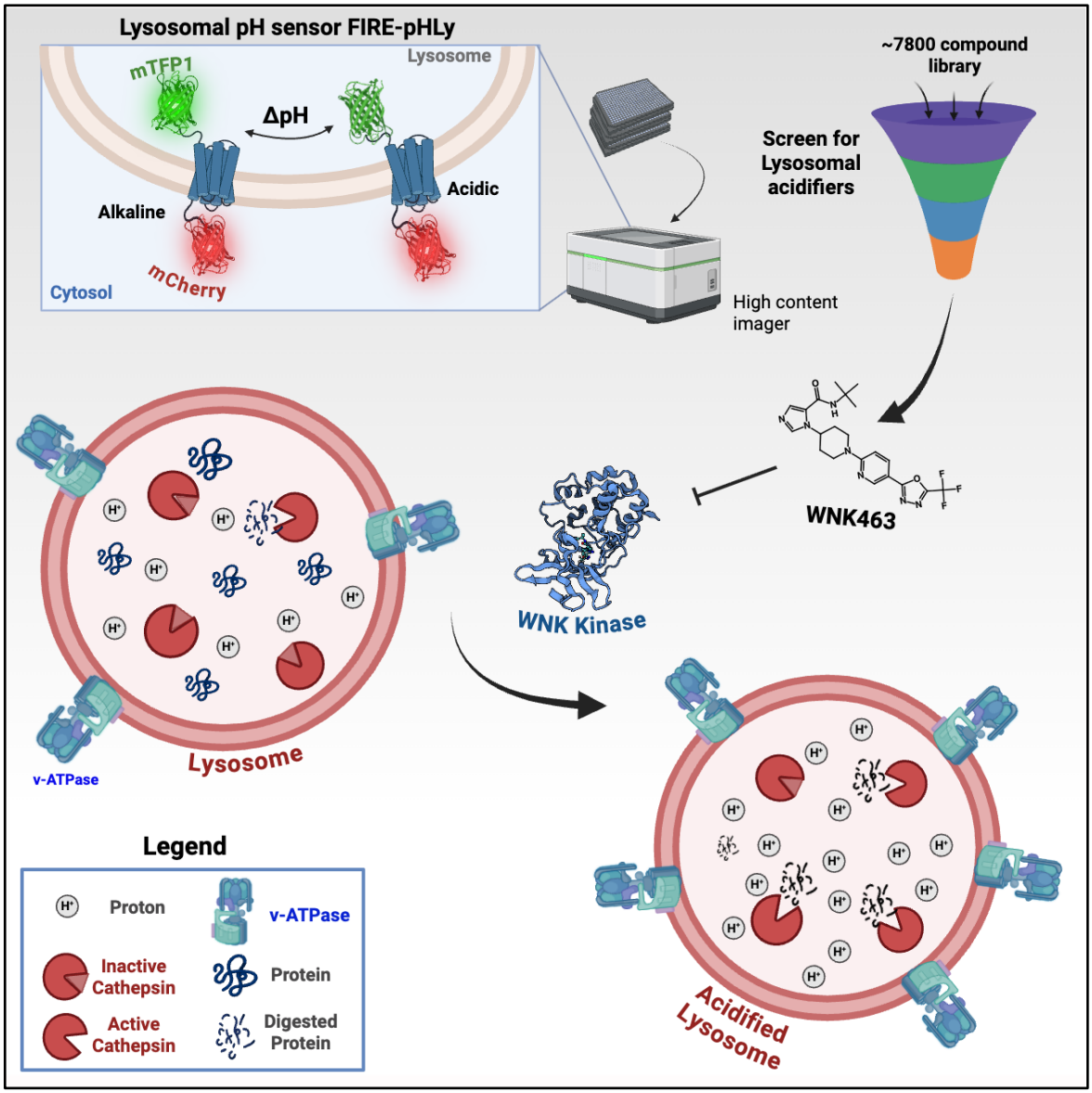


**Figure 2.13 - Graphical abstract summarizing chapter.**

Lysosomal alkalinization has been observed in several cellular models of NDs and animal models of aging. Since lysosomal acidity is crucial for its proteolytic efficiency, a loss of lysosomal acidification likely contributes to the pathobiology of neurodegenerative diseases like PD and AD. Thus, lysosomal re-acidification via small molecules could represent primary or adjunctive therapies for neurodegeneration and other diseases of aging. WNK463 was developed by

Novartis as a treatment for hypertension, but did not reach clinical trials due to an undisclosed toxicity issue in pre-clinical studies.[202] Thus, WNK463 itself is unlikely to be a viable therapeutic for NDs. However, a compound that exclusively targeted the WNK isoform involved in lysosomal pH regulation could minimize side effects. Therefore, further characterization of the pathway between WNK inhibition and lysosomal acidification could potentially lead to promising therapeutics against NDs.

# Limitations

This FIRE-pHLy screening campaign is the largest of its size and resulted in the identification of lysosomal acidifying molecules. We chose to screen SH-SY5Y cells because they are a commonly used cell model in ND research and balance scalability with physiological relevance. However, there are phenotypes observed in other cellular models, such as iPSC-derived neurons, that are not recapitulated in these cells; thus, we might have missed compounds that exclusively acidify lysosomes of terminally differentiated neurons.[244,245] Future screening of other neuronal cellular models might uncover other molecules of interest. The mechanism of lysosomal acidification via WNK inhibition was characterized but the specific WNK isoforms and substrates involved in this process remain unclear. Future work deconvoluting downstream pathways would further our understanding of lysosomal pH regulation. Acute WNK inhibitor treatment was shown to increase lysosomal function in an AD-linked mutant cell line model. Future work treating animal models chronically with WNK inhibitors would determine whether the WNK pathway is a viable target of therapeutic efforts.

# Methods

## Experimental model details

### *Cell Lines*

SH-SY5Y (human female, RRID: CVCL_0019) and HEK293FT (human female, RRID: CVCL_6911) cell lines were obtained from ATCC and Invitrogen, respectively. Neuro-2a (mouse, male) lines were obtained from Krogan lab at UCSF.[114] SH-SY5Y FIRE-pHLy and TMEM-192-3x-HA were generated for previous published studies in the Kao lab.[198,246] All cell lines were incubated in a humidified 5% $CO_2$ incubator at 37 °C. SH-SY5Y cells were cultured in Eagle's Minimum Essential Medium (EMEM)(ATCC, cat# cat#30-2003) : F12 (Gibco, cat#11765054) with 10% Fetal Bovine Serum (FBS) (ATCC, cat#30-2020) and 1% Penicillin-Streptomycin (10,000 U/mL) (Gibco, cat#15140-122). Neuro2a (N2a) cells were cultured in MEM with glutaMAX supplement (Fisher, cat#41090036) with 10% FBS, 1% MEM non-essential amino acids (NEAA) (Gibco, cat#11140050), and 1 mM sodium pyruvate (Gibco, cat# cat#11-360-070). HEK 293-FT cells were cultured in Dulbecco's Modified Eagle Medium (DMEM) (Gibco, cat#11995073) with 10% FBS and 1% Penicillin-Streptomycin (10,000 U/mL). Cell cultures were fed once every 2-3 days, grown to 90% confluence and then passaged 1:5 by trypsinization. Cell density was estimated with an automatic cell counter (Bio-Rad cat# 1450102) when cells were being plated for experiments.

### *C. elegans*

The following strains were used for experiments described in this manuscript:

- AWK611 *rocIs11* (rab-3p::mTFP1::LMP-1::mCherry)
- AWK613 *rocIs11; rocIs12* (aex-3p::SID-1;unc-119p:UNC-119)

The strains described were generated in this study. All plasmids were generated using Gibson assembly. AWK611 was created through microinjection of AK358 (rab-3p::mTFP1::LMP-1::mCherry; 50ng/µL) and the co-injection plasmid AK362 (myo-3p::BFP; 10ng/µl) into N2E. Stable transgenic lines were selected based on the blue fluorescent phenotype and integrated by UV mutagenesis and backcrossed 10 times. AWK613 was created by crossing AWK611 with AWK612, which was created through microinjection of AK364 (aex-3p::SID-1; 50ng/µL) into unc-119(-). Stable transgenic lines were selected based on rescue of the uncoordinated phenotype and integrated by UV mutagenesis and backcrossed 10 times.

C. elegans strains were maintained at 20°C on nematode growth medium (NGM) (Fisher, cat# NC9270887) agar plates seeded with *Escherichia coli* strain OP50 (RRID:WB-STRAIN:WBStrain00041974).[247]

# Method Details

## *FIRE-pHLy assay*

For the FIRE-pHLy primary screen and dose-response curves: SH-SY5Y Fire-pHLy cells were plated in collagen-coated 384-well plates (Greiner cat#781956) at a seeding density of 8 thousand cells in 25 µL of media per well. The next day, compounds in DMSO were added to the plates with an Echo liquid dispenser (Beckman Coulter, Echo 655T). Plates were placed in an incubator for the stated treatment time (1-24 hours) and then fixed by adding 25 µL of 4% Paraformaldehyde to each well with a plate washer dispenser (Biotek, EL406). The plates were incubated at room temperature for 15 minutes and then washed with 25 µL per well of DPBS with calcium and magnesium (subsequently referred to as DPBS +/+) (Gibco, cat# 14040216). Next, 25 µL of 2 µM of Hoescht (Invitrogen, cat#33342) in DPBS +/+ were added, plates were incubated

again at room temperature for 15 minutes, washed again with DPBS +/+, followed by a final addition of 50 μL of DPBS +/+.

The primary screen was composed of 24 384-well plates, which were split into 2 batches of 12 completed on two subsequent weeks. 32 wells of each plate were treated with DMSO (as a negative control); 16 wells per plate were treated with 100 nM of BaF (Fisher, cat#AAJ61835MCR) as a control for lysosomal alkalinization; and 16 were treated with 20 μM of OXA-01 (Medchem Express, cat#HY-111065) as a control for lysosomal acidification. One well was treated per compound from the TargetMol Bioactive Compound Library (Target Mol, cat#L4000) with a final concentration of 10 μM. The final concentration of DMSO in each well was 0.1% and the treatment time was 6 hours.

Dose-response curves with the FIRE-pHLy assay were generated in a similar manner. The Echo liquid dispenser was used to add 2.5 – 100 nL of compounds to each well, followed by addition of DMSO at a volume that would result in a total DMSO composition per well of 0.4%. The 190 “candidate” compounds were cherry-picked from Targetmol’s bioactive compound library. Dose response curves from the screen of candidate compounds were composed of 16 doses ranging from 0.1 to 40 μM in duplicate. Treatment time was 6 hours. All other dose response curves were generated in triplicate.

Experiments where compounds were tested at 1-3 doses were done in collagen-coated 96-well plates (Revvity, cat#6005810) and imaged live. SH-SY5Y cells were seeded at a density of 30,000 cells per well and incubated overnight. Cells were then incubated with media containing 1 μM of Hoescht for 5 minutes. Cells were washed twice with SH-SY5Y live imaging media, which consisted of EMEM without phenol red (Quality-biological, cat# 112-212-101): F-12 without phenol red (Innovative research, cat#IHAMSF120813500ML) with 10% FBS. Compounds in live imaging media were added with electronic multi-channel pipette with a total DMSO concentration of 0.1%. Cells were incubated for 4 hours and then imaged.

## *Imaging for FIRE-pHLy assay*

Primary screen and candidate compound screen were imaged with an IN Cell 6500 HS Analyzer (General Electric Life Sciences/Cytiva) with a NIKON 20×/0.75, Plan Apo, CFI/60 objective lens with the following excitation lasers: 405 nm (Hoescht), 488 (mTFP1) 561 nm (mCherry). Four frames per well were obtained.

Images were analyzed with high-content image analysis software (IN Cell Developer Toolbox v1.9, GE Life Sciences), as previously described.[198] In short, Nuclei were segmented using a preset nucleus-type segmentation module, which was used to count the number of cells imaged per well. To quantify FIRE-pHLy fluorescence, a vesicle segmentation module was applied on the mCherry channel to segment lysosomes, with the following acceptance criteria: (Dens-levels >300), min/max granule size (1–10 μm), scales = 2, sensitivity = 33, low background, and no shape constraint settings. These settings created an object "mask" for lysosomes. FIRE-pHLy ratio was calculated by dividing the integrated signal of mTFP1 within the lysosome mask by that of mCherry.

Subsequent FIRE-pHLy assay experiments were imaged with an Opera Phenix high content imager (Revvity, B97236) with the imaging chamber set at 5% $CO_2$ and 37 °C. 12 frames per well were taken with a 40x water-objective. Confocal images were obtained with the following excitation lasers and emission filters: 405 nm / 435-480 nm (Hoescht), 488 nm / 500-550 nm (mTFP1), and 561 nm / 570-630 nm (mCherry).

Images taken with Opera Phenix were analyzed on Revvity's Harmony software. The "Find Nuclei" module with method "C" was used to segment nuclei in the Hoescht channel, and the cell count was estimated by summing the number of segmented nuclei in a well. The "Find Cytoplasm" module with method "B" was used with the mCherry to segment the cell body. The "Find Spots" module with method "D" was used to segment lysosomes within the cytoplasm in the mCherry channel. The exact criteria of each of these modules was modified depending on cell type to

generate accurate segmentation. The “Calculate Intensity Properties” module was used to calculate the total signal of mTFP1 and mCherry within the segmented lysosomes, “FIRE-pHLy ratio” was calculated by diving the former by the latter.

## *Differentiation of SH-SY5Y FIRE-pHLy cells*

FIRE-pHLy-expressing SH-SY5Y cells were seeded in collagen-coated 96-well plates with a density of 3,000 cells per well. The next day (day 0), the media of the cells was replaced with SH-SY5Y culturing media containing 10 µM of Retinoic acid (Sigma-Aldritch, Cat#R2625). On day 3, cells were fed by removing media and adding fresh media with retinoic acid. On day 6, the media was replaced FBS-free EMEM:F12 media with 50 ng/mL of BDNF (Gibco, cat# 450021). Compounds in BDNF-containing FBS-free media were added on day 10, and cells were fixed four hours later with the addition of PFA to a final concentration of 2%. Cells were then washed, stained with Hoescht, imaged on Phenix and segmented as explained previously.

## *Absolute lysosomal pH quantification with Dojindo kit*

Cells were seeded in collagen-coated 96-well plates with density of 30,000 cells per well for SH-SY5Y cells and that of 8,000 cells per well for N2a cells. The next day, cells were washed twice with FBS-free media. FBS-free media containing 0.05% LysoPrime Green dye (Dojindo, cat#L266-10) were added and the cells were left in incubator for 30 minutes. A vial of pHLys red dye (Dojindo, cat#L266-10) was dissolved in 20 µL of DMSO. The plates were then washed three times with FBS-free media. Followed by the addition of 0.1% pHLys Red dye and 1 µM of Hoescht in culturing media. The cells were again placed in an incubator for 30 minutes, after which they were washed once with culturing media and twice with live-imaging media. For SH-SY5Y cells, live-imaging media was composed of EMEM without phenol red: F-12 without phenol red with 10% FBS, and for N2a cells it was composed of EMEM without phenol red, 10% FBS, 1%

GlutaMAX supplement (Fisher, cat#41090036), 1% NEAA and 1% sodium pyruvate. Compounds in live imaging media were added to each well and the plate was left in an incubator for 4 hours.

To make pH titration curve, the pH of buffers from Invitrogen's intracellular pH quantification kit (Invitrogen, cat#P35379) were adjusted by adding potassium hydroxide or potassium chloride to obtain buffers with the following pH's: 3.7, 4.1, 4.5, 4.9, 5.6, 6.2, and 6.5. Valinomycin and nigericin were added fresh to all buffers to a final concentration for both of 10 μM. Cells were incubated with buffers with valinomycin and nigericin for 5 minutes.

Plates were then imaged live with an Opera Phenix high content imager, with the imaging chamber set at 5% $CO_2$ and 37 °C, while utilizing a 40x objective. Confocal images were obtained with the following excitation lasers and emission filters: 405 nm / 435-480 nm (Hoescht), 488 nm / 500-550 nm (LysoPrime Green), and 561 nm / 570-630 nm (pHLys Red).

Images were analyzed on Revvity's Harmony software. The "Find Nuclei" module with method "C" was used to segment nuclei in the Hoescht channel, and the cell count was estimated by summing the number of segmented nuclei in a well. The "Find Cytoplasm" module with method "B" was used with the LysoPrime Green channel to segment the cell body. The "Find Spots" module with method "D" was used to segment lysosomes within the cytoplasm in the LysoPrime Green channel. The exact criteria of each of these modules was modified depending on cell type to generate accurate segmentation. The "Calculate Intensity Properties" module was used to calculate the total signal of pHLys Red and LysoPrime Green within the segmented lysosomes, the ratio of the former to the latter was used as a relative estimate of lysosomal pH. For absolute pH quantification, a pH titration curve was generated in Prism 11 (Graphpad) by fitting an asymmetric sigmoidal 5-parameter curve to the pHLys Red to LysoPrime Green ratiometric signal of all the pH buffers. The estimated lysosomal pH of all treatment conditions was calculated by extrapolating from this pH titration curve.

## *Western Blots*

SH-SY5Y cells were seeded in 6-well plates at a density of 1 million cells per well. They were treated the next day with the corresponding compounds for 1 to 6 hours. Cells were detached from plates by scraping and collected into Eppendorf tubes. The samples were washed once with pre-chilled DPBS (Gibco, cat#14190250) and then lysed by suspending the cells in RIPA buffer (Thermo Fisher Scientific, cat#89900) with 1X HALT phosphatase and protease inhibitor cocktail (Thermo Fisher Scientific, cat#89900) and incubated for 30 minutes on ice. Samples were then spun down at 17,000xg for 15 minutes at 4°C and then the supernatant was transferred into new tubes. The concentration of the protein lysate was quantified with a BCA assay (Thermo Fisher Scientific, cat#23225). Equal amounts of protein from each sample were then denatured by adding NuPAGE reducing agent (Thermo Fisher Scientific, cat#NP0009) and NuPAGE LDS sample buffer (Thermo Fisher Scientific, cat#NP0007) to 1X and placing them on a heat block at 95°C for 5 minutes. Samples were separated via SDS-polyacrylamide gel electrophoresis (SDS-PAGE) and transferred to a nitrocellulose membrane (Bio-Rad, cat#1620112) through wet transfer at 300 mA for 1 hour. The blots were blocked by gently shaking them in Intercept TBS blocking buffer (LI-COR, cat#927-60010) for 1 hour at room temperature. Blots were incubated overnight with primary antibodies with gentle shaking at 4°C, and then washed three times with TBS (Teknova, cat#T1680) with 0.1% Tween-20 (Thermo Fisher Scientific, cat#78444) (TBS-T) buffer. They were then incubated with secondary antibody for 1 hour at room temperature with gentle shaking and then washed three times with TBS-T. All primary antibodies were diluted by 1000, except for anti-GAPDH, which was diluted by 4000. Secondary antibodies were diluted by a factor of 10,000. Blots were imaged with a LI-COR Odyssey Clx imager.

To quantify the degree of phosphorylation of proteins, blots were first incubated with primary antibody against the phosphorylated version of the protein. After imaging, the primary and

secondary antibodies were stripped by incubating in NewBlot Nitrocellulose Stripping buffer (LICORbio, cat#928-40030) at 1X for 10 minutes and washed 3 times with TBS. Blots were re-blocked for 1 hour at room temperature and then incubated overnight with gentle shaking at 4°C in primary antibody against the full-length version of the protein. Washing, incubation in secondary antibody, and imaging steps carried out as before.

Western Blots were quantified in Image Studio Lite version 5.2.5 (LI-COR). Rectangles around bands of interest were drawn with the “Add Rectangle” function, and the border width of the surrounding rectangle was adjusted to avoid other bands. The background was defined as the median signal at the top and bottom of the larger rectangle. To estimate phosphorylation levels, the phosphorylated signal was divided by that of the full-length protein, which was then normalized to the mean of the DMSO-treated samples within the same blot.

## *C. Elegans drug treatment*

WNK463 (MedChem Express, cat#HY-100626) was added to plates at final concentrations of 0.5 and 1 μM. Plates were seeded with concentrated 10x OP50 that had been UV-treated with a dose sufficient to arrest bacterial growth. L4-stage animals were transferred onto drug-containing plates and imaged 24 hours later as Day 1 Adults as described below.

## *C. Elegans RNAi Treatment*

Strain used for RNAi experiments over-expressed dsRNA transporter SID-1 under a neuronal promoter to ensure successful *wnk-1* in neurons.[248] NGM plates for RNAi experiments were supplemented with 100μg/mL carbenicillin (Fisher, cat#BP26485) and 1mM IPTG (Sigma, cat#I5502). Plasmids for the RNAi for *wnk-1* was obtained from the Ahringer RNAi library, a common whole-genome library for *C. elegans.*[249] RNAi cultures were grown overnight and then diluted 1:10 into fresh Luria Broth (LB) (Research products international, cat#L24040) containing

100µg/mL carbenicillin and grown at 37 °C with shaking at 200 rpm for 2 hours. IPTG was then added to a final concentration of 2 mM, and 150 µL of the induced culture was immediately spotted onto pre-warmed plates. Plates were dried overnight at 30°C. Worms were egg prepped allowed to hatch overnight in M9 buffer (Fisher scientific, cat#11006516) while rocking at 20 °C. Fourteen hours after spotting the bacteria, 30–50 synchronized L1-stage animals were transferred to the RNAi plates. Animals were imaged as Day 1 Adults three days later as described below.

## *Fluorescent imaging of FIRE-pHLy-expressing C. Elegans*

All imaged animals were hermaphrodites and the fluorescence imaging of mTFP1::LMP-1::mCherry was performed as follows. Images were collected on a Leica TCS SP8 confocal microscope with a 20× objective using LasX software (Leica). Day 1 young adult animals were immobilized in a droplet of M9 buffer containing 5mM Levamisole (Fisher Scientific, cat#AC187870100) and placed on a 2% agarose pad (Precision Biosystems, cat#PBSA1705). Images were acquired with the 488-nm laser set to 2.5% power and the 561-nm laser set to 5% power. To quantify mTFP1 and mCherry fluorescence, the background threshold was first defined on the mCherry image with a minimum threshold of 20 and a maximum threshold of 255 using ImageJ version 2.14.0/1.54p (NIH). This threshold was then used to create a mask to measure fluorescence intensity from mTFP1 and mCherry images. All values were normalized to the average intensity measured for the negative control (L4440-treated for RNAi experiment and DMSO-treated for drug treatment experiments) before graphing.

## *Autophagy flux assay*

SH-SY5Y cells were seeded in 96-well plates at a density of 30,000 cells per well and incubated overnight. Staining media consisted of 1 µg/mL of Hoescht, 0.2 µM of DAPRed stain (Dojindo, cat#A562-10), and 1 µM of DALGreen stain (Dojindo, cat#A562-10) in SH-SY5Y culturing media. Cells were washed once with culturing media before addition of staining media

and placed in incubator for 30 minutes with staining media. Cells were then washed twice with culturing media and once with EMEM without phenol red: F-12 without phenol red with 10% FBS (live-imaging media). Compounds in live-imaging media were then added to cells and then placed in an incubator for 4-6 hours. Plates were then imaged live with an Opera Phenix high content imager, with the imaging chamber set at 5% $CO_2$ and 37 °C, while utilizing a 40x objective. Confocal images were obtained with the following excitation lasers and emission filters: 405 nm / 435-480 nm (Hoescht), 488 nm / 500-550 nm (DALGreen), and 561 nm / 570-630 nm (DAPRed).

Images were analyzed on Revvity's Harmony software. The "Find Nuclei" module with method "C" was used to segment nuclei in the Hoescht channel, and the cell count was estimated by summing the number of segmented nuclei in a well. The "Find Cytoplasm" module with method "B" was used with the DAPRed channel to segment the cell body. The "Calculate Morphology" module was used to measure the area of each cell. The "Find Spots" module with method "D" was used with the DAPRed channel to segment autophagosomes and autolysosomes and with the DALGreen channel to segment autolysosomes. The "Calculate Morphology" module was used to measure the area of segmented puncta generated by both the DAPREd and DALGreen channel. Dividing the area of segmented puncta with the DAPRed channel over the cell area was used to estimate the volume of autophagosomes and autolysosomes per cell, while that of the puncta generated in the DALGreen channel over the cell area was used to estimate the volume of autolysosomes per cell.

## *Lysosomal Immunoprecipitation*

This protocol was adapted from Park *et al.* 2022.[250] SH-SY5Y cells expressing TMEM-192-3x-HA were plated onto 15 cm plates at a density of 35 million cells per plate and left in incubator overnight.[246] Cell media was then changed to that containing DMSO or a WNK inhibitor and placed in incubator for 4 hours. The plates were then washed with 3 mL of cold DPBS, and

then 1 mL if cold DPBS with 1X Halt protease and phosphatase inhibitor cocktail was added. Cells were then collected by scrapping them into 1.5 mL tubes and pelleted at 4°C by centrifugation at 600xg. The supernatant was removed and the cells were resuspended in 1 mL KPBS buffer [136 mM Potassium chloride, 10 mM potassium phosphate, 300 mM, sodium chloride, 50 mM sucrose, 1X Halt protease and phosphatase inhibitor cocktail in HPLC-grade water (Honeywell, cat#AH365-4)] and then homogenized with 30 strokes of a Dounce homogenizer (Sigma, cat#D8938-B). Samples for whole cell lysate analysis were collected by saving 50 µL of homogenate, while the rest was spun down at 1000xg for 5 minutes at 4°C. The supernatant was moved to a new tube containing 50 µL of anti-HA beads (Thermo Fisher Scientific, cat#PI88837). The samples were incubated at 4°C for 1 hour with gentle rotation. The beads were then washed three times with cold KPBS buffer by using a magnetic stand to pull down the beads. Lysosomal proteins were then precipitated by incubating the beads with gentle rotation for 20 minutes at 4°C in 100 uL of 0.05% v/v NP-40 in KPBS buffer (Thermo Scientific, cat#28324). The concentration of proteins in the whole-cell lysate and Lyso-IP samples were determined with BCA assays (Thermo Fisher scientific, cat#23225) and flash-frozen for later analysis.

The whole cell lysate and Lyso-IP samples were then purified for mass spectrometry analysis by using the solved precipitation single-pot, solid-phase-enhanced sample preparation (SP4) method.[251] To perform the protocol, glass spheres were prepared as follows: 100 mg of 9-13 µm glass spheres (Millipore Sigma, cat#440345) were suspended in ultrapure water by vortexing, and spun down at 500xg for 1 minute. Supernatant, including floating beads, was removed and wash step was repeated once with acetonitrile, once in 100 mM of ammonium bicarbonate (Millipore Sigma, cat# S2454) and twice with ultrapure water. Beads were finally re-suspended in 0.9 mL of acetonitrile to a final concentration of 50 mg/mL. After Lyso-IP and whole cell lysate samples were thawed, TCEP (Sigma Aldritch, cat#T2556) and 2-Chloroacetamide (Millipore Sigma, cat#C0267) were added for a final concentration of 10 mM and 40 mM,

respectively. Samples were then incubated at 95°C for 5 minutes. Four-times the volume of glass beads in acetonitrile were then added so that the final concentration of glass beads was 2.5-fold higher than that of the proteins in samples. Samples were then mixed by vortexing for 5 seconds, and centrifuged at 16,000xg for 5 minutes. The supernatant was removed and 1 mL of ethanol was added, and then samples were again centrifuged at 16,000xg for 2 minutes. Wash steps with ethanol were repeated twice. Next, as much ethanol was removed and glass beads were re-suspended in 100 mM of ammonium bicarbonate buffer. Trypsin (Worthington Biochemical Corporation, cat#LS003740) at a 1:30 trypsin:protein ratio was then added, and samples were incubated in a thermomixer with shaking at 1000 rpm and at 37°C for 18 hours. Next, samples were spun down at 16,000xg for 2 minutes, and the supernatant was collected and filtered through a cellulase acetate filter in spin cups (Thermo Fisher Scientific, cat# 69702).

## *Mass spectrometry data acquisition*

Samples were separated over a 10-minute linear gradient of 2-35% solvent B (solvent A: 0.1% formic acid water, solvent B: 0.1% formic acid acetonitrile) for 10 minutes, and 35-95% solvent B for 2 minutes on a PepSep MAX HT (150µm, 1.9µm) column (Bruker, 1903885) using a nanoElute 2 system (Bruker) and injected into a timsTOF HT mass spectrometer (Bruker). Experiments were run as data-independent acquisitions (DIA) with parallel accumulation-serial fragmentation (PASEF) and enabled trapped ion mobility spectrometry (TIMS). MS and MS/MS spectra were collected with a mass range from 100 to 1700 m/z.

## *Mass spectrometry data processing*

Mass spectrometry files were processed using Biognosys' Spectronaut software (version 19). Peptides were searched against Uniport's human proteome (Uniprot, Proteome ID: UP000005640). Enzyme cleavage rules were set to Trypsin, with at most two missed cleavages. The peptide length was restricted to 7-52 amino acids. Accepted peptide modifications were set

up as follows: carbamidomethyl in cysteine residues as a fixed modification, and oxidation in methionine residues and acetylation in the N-terminus as variable modifications. MS2 peak area quantification was used, and the imputation strategy was set up as background signal. The differential abundance grouping was calculated at the protein level. $Log_2$ ratio candidate filter was set at 0.58. Unpaired t-tests were used to calculate significance.

## *Lentiviral packaging*

HEK293FT were seeded in 10 cm plates with a density of 2 million cells per plate. The next day, 48 µL of Xtreme HP transfection reagent, 4 µg of PsPAX2 plasmid, 4 µg VSVG envelope plasmid and 8 µg of pLV_3xFLAG-ATP6V0A3-mScarlet (Addgene, cat#228867) or pLV_3XHA-ATP6V1B2-mNeonGreen (Addgene, cat#228865) were added to 1 mL of OptiMEM (Gibco, cat#31985062) media. Transfection reagent was added first and left to incubate for 5 minutes, followed by addition of the DNA and a 15-min incubation. Media was removed from the plates containing the HEK293FT cells, 9 mL of fresh media was added, followed with the drop-wise addition of 1 mL of OptiMEM containing the transfection reagents. Cells were left to incubate overnight, and the media was changed the next day. The media was collected 2 and 3 days after transfection and pooled. The pooled media was spun down for 500xg for 10 minutes. The supernatant was collected and 1/3 of its volume in Lenti-X concentrator (Takara bio, cat#631231) was added and then mixed gently by inversion. The samples were incubated on ice for 1 hour, and then spun down at 1,500xg for 15 minutes at 4°C. The pellet was then re-suspended in DPBS with 1% of its original volume.

## *Generation of fluorescent vATPase SH-SY5Y cell line*

SH-SY5Y cells were seeded at a density of 200-thousand cells per well in 6-well plates and incubated overnight. Concentrated lentivirus of ATP6V0A3-mScarlet and ATP6V1B2-mNeonGreen was diluted by a factor of 100 in SH-SY5Y media containing 6 µg/mL of polybrene

(Millipore Sigma, cat#TR-1003-G). Four 3-fold dilutions of the lentivirus-containing media were then performed with media containing 6 µg/mL of polybrene, which were then used to treat 1-well of SH-SY5Y cells. Cells were left in incubator overnight, and the media was changed to regular culturing media the following day. Cell selection was begun 3 days after infection, with media containing 50 µg/mL of Hygromycin (Fisher Scientific, cat#10-687-010) and 5 µg/mL of Blasticidin (Fisher Scientific, cat#R21001). The well with surviving cells with that was infected with the lowest virus titter was expanded and used for future experiments.

## *Fluorescent-vATPase imaging assay*

SH-SY5Y cells expressing ATP6V0A3-mScarlet and ATP6V1B2-mNeonGreen were seeded in collagen-coated 96-well plates at a density of 30,000 cells per well and incubated overnight. Cells were stained with 1 µg/mL of Hoescht and 0.1% LysoPrime Deep Red dye (Dojindo, cat#L264-10) in culturing media for 30 minutes. They were then washed once with culturing media and once with SH-SY5Y live-imaging media, which was composed of EMEM without phenol red: F-12 without phenol red with 10% FBS. WNK464 was then diluted by a factor of 1000 in live imaging media and added to the corresponding wells for a final concentration of 1 or 5 µM. Wells treated with media containing 0.1% DMSO were used as the negative control. Four hours after compound treatment, the cells were imaged live with an Opera Phenix high content imager, with the imaging chamber set at 5% $CO_2$ and 37°C, while utilizing a 40x objective. Confocal images were obtained with the following excitation lasers and emission filters: 405 nm / 435-480 nm (Hoescht), 488 nm / 500-550 nm (mNeonGreen), 561 nm / 570-630 nm (mScarlet), and 640 nm / 650-760 nm (LysoPrime Deep Red).

Images were analyzed on Revvity's Harmony software. The "Find Nuclei" module with method "C" was used to segment nuclei in the Hoescht channel, and the cell count was estimated by summing the number of segmented nuclei in a well. The "Find Cytoplasm" module with method

“B” was used with the LysoPrime Deep Red channel to segment the cell body. The “Find Spots” module with method “C” was used to segment lysosomes within the cytoplasm in the LysoPrime Deep Red channel and V0A3-puncta in the mScarlet channel. The “Calculate Intensity Properties” module was used to measure the total signal of V1B2-mNeonGreen, V0A3-mScarlet and LysoPrime Deep Red in total within a cell, in segmented lysosomes and in segmented V0A3-puncta. The “Calculate Morphology Properties” module was used to measure the area of segmented V0A3-puncta and segmented lysosomes. The total signal of V1B2-mNeonGreen and V0A3-mScarlet within cells was divided by the cell count to measure changes of total V1B2 and V0A3 subunit abundance within cells, respectively. The total signal of V1B2-mNeonGreen and LysoPrime Deep Red within segmented V0A3-puncta were divided by the total area of segmented V0A3-puncta as an estimate of $V_0$ and $V_1$ complexes bound together and lysosomal overlap with $V_0$, respectively. The total signal of V1B2-mNeonGreen and V0A3-mScarlet within lysosomes were divided by the area of segmented lysosomes as an estimate of $V_1$ and $V_0$ complexes localized within lysosomes, respectively.

## *Cathepsin activity and lysosomal proteolytic activity assays*

Cells were seeded in collagen-coated 96-well plates with density of 30,000 cells per well for SH-SY5Y cells and that of 8,000 cells per well for N2a cells. After an overnight incubation, the cells were stained with 2 µg/mL of Hoescht in culturing media for 5 minutes, followed by one wash in culturing media and one wash with live-imaging media. For SH-SY5Y cells, live-imaging media was composed of EMEM without phenol red: F-12 without phenol red with 10% FBS, and for N2a cells it was composed of EMEM without phenol red, 10% FBS, 1% GlutaMAX supplement, 1% NEAA and 1% sodium pyruvate. The compounds being tested were diluted in live imaging media to a final concentration of DMSO of 0.1%, which were added to cells and placed in incubator. 50 µL of each compound was added per well. For measure of active cathepsin D, cells were treated with compounds for 4 hours. Then 12.5 µL of 2.5 µM BODIPY-Pepstatin A (Thermo Fisher

Scientific, cat#P12271) in live-imaging media were added to each well for a final concentration of 0.5 μM. The cells were incubated for 45 minutes, then washed once with live imaging media and then imaged. For magic red substrate assays, cells were treated with pH-modifying compounds for 4 hours, after which 5.5 μL of 2 μM magic red substrate for cathepsin B (Abcam, cat#ab270772) or for cathepsin L (Abcam, cat#ab270774) in live-imaging media were added to each well for a final concentration of 0.2 μM. Cells were incubated for 1 hour and then imaged. For DQ-BSA assays, cells were treated with pH-modifying compounds for 3 hours, after which 5.5 μL of 100 μg/mL DQ-BSA (Thermo Fisher, cat#D12051) in live imaging media was added for a final concentration of 10 μg/mL. For the time-course with SH-SY5Y cells, cells were imaged every 30 minutes starting 1 hour after DQ-BSA addition for 5.5 hours. For the experiment with N2a cells, cells were imaged 3 hours after DQ-BSA addition. Confocal images were obtained with the following excitation lasers and emission filters: 405 nm / 435-480 nm (Hoescht), 488 nm / 500-550 nm (BODIPY), and 561 nm / 570-630 nm (DQ-BSA and magic red substrates).

Images were analyzed on Revvity's Harmony software. The "Find Nuclei" module with method "C" was used to segment nuclei in the Hoescht channel, and the cell count was estimated by summing the number of segmented nuclei in a well. The "Find Cytoplasm" module with method "B" was used with the BODIPY, Magic Red substrate, or DQ-BSA channels to segment the cell body. The "Find Spots" module with method "C" was used to segment puncta in the BODIPY and magic red channels, and with method "D" to segment puncta in the DQ-BSA channel. The "Calculate Intensity Properties" module was used to measure the total signal within segmented puncta of BODIPY-pepstatin A, magic red substrate or DQ-BSA within their respective channels. Each of these was divided by the number of cells within a well to estimate the total signal of each of the probes per cell as an estimate of mature cathepsin D for BODIPY-pepstatin A, cathepsin B or L activity for magic red substrates, and lysosomal proteolytic activity for DQ-BSA.

## *Mitophagy assay*

N2a cells were seeded in collagen-coated 96-well plates at a density of 8,000 cells per well. After an overnight incubation, the cells were incubated in 1 µg/mL of Hoescht and 100 nM of Mtphagy dye (Dojindo, cat#MT02) in FBS-free media for 30 minutes. Cells were then washed once with FBS-free media and twice with live-imaging media, which was composed of EMEM without phenol red, 10% FBS, 1% GlutaMAX supplement, 1% NEAA and 1% sodium pyruvate. Next, 50 µL of live-imaging media containing 0.1% DMSO, 100 nM BaF or 5 µM WNK463 were added to each well. Mitophagy was then induced with the addition of 5.5 µL of live-imaging media containing 100 µM of FCCP (MedChem Express, cat#HY-100410) and 100 µM of oligomycin (MedChem Express, cat#HY-N6782) for a final concentration of 10 µM for both. Cells were then incubated for an additional 4 hours and then imaged live with an Opera Phenix high content imager. Confocal images were obtained with the following excitation lasers and emission filters: 405 nm / 435-480 nm (Hoescht), and 561 nm / 570-630 nm (Mtphagy dye).

Images were analyzed on Revvity's Harmony software. The "Find Nuclei" module with method "C" was used to segment nuclei in the Hoescht channel, and the cell count was estimated by summing the number of segmented nuclei in a well. The "Find Cytoplasm" module with method "B" was used with the Mtphagy dye channel to segment the cell body. The "Find Spots" module with method "D" was used to segment puncta in the Mtphagy dye channel. The "Calculate Intensity Properties" module was used to measure the total Mtphagy signal within the segmented puncta. This measure was divided by the number of cells per well to measure the Mtphagy signal per cell to measure the volume of acidified mitochondria per cell which is correlated to the amount of mitophagy occurring.

## Quantification and statistical analysis

### *Quantification of FIRE-pHLy primary screen*

FIRE-pHLy primary screen data was analyzed on SMDC HiTS version 2.4 (UCSF), where FIRE-pHLy Ratio percent relative effect, FIRE-pHLy Ratio fold-change, FIRE-pHLy Ratio b-score, and mCherry signal per cell fold-change values were calculated for every screened compound.

### *Selection of Active compounds from candidate compound screen*

We selected “active” compounds based on the following four properties: a) bottom plateau of FIRE-pHLy ratio FC curve of 0.85 or 65% relative to OXA-01 (b) dose-dependent decrease in FIRE-pHly ratio (c) bottom plateau of nuclear count greater than 0.3 fold-change or an $EC_{50}$ for nuclear count that was at least 5-times greater than that for FIRE-pHLy ratio d) top plateau of mCherry signal per cell FC curve less than 2.5 fold-change. Thirty-two compounds passed the activity threshold. Eight compounds were removed due to weak or poor-quality dose-responses, a further nine compounds were toxic, and four increased mCherry signal per cell. Eleven compounds remained and were ordered from commercial vendors for further testing.

### *Quantification of proteomics data*

Lyso-IP method was validated by showing that most lysosomal proteins were enriched in Lyso-IP fraction compared to whole cell lysate. Proteins were classified as “lysosomal” if their Gene Ontology Cellular component annotations contained “lysosome” or “lysosomal”.

Gene enrichment analysis was performed using STRING version 12.0 (Swiss Institute of Bioinformatics). Comparison between the lysosomal fraction of WNK463-treated cells and the lysosomal fraction of DMSO-treated cells was used as the data set, with proteins ranked by $\log_2$

protein abundance values. V-ATPase proteins were removed from dataset because if they were included most significantly enriched categories reached significance due to them.

## *Statistical Analysis*

All other statistical analyses were performed using GraphPad Prism 8. The experimental data were presented in the form of mean ± standard error (SEM), unless otherwise specified. Information on statistical tests used and the number of biological replicates analyzed (*n*) in each experiment is found in the figure legends.

Plots were designed on Prism, the graphical abstract and screen workflow from Figure 2.2.F were designed with BioRender, and figures were arranged with Adobe Illustrator.

# References


1. Perera, R.M., and Zoncu, R. (2016). The Lysosome as a Regulatory Hub. Annu Rev Cell Dev Biol *32*, 223–253. https://doi.org/10.1146/annurev-cellbio-111315-125125.

2. Trivedi, P.C., Bartlett, J.J., and Pulinilkunnil, T. (2020). Lysosomal Biology and Function: Modern View of Cellular Debris Bin. Cells *9*, 1131. https://doi.org/10.3390/cells9051131.

3. Kaushik, S. (2025). Chaperone-Mediated Autophagy in Health and Disease. In Autophagy - From Molecular Mechanisms to Flux Control in Health and Disease, B. Loos and D. J. Klionsky, eds. (Springer Nature Switzerland), pp. 283–309. https://doi.org/10.1007/978-3-031-88121-3_11.

4. Sakai, Y., Behrends, C., Debnath, J., Izumi, M., Jenny, A., Molinari, M., Nakamura, S., Oku, M., Otegui, M.S., Santambrogio, L., et al. (2026). Microautophagy: current understanding of its molecular mechanisms and functions. Autophagy Rep *5*. https://doi.org/10.1080/27694127.2026.2626661.

5. Reggiori, F., and Klumperman, J. (2016). Lysosome Biogenesis and Autophagy. In Lysosomes: Biology, Diseases, and Therapeutics (John Wiley & Sons, Ltd), pp. 7–31. https://doi.org/10.1002/9781118978320.ch2.

6. Piras, A., Collin, L., Grüninger, F., Graff, C., and Rönnbäck, A. (2016). Autophagic and lysosomal defects in human tauopathies: analysis of post-mortem brain from patients with familial Alzheimer disease, corticobasal degeneration and progressive supranuclear palsy. Acta Neuropathol Commun *4*, 22. https://doi.org/10.1186/s40478-016-0292-9.

7. Hassiotis, S., Manavis, J., Blumbergs, P.C., Hattersley, K.J., Carosi, J.M., Kamei, M., and Sargeant, T.J. (2018). Lysosomal LAMP1 immunoreactivity exists in both diffuse and neuritic amyloid plaques in the human hippocampus. Eur. J. Neurosci. *47*, 1043–1053. https://doi.org/10.1111/ejn.13913.

8. Wallings, R.L., Humble, S.W., Ward, M.E., and Wade-Martins, R. (2019). Lysosomal Dysfunction at the Centre of Parkinson's Disease and Frontotemporal Dementia/Amyotrophic Lateral Sclerosis. Trends Neurosci *42*, 899–912. https://doi.org/10.1016/j.tins.2019.10.002.

9. Nixon, R.A. (2020). The aging lysosome: An essential catalyst for late-onset neurodegenerative diseases. Biochimica et Biophysica Acta (BBA) - Proteins and Proteomics *1868*, 140443. https://doi.org/10.1016/j.bbapap.2020.140443.

10. Lane-Donovan, C., Paredes, M., and Kao, A.W. (2025). The lysosome and proteostatic stress at the intersection of pediatric neurological disorders and adult neurodegenerative diseases. Prog Neurobiol *255*, 102854. https://doi.org/10.1016/j.pneurobio.2025.102854.

11. Nixon, R.A., and Rubinsztein, D.C. (2024). Mechanisms of autophagy-lysosome dysfunction in neurodegenerative diseases. Nat Rev Mol Cell Biol *25*, 926–946. https://doi.org/10.1038/s41580-024-00757-5.

12. Giovedì, S., Ravanelli, M.M., Parisi, B., Bettegazzi, B., and Guarnieri, F.C. (2020). Dysfunctional Autophagy and Endolysosomal System in Neurodegenerative Diseases: Relevance and Therapeutic Options. Front Cell Neurosci *14*, 602116. https://doi.org/10.3389/fncel.2020.602116.

13. Ohkuma, S., and Poole, B. (1978). Fluorescence probe measurement of the intralysosomal pH in living cells and the perturbation of pH by various agents. Proc Natl Acad Sci U S A *75*, 3327–3331. https://doi.org/10.1073/pnas.75.7.3327.

14. Anderson, R.G., Falck, J.R., Goldstein, J.L., and Brown, M.S. (1984). Visualization of acidic organelles in intact cells by electron microscopy. Proc Natl Acad Sci U S A *81*, 4838–4842. https://doi.org/10.1073/pnas.81.15.4838.

15. Meyer-Schwesinger, C. (2021). Lysosome function in glomerular health and disease. Cell Tissue Res *385*, 371–392. https://doi.org/10.1007/s00441-020-03375-7.

16. Hsu, A., Podvin, S., and Hook, V. (2018). Lysosomal Cathepsin Protease Gene Expression Profiles in the Human Brain During Normal Development. J Mol Neurosci *65*, 420–431. https://doi.org/10.1007/s12031-018-1110-6.

17. Reif, M.M., Mach, L., and Oostenbrink, C. (2012). Molecular Insight into Propeptide–Protein Interactions in Cathepsins L and O. Biochemistry *51*, 8636–8653. https://doi.org/10.1021/bi300802a.

18. Mason, S.D., and Joyce, J.A. (2011). Proteolytic networks in cancer. Trends in Cell Biology *21*, 228–237. https://doi.org/10.1016/j.tcb.2010.12.002.

19. Chen, C.S., Chen, W.N., Zhou, M., Arttamangkul, S., and Haugland, R.P. (2000). Probing the cathepsin D using a BODIPY FL-pepstatin A: applications in fluorescence polarization and microscopy. J Biochem Biophys Methods *42*, 137–151. https://doi.org/10.1016/s0165-022x(00)00048-8.

20. Banay-Schwartz, M., Bracco, F., Dahl, D., Deguzman, T., Turk, V., and Lajtha, A. (1985). The pH dependence of breakdown of various purified brain proteins by cathepsin D preparations. Neurochem Int *7*, 607–614. https://doi.org/10.1016/0197-0186(85)90057-9.

21. Yasuda, Y., Kageyama, T., Akamine, A., Shibata, M., Kominami, E., Uchiyama, Y., and Yamamoto, K. (1999). Characterization of new fluorogenic substrates for the rapid and sensitive assay of cathepsin E and cathepsin D. J Biochem *125*, 1137–1143. https://doi.org/10.1093/oxfordjournals.jbchem.a022396.

22. Turk, B., Dolenc, I., Lenarcic, B., Krizaj, I., Turk, V., Bieth, J.G., and Björk, I. (2001). Acidic pH as a physiological regulator of human cathepsin L activity. Eur J Biochem *259*, 926–932. https://doi.org/10.1046/j.1432-1327.1999.00145.x.

23. Jordans, S., Jenko-Kokalj, S., Kühl, N.M., Tedelind, S., Sendt, W., Brömme, D., Turk, D., and Brix, K. (2009). Monitoring compartment-specific substrate cleavage by cathepsins B, K, L,

and S at physiological pH and redox conditions. BMC Biochem *10*, 23. https://doi.org/10.1186/1471-2091-10-23.

24. Yoon, M.C., Solania, A., Jiang, Z., Christy, M.P., Podvin, S., Mosier, C., Lietz, C.B., Ito, G., Gerwick, W.H., Wolan, D.W., et al. (2021). Selective Neutral pH Inhibitor of Cathepsin B Designed Based on Cleavage Preferences at Cytosolic and Lysosomal pH Conditions. ACS Chem Biol *16*, 1628–1643. https://doi.org/10.1021/acschembio.1c00138.

25. Sampognaro, P.J., Arya, S., Knudsen, G.M., Gunderson, E.L., Sandoval-Perez, A., Hodul, M., Bowles, K., Craik, C.S., Jacobson, M.P., and Kao, A.W. (2023). Mutations in α-synuclein, TDP-43 and tau prolong protein half-life through diminished degradation by lysosomal proteases. Molecular Neurodegeneration *18*, 29. https://doi.org/10.1186/s13024-023-00621-8.

26. Lane-Donovan, C., Smith, A.W., Saloner, R., Miller, B.L., Casaletto, K.B., and Kao, A.W. (2025). Tau phosphorylation at Alzheimer's disease biomarker sites impairs its cleavage by lysosomal proteases. Alzheimers Dement *21*, e70320. https://doi.org/10.1002/alz.70320.

27. Freeman, S.A., Grinstein, S., and Orlowski, J. (2023). Determinants, maintenance, and function of organellar pH. Physiol. Rev *103*, 515–606. https://doi.org/10.1152/physrev.00009.2022.

28. Chin, M.Y., Espinosa, J.A., Pohan, G., Markossian, S., and Arkin, M.R. (2021). Reimagining dots and dashes: Visualizing structure and function of organelles for high-content imaging analysis. Cell Chem Biol *28*, 320–337. https://doi.org/10.1016/j.chembiol.2021.01.016.

29. Wolfe, D.M., Lee, J.-H., Kumar, A., Lee, S., Orenstein, S.J., and Nixon, R.A. (2013). Autophagy failure in Alzheimer's disease and the role of defective lysosomal acidification. Eur J Neurosci *37*, 1949–1961. https://doi.org/10.1111/ejn.12169.

30. Sarić, A., Grinstein, S., and Freeman, S.A. (2017). Measurement of Autolysosomal pH by Dual-Wavelength Ratio Imaging. In Methods in Enzymology (Academic Press), pp. 15–29. https://doi.org/10.1016/bs.mie.2016.09.073.

31. Liv, N., Fermie, J., Ten Brink, C.B.M., de Heus, C., and Klumperman, J. (2023). Functional characterization of endo-lysosomal compartments by correlative live-cell and volume electron microscopy. In Volume Electron Microscopy Methods in Cell Biology. (Elsevier), pp. 301–326. https://doi.org/10.1016/bs.mcb.2022.12.022.

32. Lee, J.-H., Yang, D.-S., Goulbourne, C.N., Im, E., Stavrides, P., Pensalfini, A., Chan, H., Bouchet-Marquis, C., Bleiwas, C., Berg, M.J., et al. (2022). Faulty autolysosome acidification in Alzheimer's disease mouse models induces autophagic build-up of Aβ in neurons, yielding senile plaques. Nat Neurosci *25*, 688–701. https://doi.org/10.1038/s41593-022-01084-8.

33. Harter, C., and Mellman, I. (1992). Transport of the lysosomal membrane glycoprotein lgp120 (lgp-A) to lysosomes does not require appearance on the plasma membrane. J Cell Biol *117*, 311–325. https://doi.org/10.1083/jcb.117.2.311.

34. Thermo Fisher Scientific (2013). LysoTracker® and LysoSensor™ Probes.

35. Millot, C., Millot, J.M., Morjani, H., Desplaces, A., and Manfait, M. (1997). Characterization of acidic vesicles in multidrug-resistant and sensitive cancer cells by acridine orange staining and confocal microspectrofluorometry. J Histochem Cytochem *45*, 1255–1264. https://doi.org/10.1177/002215549704500909.

36. Vergne, I., Constant, P., and Lanéelle, G. (1998). Phagosomal pH determination by dual fluorescence flow cytometry. Anal Biochem *255*, 127–132. https://doi.org/10.1006/abio.1997.2466.

37. Hoffmann, B., and Kosegarten, H. (1995). FITC-dextran for measuring apoplast pH and apoplastic pH gradients between various cell types in sunflower leaves. Physiologia Plantarum *95*, 327–335. https://doi.org/10.1111/j.1399-3054.1995.tb00846.x.

38. Chen, Y., Liu, P., Zhong, Z., Zhang, H., Sun, A., and Wang, Y. (2024). STIM1 functions as a proton sensor to coordinate cytosolic pH with store-operated calcium entry. J Biol Chem *300*, 107924. https://doi.org/10.1016/j.jbc.2024.107924.

39. Chin, M.Y., Patwardhan, A.R., Ang, K.-H., Wang, A.L., Alquezar, C., Welch, M., Nguyen, P.T., Grabe, M., Molofsky, A.V., Arkin, M.R., et al. (2021). Genetically Encoded, pH-Sensitive mTFP1 Biosensor for Probing Lysosomal pH. ACS Sens *6*, 2168–2180. https://doi.org/10.1021/acssensors.0c02318.

40. Webb, B.A., Aloisio, F.M., Charafeddine, R.A., Cook, J., Wittmann, T., and Barber, D.L. (2021). pHLARE: a new biosensor reveals decreased lysosome pH in cancer cells. MBoC *32*, 131–142. https://doi.org/10.1091/mbc.E20-06-0383.

41. Ponsford, A.H., Ryan, T.A., Raimondi, A., Cocucci, E., Wycislo, S.A., Fröhlich, F., Swan, L.E., and Stagi, M. (2021). Live imaging of intra-lysosome pH in cell lines and primary neuronal culture using a novel genetically encoded biosensor. Autophagy *17*, 1500–1518. https://doi.org/10.1080/15548627.2020.1771858.

42. Stransky, L.A., and Forgac, M. (2015). Amino Acid Availability Modulates Vacuolar H+-ATPase Assembly. J Biol Chem *290*, 27360–27369. https://doi.org/10.1074/jbc.M115.659128.

43. Kane, P.M., and Parra, K.J. (2000). Assembly and Regulation of the Yeast Vacuolar H+-ATPase. J Exp Biol *203*, 81–87. https://doi.org/10.1242/jeb.203.1.81.

44. Sautin, Y.Y., Lu, M., Gaugler, A., Zhang, L., and Gluck, S.L. (2005). Phosphatidylinositol 3-Kinase-Mediated Effects of Glucose on Vacuolar H+-ATPase Assembly, Translocation, and Acidification of Intracellular Compartments in Renal Epithelial Cells. Mol Cell Biol *25*, 575–589. https://doi.org/10.1128/MCB.25.2.575-589.2005.

45. Ratto, E., Chowdhury, S.R., Siefert, N.S., Schneider, M., Wittmann, M., Helm, D., and Palm, W. (2022). Direct control of lysosomal catabolic activity by mTORC1 through regulation of V-ATPase assembly. Nat Commun *13*, 4848. https://doi.org/10.1038/s41467-022-32515-6.

46. Ishida, Y., Nayak, S., Mindell, J.A., and Grabe, M. (2013). A model of lysosomal pH regulation. Journal of General Physiology *141*, 705–720. https://doi.org/10.1085/jgp.201210930.

47. Tian, Z., Chen, R., Fang, G., Qiu, K., Wu, W., Shao, X., Liu, D., Que, H., Wang, X., Gao, J., et al. (2026). Mitochondria acidify lysosomes through membrane contacts. Cell Rep *45*. https://doi.org/10.1016/j.celrep.2026.117112.

48. Liu, Q., Yoo, S., Zhang, Z.A., Li, L., Su, H., Vannur, L., Wooldredge, A.C., Hughes, J.-W.B., Desprez, P.-Y., Hao, N., et al. (2026). Mitochondria-lysosome coupling contributes to lysosome acidification and aging. Mol Cell *0*. https://doi.org/10.1016/j.molcel.2026.05.004.

49. Kosmidis, E., Shuttle, C.G., Preobraschenski, J., Ganzella, M., Johnson, P.J., Veshaguri, S., Holmkvist, J., Møller, M.P., Marantos, O., Marcoline, F., et al. (2022). Regulation of the mammalian-brain V-ATPase through ultraslow mode-switching. Nature *611*, 827–834. https://doi.org/10.1038/s41586-022-05472-9.

50. Johnson, D.E., Ostrowski, P., Jaumouillé, V., and Grinstein, S. (2016). The position of lysosomes within the cell determines their luminal pH. J Cell Biol *212*, 677–692. https://doi.org/10.1083/jcb.201507112.

51. Yoshimori, T., Yamamoto, A., Moriyama, Y., Futai, M., and Tashiro, Y. (1991). Bafilomycin A1, a specific inhibitor of vacuolar-type H(+)-ATPase, inhibits acidification and protein degradation in lysosomes of cultured cells. J Biol Chem *266*, 17707–17712. https://doi.org/10.1016/S0021-9258(19)47429-2.

52. Verma, S., Tirumala, N.A., Zhu, X., De Pace, R., and Bonifacino, J.S. (2025). Spatial Regulation of Lysosomal Vesicle Acidification Along the Axon via mRAVE-Dependent v-

ATPase Assembly. bioRxiv, 2025.12.22.696043. https://doi.org/10.64898/2025.12.22.696043.

53. Myers, B.M., Tietz, P.S., Tarara, J.E., and LaRusso, N.F. (1995). Dynamic measurements of the acute and chronic effects of lysosomotropic agents on hepatocyte lysosomal pH using flow cytometry. Hepatology *22*, 1519–1526.

54. Tang, Q., Liu, M., Liu, Y., Hwang, R.-D., Zhang, T., and Wang, J. (2021). NDST3 deacetylates α-tubulin and suppresses V-ATPase assembly and lysosomal acidification. The EMBO Journal. https://doi.org/10.15252/embj.2020107204.

55. Hu, M., Li, P., Wang, C., Feng, X., Geng, Q., Chen, W., Marthi, M., Zhang, W., Gao, C., Reid, W., et al. (2022). Parkinson's disease-risk protein TMEM175 is a proton-activated proton channel in lysosomes. Cell *185*, 2292-2308.e20. https://doi.org/10.1016/j.cell.2022.05.021.

56. Hughes, A.L., and Gottschling, D.E. (2012). An Early-Age Increase in Vacuolar pH Limits Mitochondrial Function and Lifespan in Yeast. Nature *492*, 261–265. https://doi.org/10.1038/nature11654.

57. Dehay, B., Ramirez, A., Martinez-Vicente, M., Perier, C., Canron, M.-H., Doudnikoff, E., Vital, A., Vila, M., Klein, C., and Bezard, E. (2012). Loss of P-type ATPase ATP13A2/PARK9 function induces general lysosomal deficiency and leads to Parkinson disease neurodegeneration. Proc Natl Acad Sci USA *109*, 9611–9616. https://doi.org/10.1073/pnas.1112368109.

58. Kim, S.-H., Cho, Y.-S., Kim, Y., Park, J., Yoo, S.-M., Gwak, J., Kim, Y., Gwon, Y., Kam, T., and Jung, Y.-K. (2023). Endolysosomal impairment by binding of amyloid beta or MAPT/Tau to V-ATPase and rescue via the HYAL-CD44 axis in Alzheimer disease. Autophagy *19*, 2318–2337. https://doi.org/10.1080/15548627.2023.2181614.

59. Baltazar, G.C., Guha, S., Lu, W., Lim, J., Boesze-Battaglia, K., Laties, A.M., Tyagi, P., Kompella, U.B., and Mitchell, C.H. (2012). Acidic Nanoparticles Are Trafficked to Lysosomes

and Restore an Acidic Lysosomal pH and Degradative Function to Compromised ARPE-19 Cells. PLoS One *7*, e49635. https://doi.org/10.1371/journal.pone.0049635.

60. Zeng, J., Shirihai, O.S., and Grinstaff, M.W. (2020). Modulating lysosomal pH: a molecular and nanoscale materials design perspective. J Life Sci (Westlake Village) *2*, 25–37. https://doi.org/10.36069/jols/20201204.

61. Bourdenx, M., Daniel, J., Genin, E., Soria, F.N., Blanchard-Desce, M., Bezard, E., and Dehay, B. (2016). Nanoparticles restore lysosomal acidification defects: Implications for Parkinson and other lysosomal-related diseases. Autophagy *12*, 472–483. https://doi.org/10.1080/15548627.2015.1136769.

62. Chung, C.Y.-S., Shin, H.R., Berdan, C.A., Ford, B., Ward, C.C., Olzmann, J.A., Zoncu, R., and Nomura, D.K. (2019). Covalent targeting of the vacuolar H+-ATPase activates autophagy via mTORC1 inhibition. Nat Chem Biol *15*, 776–785. https://doi.org/10.1038/s41589-019-0308-4.

63. Zhou, X., Zhao, S., Liu, T., Yao, L., Zhao, M., Ye, X., Zhang, X., Guo, Q., Tu, P., and Zeng, K. (2022). Schisandrol A protects AGEs-induced neuronal cells death by allosterically targeting ATP6V0d1 subunit of V-ATPase. Acta Pharmaceutica Sinica B *12*, 3843–3860. https://doi.org/10.1016/j.apsb.2022.06.013.

64. Vest, R.T., Chou, C.-C., Zhang, H., Haney, M.S., Li, L., Laqtom, N.N., Chang, B., Shuken, S., Nguyen, A., Yerra, L., et al. (2022). Small molecule C381 targets the lysosome to reduce inflammation and ameliorate disease in models of neurodegeneration. Proc Natl Acad Sci USA *119*, e2121609119. https://doi.org/10.1073/pnas.2121609119.

65. Afghah, Z., Khan, N., Datta, G., Halcrow, P.W., Geiger, J.D., and Chen, X. (2024). Involvement of Endolysosomes and Aurora Kinase A in the Regulation of Amyloid β Protein Levels in Neurons. Int Mol Sci *25*, 6200. https://doi.org/10.3390/ijms25116200.

66. Chin, M.Y., Ang, K.-H., Davies, J., Alquezar, C., Garda, V.G., Rooney, B., Leng, K., Kampmann, M., Arkin, M.R., and Kao, A.W. (2022). Phenotypic Screening Using High-Content Imaging to Identify Lysosomal pH Modulators in a Neuronal Cell Model. ACS Chem Neurosci *13*, 1505–1516. https://doi.org/10.1021/acschemneuro.1c00804.

67. Bruns, H., Stegelmann, F., Fabri, M., Döhner, K., van Zandbergen, G., Wagner, M., Skinner, M., Modlin, R.L., and Stenger, S. (2012). Abelson Tyrosine Kinase Controls Phagosomal Acidification Required for Killing of Mycobacterium tuberculosis in Human Macrophages. J Immunol *189*, 4069–4078. https://doi.org/10.4049/jimmunol.1201538.

68. Im, E., Jiang, Y., Stavrides, P.H., Darji, S., Erdjument-Bromage, H., Neubert, T.A., Choi, J.Y., Wegiel, J., Lee, J.-H., and Nixon, R.A. (2023). Lysosomal dysfunction in Down syndrome and Alzheimer mouse models is caused by v-ATPase inhibition by Tyr682-phosphorylated APP βCTF. Sci Adv *9*, eadg1925. https://doi.org/10.1126/sciadv.adg1925.

69. Avrahami, L., Farfara, D., Shaham-Kol, M., Vassar, R., Frenkel, D., and Eldar-Finkelman, H. (2013). Inhibition of glycogen synthase kinase-3 ameliorates β-amyloid pathology and restores lysosomal acidification and mammalian target of rapamycin activity in the Alzheimer disease mouse model: in vivo and in vitro studies. J Biol Chem *288*, 1295–1306. https://doi.org/10.1074/jbc.M112.409250.

70. He, D.-L., Wu, Z., Jia, R.-J., Wu, T.-Y., Qiu, Y.-M., and Fan, Y.-G. (2026). AS1842856 Reduces β-Amyloid Burden via Inhibiting PLA2G4A-Mediated Lysosomal Dysfunction in APP/PS1 Mice. CNS Neurosci Ther *32*, e70910. https://doi.org/10.1002/cns.70910.

71. Sanyal, A., Novis, H.S., Gasser, E., Lin, S., and LaVoie, M.J. (2020). LRRK2 Kinase Inhibition Rescues Deficits in Lysosome Function Due to Heterozygous GBA1 Expression in Human iPSC-Derived Neurons. Front Neurosci *14*, 442. https://doi.org/10.3389/fnins.2020.00442.

72. Riederer, E., Mikusevic, V., Tang, T., Martin, L., Mindell, J.A., and Ren, D. (2025). TMEM175 does not function as a proton-selective ion channel to prevent lysosomal over-acidification. J Cell Biol *225*, e202501145. https://doi.org/10.1083/jcb.202501145.

73. Kang, H.T., Park, J.T., Choi, K., Kim, Y., Choi, H.J.C., Jung, C.W., Lee, Y.-S., and Park, S.C. (2017). Chemical screening identifies ATM as a target for alleviating senescence. Nat Chem Biol *13*, 616–623. https://doi.org/10.1038/nchembio.2342.

74. Deivasigamani, S., Thekkan, S., Vergara, H.M., Conolly, O., Cosden, M., Phan, T., Smith, S., Marcus, J., Uslaner, J., Venkat, D., et al. (2025). Multimodal Blood-Based Biomarker Panel Reveals Altered Lysosomal Ionic Content in Alzheimer's Disease. ACS Chem Biol *20*, 137–152. https://doi.org/10.1021/acschembio.4c00602.

75. Hui, L., Soliman, M.L., Geiger, N.H., Miller, N.M., Afghah, Z., Lakpa, K.L., Chen, X., and Geiger, J.D. (2019). Acidifying Endolysosomes Prevented Low-Density Lipoprotein-Induced Amyloidogenesis. J Alzheimers Dis *67*, 393–410. https://doi.org/10.3233/JAD-180941.

76. Garda, V.G., Debnath, M., Hodul, M., Mambou, E.A., Bruemmer, K.J., Burris, K.D., Limas, J.C., Kao, A.W., and Arkin, M. (2026). WNK Inhibitors Acidify Lysosomes and Enhance Lysosomal Proteolytic Activity. Preprint at Social Science Research Network, https://doi.org/10.2139/ssrn.6754482 https://doi.org/10.2139/ssrn.6754482.

77. Tong, B.C.-K., Wu, A.J., Huang, A.S., Dong, R., Malampati, S., Iyaswamy, A., Krishnamoorthi, S., Sreenivasmurthy, S.G., Zhu, Z., Su, C., et al. (2021). Lysosomal TPCN (two pore segment channel) inhibition ameliorates beta-amyloid pathology and mitigates memory impairment in Alzheimer disease. Autophagy *18*, 624–642. https://doi.org/10.1080/15548627.2021.1945220.

78. Lee, J.-H., Wolfe, D.M., Darji, S., McBrayer, M.K., Colacurcio, D.J., Kumar, A., Stavrides, P., Mohan, P.S., and Nixon, R.A. (2020). β2-adrenergic Agonists Rescue Lysosome

Acidification and Function in PSEN1 Deficiency by Reversing Defective ER-to-lysosome Delivery of ClC-7. J Mol Biol *432*, 2633–2650. https://doi.org/10.1016/j.jmb.2020.02.021.

79. Yu, H., Chen, J., Wang, F., Jia, D., Bi, S., Mao, Y., Zhang, Y., Gao, T., Yang, L., Du, J., et al. (2025). Capsaicin Alleviates Autophagy-Lysosomal Dysfunction via PPARA-Mediated V-ATPase Subunit ATP6V0E1 Signaling in 3xTg-AD Mice. Adv Sci e02707. https://doi.org/10.1002/advs.202502707.

80. Wallings, R., Connor-Robson, N., and Wade-Martins, R. (2019). LRRK2 interacts with the vacuolar-type H+-ATPase pump a1 subunit to regulate lysosomal function. Hum Mol Genet *28*, 2696–2710. https://doi.org/10.1093/hmg/ddz088.

81. Samaddar, M., Fitzgerald, G.A., Nguyen, A.H., Davis, S.S., Jain, S., Guo, J., Propson, N.E., van Lengerich, B., Shi, Y., Balasundar, S., et al. (2025). Lysosomal polyamine storage upon ATP13A2 loss impairs β-glucocerebrosidase via altered lysosomal pH and electrostatic hydrolase-lipid interactions. Cell Rep *44*, 116179. https://doi.org/10.1016/j.celrep.2025.116179.

82. Wang, F.-W., Zhao, F., Qian, X.-Y., Yu, Z.-Z., Zhao, J., Su, L., Zhang, Y., Zhang, S.-L., Zhao, B.-X., and Miao, J.-Y. (2014). Identification of a small molecule preventing BMSC senescence in vitro by improving intracellular homeostasis via ANXA7 and Hmbox1. RSC Adv *4*, 56722–56730. https://doi.org/10.1039/C4RA10404H.

83. Lee, Y., Miller, M.R., Fernandez, M.A., Berg, E.L., Prada, A.M., Ouyang, Q., Schmidt, M., Silverman, J.L., Young-Pearse, T.L., and Morrow, E.M. (2021). Early lysosome defects precede neurodegeneration with amyloid-β and tau aggregation in NHE6-null rat brain. Brain *145*, 3187–3202. https://doi.org/10.1093/brain/awab467.

84. Folts, C.J., Scott-Hewitt, N., Pröschel, C., Mayer-Pröschel, M., and Noble, M. (2016). Lysosomal Re-acidification Prevents Lysosphingolipid-Induced Lysosomal Impairment and Cellular Toxicity. PLOS Biol *14*, e1002583. https://doi.org/10.1371/journal.pbio.1002583.

85. Yao, X.C., Xue, X., Zhang, H.T., Zhu, M.M., Yang, X.W., Wu, C.F., and Yang, J.Y. (2019). Pseudoginsenoside-F11 alleviates oligomeric β-amyloid-induced endosome-lysosome defects in microglia. Traffic *20*, 61–70. https://doi.org/10.1111/tra.12620.

86. Nie, J., Jiang, L.-S., Zhang, Y., Tian, Y., Li, L.-S., Lu, Y.-L., Yang, W.-J., and Shi, J.-S. (2018). Dendrobium nobile Lindl. Alkaloids Decreases the Level of Intracellular β-Amyloid by Improving Impaired Autolysosomal Proteolysis in APP/PS1 Mice. Front Pharmacol *9*. https://doi.org/10.3389/fphar.2018.01479.

87. Wu, Y., Liu, X., Luo, G., Li, Q., Guo, B., Li, L., and Nie, J. (2025). DNLA Delayed the Appearance of Learning and Memory Impairment of APP/PS1 Mice: Involvement of mTOR/TFEB/v-ATPase Signaling Pathway. CNS Neurosci Ther *31*, e70300. https://doi.org/10.1111/cns.70300.

88. Liang, Y., Zheng, D., Peng, S., Lin, D., Jing, X., Zeng, Z., Chen, Y., Huang, K., Xie, Y., Zhou, T., et al. (2020). Rifampicin attenuates rotenone-treated microglia inflammation via improving lysosomal function. Toxicol In Vitro *63*, 104690. https://doi.org/10.1016/j.tiv.2019.104690.

89. Wang, L., Han, X., Qu, G., Su, L., Zhao, B., and Miao, J. (2018). A pH probe inhibits senescence in mesenchymal stem cells. Stem Cell Res Ther *9*, 343. https://doi.org/10.1186/s13287-018-1081-0.

90. Prieto, L.I., Graves, S.I., and Baker, D.J. (2020). Insights from In Vivo Studies of Cellular Senescence. Cells *9*, 954. https://doi.org/10.3390/cells9040954.

91. Huang, Y., Li, Y., Qu, Y., Zheng, Y., Ouyang, M., Zhang, Y., Lai, W., and Xu, Q. (2019). UVA-induced photoaging inhibits autophagic degradation by impairing lysosomal function in dermal fibroblasts. Biochem Biophys Res Commun *518*, 611–618. https://doi.org/10.1016/j.bbrc.2019.08.103.

92. Loo, T.M., Zhou, X., Tanaka, Y., Sugawara, S., Yamauchi, S., Kawasaki, H., Matsuoka, Y., Sugiura, Y., Sakuma, S., Yamanishi, Y., et al. (2025). Senescence-associated lysosomal

dysfunction impairs cystine deprivation-induced lipid peroxidation and ferroptosis. Nat Commun *16*, 6617. https://doi.org/10.1038/s41467-025-61894-9.

93. Li, W., Kawaguchi, K., Tanaka, S., He, C., Maeshima, Y., Suzuki, E., and Toi, M. (2023). Cellular senescence triggers intracellular acidification and lysosomal pH alkalinized via ATP6AP2 attenuation in breast cancer cells. Commun Biol *6*, 1147. https://doi.org/10.1038/s42003-023-05433-6.

94. Curnock, R., Yalci, K., Palmfeldt, J., Jäättelä, M., Liu, B., and Carroll, B. (2023). TFEB-dependent lysosome biogenesis is required for senescence. EMBO J *42*, e111241. https://doi.org/10.15252/embj.2022111241.

95. Burrinha, T., Martinsson, I., Gomes, R., Terrasso, A.P., Gouras, G.K., and Almeida, C.G. (2021). Upregulation of APP endocytosis by neuronal aging drives amyloid-dependent synapse loss. J Cell Sci *134*, jcs255752. https://doi.org/10.1242/jcs.255752.

96. Burrinha, T., Cunha, C., Hall, M.J., Lopes-da-Silva, M., Seabra, M.C., and Guimas Almeida, C. (2023). Deacidification of endolysosomes by neuronal aging drives synapse loss. Traffic *24*, 334–354. https://doi.org/10.1111/tra.12889.

97. Mollinari, C., Zhao, J., Lupacchini, L., Garaci, E., Merlo, D., and Pei, G. (2018). Transdifferentiation: a new promise for neurodegenerative diseases. Cell Death Dis *9*, 830. https://doi.org/10.1038/s41419-018-0891-4.

98. Chou, C.-C., Vest, R., Prado, M.A., Wilson-Grady, J., Paulo, J.A., Shibuya, Y., Moran-Losada, P., Lee, T.-T., Luo, J., Gygi, S.P., et al. (2025). Proteostasis and lysosomal repair deficits in transdifferentiated neurons of Alzheimer's disease. Nat Cell Biol *27*, 619–632. https://doi.org/10.1038/s41556-025-01623-y.

99. He, C., Zhou, C., and Kennedy, B.K. (2018). The yeast replicative aging model. Biochim Biophys Acta Mol Basis Dis *1864*, 2690–2696. https://doi.org/10.1016/j.bbadis.2018.02.023.

100. Ghavidel, A., Baxi, K., Prusinkiewicz, M., Swan, C., Belak, Z.R., Eskiw, C.H., Carvalho, C.E., and Harkness, T.A. (2018). Rapid Nuclear Exclusion of Hcm1 in Aging Saccharomyces cerevisiae Leads to Vacuolar Alkalization and Replicative Senescence. G3 (Bethesda) *8*, 1579–1592. https://doi.org/10.1534/g3.118.200161.

101. Ruckenstuhl, C., Netzberger, C., Entfellner, I., Carmona-Gutierrez, D., Kickenweiz, T., Stekovic, S., Gleixner, C., Schmid, C., Klug, L., Sorgo, A.G., et al. (2014). Lifespan Extension by Methionine Restriction Requires Autophagy-Dependent Vacuolar Acidification. PLoS Genet *10*, e1004347. https://doi.org/10.1371/journal.pgen.1004347.

102. Hashmi, F., and Kane, P.M. (2025). V-ATPase Disassembly at the Yeast Lysosome-Like Vacuole Is a Phenotypic Driver of Lysosome Dysfunction in Replicative Aging. Aging Cell *24,* 5. https://doi.org/10.1111/acel.14487.

103. Henderson, K.A., Hughes, A.L., and Gottschling, D.E. (2014). Mother-daughter asymmetry of pH underlies aging and rejuvenation in yeast. eLife *3*, e03504. https://doi.org/10.7554/eLife.03504.

104. Jeayeng, S., Thongsroy, J., and Chuaijit, S. (2024). Caenorhabditis elegans as a Model to Study Aging and Photoaging. Biomolecules *14*, 1235. https://doi.org/10.3390/biom14101235.

105. Baxi, K., and de Carvalho, C.E. (2018). Assessing Lysosomal Alkalinization in the Intestine of Live Caenorhabditis elegans. J Vis Exp, 57414. https://doi.org/10.3791/57414.

106. Imanikia, S., Özbey, N.P., Krueger, C., Casanueva, M.O., and Taylor, R.C. (2019). Neuronal XBP-1 Activates Intestinal Lysosomes to Improve Proteostasis in C. elegans. Curr Biol *29*, 2322-2338.e7. https://doi.org/10.1016/j.cub.2019.06.031.

107. Sun, Y., Li, M., Zhao, D., Li, X., Yang, C., and Wang, X. (2020). Lysosome activity is modulated by multiple longevity pathways and is important for lifespan extension in C. elegans. eLife *9*, e55745. https://doi.org/10.7554/eLife.55745.

108. Yin, X., Dai, F., Ran, D., Zhang, Y., Qu, Z., and Zheng, S. (2024). Cysteine protease cathepsin B promotes lysosome integrity to extend the lifespan of alternative day fasting worms. Aging Cell *23*, e14286. https://doi.org/10.1111/acel.14286.

109. Baxi, K., Ghavidel, A., Waddell, B., Harkness, T.A., and de Carvalho, C.E. (2017). Regulation of Lysosomal Function by the DAF-16 Forkhead Transcription Factor Couples Reproduction to Aging in Caenorhabditis elegans. Genetics *207*, 83–101. https://doi.org/10.1534/genetics.117.204222.

110. Ansari, M.Y., Ball, H.C., Wase, S.J., Novak, K., and Haqqi, T.M. (2021). Lysosomal dysfunction in osteoarthritis and aged cartilage triggers apoptosis in chondrocytes through BAX mediated release of Cytochrome c. Osteoarthr Cartil *29*, 100–112. https://doi.org/10.1016/j.joca.2020.08.014.

111. Truschel, S.T., Clayton, D.R., Beckel, J.M., Yabes, J.G., Yao, Y., Wolf-Johnston, A., Birder, L.A., and Apodaca, G. (2018). Age-related endolysosome dysfunction in the rat urothelium. PLOS ONE *13*, e0198817. https://doi.org/10.1371/journal.pone.0198817.

112. Narayanaswamy, N., Chakraborty, K., Saminathan, A., Zeichner, E., Leung, K., Devany, J., and Krishnan, Y. (2019). A pH-correctable, DNA-based fluorescent reporter for organellar calcium. Nat Methods *16*, 95–102. https://doi.org/10.1038/s41592-018-0232-7.

113. Prasad, H., and Rao, R. (2018). Amyloid clearance defect in ApoE4 astrocytes is reversed by epigenetic correction of endosomal pH. Proc Natl Acad Sci U S A *115*, E6640–E6649. https://doi.org/10.1073/pnas.1801612115.

114. Krogsaeter, E.K., McKetney, J., Valiente-Banuet, L., Marquez, A., Willis, A., Cakir, Z., Stevenson, E., Jang, G.M., Rao, A., Li, E., et al. (2025). Lysosomal proteomics reveals mechanisms of neuronal APOE4-associated lysosomal dysfunction. Autophagy *21*, 3240–3265. https://doi.org/10.1080/15548627.2025.2576613.

115. Satoh, J., Yamamoto, Y., Asahina, N., Kitano, S., and Kino, Y. (2014). RNA-Seq Data Mining: Downregulation of NeuroD6 Serves as a Possible Biomarker for Alzheimer's Disease Brains. Dis Markers *2014*, 123165. https://doi.org/10.1155/2014/123165.

116. Wang, M., Li, A., Sekiya, M., Beckmann, N.D., Quan, X., Schrode, N., Fernando, M.B., Yu, A., Zhu, L., Cao, J., et al. (2021). Transformative Network Modeling of Multi-omics Data Reveals Detailed Circuits, Key Regulators, and Potential Therapeutics for Alzheimer's Disease. Neuron *109*, 257-272.e14. https://doi.org/10.1016/j.neuron.2020.11.002.

117. Zhou, Z., Bai, J., Zhong, S., Zhang, R., Kang, K., Zhang, X., Xu, Y., Zhao, C., and Zhao, M. (2021). Downregulation of ATP6V1A Involved in Alzheimer's Disease via Synaptic Vesicle Cycle, Phagosome, and Oxidative Phosphorylation. Oxid Med Cell Longev *2021*, 5555634. https://doi.org/10.1155/2021/5555634.

118. Zi, Z., Zhang, Z., Feng, Q., Kim, C., Wang, X.-D., Scherer, P.E., Gao, J., Levine, B., and Yu, Y. (2022). Quantitative phosphoproteomic analyses identify STK11IP as a lysosome-specific substrate of mTORC1 that regulates lysosomal acidification. Nat Commun *13*, 1760. https://doi.org/10.1038/s41467-022-29461-8.

119. Ma, K., Bin, N.-R., Shi, S., Harada, H., Wada, Y., Wada, G.-H.-S., Monnier, P.P., Sugita, S., and Zhang, L. (2019). Observations From a Mouse Model of Forebrain Voa1 Knockout: Focus on Hippocampal Structure and Function. Front. Cell Neurosci *13*. https://doi.org/10.3389/fncel.2019.00484.

120. Coffey, E.E., Beckel, J.M., Laties, A.M., and Mitchell, C.H. (2014). Lysosomal alkalization and dysfunction in human fibroblasts with the Alzheimer's disease-linked presenilin 1 A246E mutation can be reversed with cAMP. Neuroscience *263*, 111–124. https://doi.org/10.1016/j.neuroscience.2014.01.001.

121. Jiang, Y., Sato, Y., Im, E., Berg, M., Bordi, M., Darji, S., Kumar, A., Mohan, P.S., Bandyopadhyay, U., Diaz, A., et al. (2019). Lysosomal Dysfunction in Down Syndrome Is

APP-Dependent and Mediated by APP-βCTF (C99). J Neurosci *39*, 5255–5268. https://doi.org/10.1523/JNEUROSCI.0578-19.2019.

122. Long, Z., Ge, C., Zhao, Y., Liu, Y., Zeng, Q., Tang, Q., Dong, Z., and He, G. (2025). Enhanced autophagic clearance of amyloid-β via histone deacetylase 6-mediated V-ATPase assembly and lysosomal acidification protects against Alzheimer's disease in vitro and in vivo. Neural Regen Res *20*, 2633. https://doi.org/10.4103/NRR.NRR-D-23-01633.

123. Ge, C., Wang, K., Tang, H., Ke, Y., Wang, H., Fu, Q., Xiu, Y., Guo, Y., Jia, Y.-F., Long, Z., et al. (2026). NDST3 suppression restores lysosomal acidification and ameliorates amyloid-β and MAPT/tau pathology in Alzheimer's disease. Transl Neurodegener *15*, 16. https://doi.org/10.1186/s40035-026-00549-1.

124. Tong, B.C.-K., Huang, A.S., Wu, A.J., Iyaswamy, A., Ho, O.K.-Y., Kong, A.H.-Y., Sreenivasmurthy, S.G., Zhu, Z., Su, C., Liu, J., et al. (2022). Tetrandrine ameliorates cognitive deficits and mitigates tau aggregation in cell and animal models of tauopathies. J Biomed Sci *29*, 85. https://doi.org/10.1186/s12929-022-00871-6.

125. Ye, C.-Y., Zeng, P., Liu, Y.-C., Shi, Y., Liu, G.-P., Wang, J.-Z., Zhou, X.-W., and Tian, Q. (2023). Tau overload associated insufficient lysosomal hydrolysis activity through deacidification of lysosomes. ResearchSquare. https://doi.org/10.21203/rs.3.rs-3294833/v1.

126. Rose, K., Jepson, T., Shukla, S., Maya-Romero, A., Kampmann, M., Xu, K., and Hurley, J.H. (2024). Tau fibrils induce nanoscale membrane damage and nucleate cytosolic tau at lysosomes. Proc Natl Acad Sci U S A *121*, e2315690121. https://doi.org/10.1073/pnas.2315690121.

127. Kaur, B., Nada, H., Zhang, L., and Gabr, M. (2026). Structure-Guided Optimization of CHI3L1 Modulators Reveals G721–0377 as a Lead Compound for Restoring Astrocyte Function in Alzheimer's Disease. ACS Bio Med Chem Au. https://doi.org/10.1021/acsbiomedchemau.5c00279.

128. Wang, M.-X., Cheng, X.-Y., Jin, M., Cao, Y.-L., Yang, Y.-P., Wang, J.-D., Li, Q., Wang, F., Hu, L.-F., and Liu, C.-F. (2015). TNF compromises lysosome acidification and reduces α-synuclein degradation via autophagy in dopaminergic cells. Exp Neurol *271*, 112–121. https://doi.org/10.1016/j.expneurol.2015.05.008.

129. Leng, K., Rooney, B., McCarthy, F., Xia, W., Rose, I.V.L., Bax, S., Chin, M., Fathi, S., Herrington, K.A., Leonetti, M., et al. (2024). mTOR activation induces endolysosomal remodeling and nonclassical secretion of IL-32 via exosomes in inflammatory reactive astrocytes. J Neuroinflammation *21*, 198. https://doi.org/10.1186/s12974-024-03165-w.

130. Lee, J.-H., Yu, W.H., Kumar, A., Lee, S., Mohan, P.S., Peterhoff, C.M., Wolfe, D.M., Martinez-Vicente, M., Massey, A.C., Sovak, G., et al. (2010). Lysosomal Proteolysis and Autophagy Require Presenilin 1 and Are Disrupted by Alzheimer-Related PS1 Mutations. Cell *141*, 1146–1158. https://doi.org/10.1016/j.cell.2010.05.008.

131. Lee, J.-H., McBrayer, M.K., Wolfe, D.M., Haslett, L.J., Kumar, A., Sato, Y., Lie, P.P.Y., Mohan, P., Coffey, E.E., Kompella, U., et al. (2015). Presenilin 1 Maintains Lysosomal Ca2+ Homeostasis via TRPML1 by Regulating vATPase-Mediated Lysosome Acidification. Cell Reports *12*, 1430–1444. https://doi.org/10.1016/j.celrep.2015.07.050.

132. Serafini, S., Ferretti, G., Monterosso, P., Angiolillo, A., Di Costanzo, A., and Matrone, C. (2024). TNF-α Levels Are Increased in Patients with Subjective Cognitive Impairment and Are Negatively Correlated with β Amyloid-42. Antioxidants (Basel) *13*, 216. https://doi.org/10.3390/antiox13020216.

133. Xue, Z., Zhao, H., Liu, J., Han, J., and Han, S. (2017). Imaging Lysosomal pH Alteration in Stressed Cells with a Sensitive Ratiometric Fluorescence Sensor. ACS Sens *2*, 436–442. https://doi.org/10.1021/acssensors.7b00035.

134. Pase, M.P., Himali, J.J., Puerta, R., Beiser, A.S., Gonzales, M.M., Satizabal, C.L., Yang, Q., Aparicio, H.J., Kojis, D.J., Decarli, C.S., et al. (2024). Association of Plasma YKL-40 With

MRI, CSF, and Cognitive Markers of Brain Health and Dementia. Neurology *102*, e208075. https://doi.org/10.1212/WNL.0000000000208075.

135. Korvatska, O., Strand, N.S., Berndt, J.D., Strovas, T., Chen, D.-H., Leverenz, J.B., Kiianitsa, K., Mata, I.F., Karakoc, E., Greenup, J.L., et al. (2013). Altered splicing of ATP6AP2 causes X-linked parkinsonism with spasticity (XPDS). Hum Mol Genet *22*, 3259–3268. https://doi.org/10.1093/hmg/ddt180.

136. Hirose, T., Cabrera-Socorro, A., Chitayat, D., Lemonnier, T., Féraud, O., Cifuentes-Diaz, C., Gervasi, N., Mombereau, C., Ghosh, T., Stoica, L., et al. (2019). *ATP6AP2* variant impairs CNS development and neuronal survival to cause fulminant neurodegeneration. J Clin Invest *129*, 2145–2162. https://doi.org/10.1172/JCI79990.

137. Malpartida, A.B., Williamson, M., Narendra, D.P., Wade-Martins, R., and Ryan, B.J. (2021). Mitochondrial Dysfunction and Mitophagy in Parkinson's Disease: From Mechanism to Therapy. Trends Biochem Sci *46*, 329–343. https://doi.org/10.1016/j.tibs.2020.11.007.

138. Nascimento, A.C., Erustes, A.G., Reckziegel, P., Bincoletto, C., Ureshino, R.P., Pereira, G.J.S., and Smaili, S.S. (2020). α-Synuclein Overexpression Induces Lysosomal Dysfunction and Autophagy Impairment in Human Neuroblastoma SH-SY5Y. Neurochem Res *45*, 2749–2761. https://doi.org/10.1007/s11064-020-03126-8.

139. Lo, C.H., Ren, M., Loi, G.W.Z., Saipuljumri, E.N., Indajang, J., Lim, K.L., and Zeng, J. (2026). Lysosome-Acidifying Nanoparticles Rescue A30P α-Synuclein Induced Neuronal Death in Cellular and Drosophila Models of Parkinson's Disease. Adv Healthc Mater e02906. https://doi.org/10.1002/adhm.202502906.

140. Arotcarena, M.-L., Soria, F.N., Cunha, A., Doudnikoff, E., Prévot, G., Daniel, J., Blanchard-Desce, M., Barthélémy, P., Bezard, E., Crauste-Manciet, S., et al. (2022). Acidic nanoparticles protect against α-synuclein-induced neurodegeneration through the restoration of lysosomal function. Aging Cell *21*, e13584. https://doi.org/10.1111/acel.13584.

141. Wang, Y., Ma, Z., Jin, Z., Kou, L., Xiong, N., Wang, T., and Xia, Y. (2026). Dysregulation of the TFEB-ATP6V0C axis in microglia exacerbates α-synuclein pathology through impaired lysosomal acidification in Parkinson's disease. Cell Death Differ, 1–17. https://doi.org/10.1038/s41418-026-01800-y.

142. Sanyal, A., DeAndrade, M.P., Novis, H.S., Lin, S., Chang, J., Lengacher, N., Tomlinson, J.J., Tansey, M.G., and LaVoie, M.J. (2020). Lysosome and Inflammatory Defects in GBA1-Mutant Astrocytes Are Normalized by LRRK2 Inhibition. Mov Disord *35*, 760–773. https://doi.org/10.1002/mds.27994.

143. Navarro-Romero, A., Fernandez-Gonzalez, I., Riera, J., Montpeyo, M., Albert-Bayo, M., Lopez-Royo, T., Castillo-Sanchez, P., Carnicer-Caceres, C., Arranz-Amo, J.A., Castillo-Ribelles, L., et al. (2022). Lysosomal lipid alterations caused by glucocerebrosidase deficiency promote lysosomal dysfunction, chaperone-mediated-autophagy deficiency, and alpha-synuclein pathology. NPJ Parkinsons Dis *8*, 126. https://doi.org/10.1038/s41531-022-00397-6.

144. Pascual, A., Moulka, T., de Fàbregues, O., Repossi, R., García-Ruiz, P.J., Ortolano, S., De Lucca, M., Vela-Desojo, L., Alves-Villar, M., Frías, M., et al. (2025). Lysosomal Network Defects in Early-Onset Parkinson's Disease Patients Carrying Rare Variants in Lysosomal Hydrolytic Enzyme Genes. Int J Mol Sci *26*, 9454. https://doi.org/10.3390/ijms26199454.

145. Cheng, C., Yang, H., Tian, L., Ni, Y., Jia, C., Le, W., and Wang, Q. (2025). Nurr1 deficiency impairs autophagy-lysosomal function through GBA-dependent transcriptional regulation in Parkinson's disease pathogenesis. Front. Aging Neurosci *17*. https://doi.org/10.3389/fnagi.2025.1612389.

146. Zeng, J., Martin, A., Han, X., Shirihai, O.S., and Grinstaff, M.W. (2019). Biodegradable PLGA nanoparticles restore lysosomal acidity and protect neural PC-12 cells against mitochondrial toxicity. Ind Eng Chem Res *58*, 13910–13917. https://doi.org/10.1021/acs.iecr.9b02003.

147. Pascua-Maestro, R., Diez-Hermano, S., Lillo, C., Ganfornina, M.D., and Sanchez, D. (2017). Protecting cells by protecting their vulnerable lysosomes: Identification of a new mechanism for preserving lysosomal functional integrity upon oxidative stress. PLOS Genetics *13*, e1006603. https://doi.org/10.1371/journal.pgen.1006603.

148. Schapansky, J., Khasnavis, S., DeAndrade, M.P., Nardozzi, J.D., Falkson, S.R., Boyd, J.D., Sanderson, J.B., Bartels, T., Melrose, H.L., and LaVoie, M.J. (2018). Familial knockin mutation of LRRK2 causes lysosomal dysfunction and accumulation of endogenous insoluble α-synuclein in neurons. Neurobiol Dis *111*, 26–35. https://doi.org/10.1016/j.nbd.2017.12.005.

149. Banerjee, R., Santhoshkumar, R., Holla, V., Kamble, N., Yadav, R., Pal, P.K., and Datta, I. (2026). LRRK2 I1371V Mutation Drives Astrocytic Glucose Metabolism Failure and Induces Integrated ER–Mitochondria–Lysosome Dysfunction in Parkinson's Disease. Int J Mol Sci https://doi.org/10.3390/ijms27083463.

150. Henry, A.G., Aghamohammadzadeh, S., Samaroo, H., Chen, Y., Mou, K., Needle, E., and Hirst, W.D. (2015). Pathogenic LRRK2 mutations, through increased kinase activity, produce enlarged lysosomes with reduced degradative capacity and increase ATP13A2 expression. Hum Mol Genet *24*, 6013–6028. https://doi.org/10.1093/hmg/ddv314.

151. Maloney, M.T., Wang, X., Ghosh, R., Andrews, S.V., Maciuca, R., Masoud, S.T., Agam, M., Caprioli, R.M., Astarita, G., Bondar, V.V., et al. (2025). LRRK2 kinase activity regulates Parkinson's disease-relevant lipids at the lysosome. Mol Neurodegeneration *20*, 89. https://doi.org/10.1186/s13024-025-00880-7.

152. Wie, J., Liu, Z., Song, H., Tropea, T.F., Yang, L., Wang, H., Liang, Y., Cang, C., Aranda, K., Lohmann, J., et al. (2021). A growth-factor-activated lysosomal K+ channel regulates Parkinson's pathology. Nature *591*, 431–437. https://doi.org/10.1038/s41586-021-03185-z.

153. Jinn, S., Blauwendraat, C., Toolan, D., Gretzula, C.A., Drolet, R.E., Smith, S., Nalls, M.A., Marcus, J., Singleton, A.B., and Stone, D.J. (2019). Functionalization of the TMEM175 p.M393T variant as a risk factor for Parkinson disease. Hum Mol Genet *28*, 3244–3254. https://doi.org/10.1093/hmg/ddz136.

154. Li, Y., Wang, Y., Kou, L., Yin, S., Chi, X., Sun, Y., Wu, J., Jin, Z., Zhou, Q., Zou, W., et al. (2024). Plasma exosomes impair microglial degradation of α-synuclein through V-ATPase subunit V1G1. CNS Neurosci Ther *30*, e14738. https://doi.org/10.1111/cns.14738.

155. Singleton, A.B., Farrer, M., Johnson, J., Singleton, A., Hague, S., Kachergus, J., Hulihan, M., Peuralinna, T., Dutra, A., Nussbaum, R., et al. (2003). alpha-Synuclein locus triplication causes Parkinson's disease. Science *302*, 841. https://doi.org/10.1126/science.1090278.

156. Ferese, R., Modugno, N., Campopiano, R., Santilli, M., Zampatti, S., Giardina, E., Nardone, A., Postorivo, D., Fornai, F., Novelli, G., et al. (2015). Four Copies of SNCA Responsible for Autosomal Dominant Parkinson's Disease in Two Italian Siblings. Parkinsons Dis *2015*, 546462. https://doi.org/10.1155/2015/546462.

157. Tanner, C.M., Kamel, F., Ross, G.W., Hoppin, J.A., Goldman, S.M., Korell, M., Marras, C., Bhudhikanok, G.S., Kasten, M., Chade, A.R., et al. (2011). Rotenone, Paraquat, and Parkinson's Disease. Environ Health Perspect *119*, 866–872. https://doi.org/10.1289/ehp.1002839.

158. AlShimemeri, S., Di Luca, D.G., and Fox, S.H. (2021). MPTP Parkinsonism and Implications for Understanding Parkinson's Disease. Mov Disord Clin Pract *9*, 42–47. https://doi.org/10.1002/mdc3.13344.

159. Lambert, C.E., and Bondy, S.C. (1989). Effects of MPTP, MPP+ and paraquat on mitochondrial potential and oxidative stress. Life Sci *44*, 1277–1284. https://doi.org/10.1016/0024-3205(89)90365-2.

160. van Veen, S., Martin, S., Van den Haute, C., Benoy, V., Lyons, J., Vanhoutte, R., Kahler, J.P., Decuypere, J.-P., Gelders, G., Lambie, E., et al. (2020). ATP13A2 deficiency disrupts lysosomal polyamine export. Nature *578*, 419–424. https://doi.org/10.1038/s41586-020-1968-7.

161. Sheshadri, P., Costa-Besada, M.A., Fisher, A., Kiraly, S., Singh, K., Kourouzidou, I., Blacker, T.S., Zeng, J., Shirihai, O.S., Grinstaff, M.W., et al. (2026). Targeting lysosomal pH restores mitochondrial quality control in GBA1-mutant Parkinson's disease. Transl Neurodegener *15*, 27. https://doi.org/10.1186/s40035-026-00559-z.

162. Cox, B.E., Griffin, E.E., Ullery, J.C., and Gray, J.W. (2007). Effects of cellular cholesterol loading on macrophage foam cell lysosome acidifications. J Lipid Res *48*, 1012–1021. https://doi.org/10.1194/jlr.M600390-JLR200.

163. Karatas, M., Dogan, S., Spahiu, E., Ašić, A., Bešić, L., and Turan, Y. (2020). Enzyme kinetics and inhibition parameters of human leukocyte glucosylceramidase. Heliyon *6*, e05191. https://doi.org/10.1016/j.heliyon.2020.e05191.

164. Yu, K., Toral-Barza, L., Shi, C., Zhang, W.-G., Lucas, J., Shor, B., Kim, J., Verheijen, J., Curran, K., Malwitz, D.J., et al. (2009). Biochemical, cellular, and in vivo activity of novel ATP-competitive and selective inhibitors of the mammalian target of rapamycin. Cancer Res *69*, 6232–6240. https://doi.org/10.1158/0008-5472.CAN-09-0299.

165. Zhang, J., Zeng, W., Han, Y., Lee, W.-R., Liou, J., and Jiang, Y. (2023). Lysosomal LAMP proteins regulate lysosomal pH by direct inhibition of the TMEM175 channel. Mol Cell *83*, 2524-2539.e7. https://doi.org/10.1016/j.molcel.2023.06.004.

166. Zhu, X., Ping, M., Liu, H., Yu, T., Jiang, Z., Liu, Z., Li, C., Hou, X., Chu, Q., Li, S., et al. (2025). Structural insights into the activation of TMEM175 by small molecule. Neuron *0*. https://doi.org/10.1016/j.neuron.2025.07.029.

167. Mackenzie, I.R.A., and H. Feldman, H. (2005). Ubiquitin Immunohistochemistry Suggests Classic Motor Neuron Disease, Motor Neuron Disease With Dementia, and Frontotemporal Dementia of the Motor Neuron Disease Type Represent a Clinicopathologic Spectrum: J Neuropathol Exp Neurol *64*, 730–739. https://doi.org/10.1097/01.jnen.0000174335.27708.0a.

168. Logan, T., Simon, M.J., Rana, A., Cherf, G.M., Srivastava, A., Davis, S.S., Low, R.L.Y., Chiu, C.-L., Fang, M., Huang, F., et al. (2021). Rescue of a lysosomal storage disorder caused by Grn loss of function with a brain penetrant progranulin biologic. Cell *184*, 4651-4668.e25. https://doi.org/10.1016/j.cell.2021.08.002.

169. Hasan, S., Fernandopulle, M.S., Humble, S.W., Frankenfield, A.M., Li, H., Prestil, R., Johnson, K.R., Ryan, B.J., Wade-Martins, R., Ward, M.E., et al. (2023). Multi-modal proteomic characterization of lysosomal function and proteostasis in progranulin-deficient neurons. Mol Neurodegener *18*, 87. https://doi.org/10.1186/s13024-023-00673-w.

170. Chen-Plotkin, A.S., Unger, T.L., Gallagher, M.D., Bill, E., Kwong, L.K., Volpicelli-Daley, L., Busch, J.I., Akle, S., Grossman, M., Van Deerlin, V., et al. (2012). TMEM106B, the Risk Gene for Frontotemporal Dementia, Is Regulated by the microRNA-132/212 Cluster and Affects Progranulin Pathways. J Neurosci *32*, 11213–11227. https://doi.org/10.1523/JNEUROSCI.0521-12.2012.

171. Busch, J.I., Unger, T.L., Jain, N., Tyler Skrinak, R., Charan, R.A., and Chen-Plotkin, A.S. (2016). Increased expression of the frontotemporal dementia risk factor TMEM106B causes C9orf72-dependent alterations in lysosomes. Hum Mol Genet *25*, 2681–2697. https://doi.org/10.1093/hmg/ddw127.

172. Chung, C.W., Zhou, A.J., Mela, I., Stephens, A.D., Miyashita, A., George-Hyslop, P.H.S., Kaminski, C.F., Knowles, T.P.J., and Schierle, G.S.K. (2022). Intracellular FUS protein accumulation leads to cytoskeletal, organelle and cellular homeostasis perturbations.

Preprint at bioRxiv, https://doi.org/10.1101/2022.10.04.510756 https://doi.org/10.1101/2022.10.04.510756.

173. Romano, R., Del Fiore, V.S., Ruotolo, G., Mazzoni, M., Rosati, J., Conforti, F.L., and Bucci, C. (2025). Lysosomal Dysfunction in Amyotrophic Lateral Sclerosis: A Familial Case Linked to the p.G376D TARDBP Mutation. Int J Mol Sci *26*, 2867. https://doi.org/10.3390/ijms26072867.

174. Bicchi, I., Morena, F., Argentati, C., Nodari, L.R., Emiliani, C., Gelati, M., Vescovi, A.L., and Martino, S. (2021). Storage of Mutant Human SOD1 in Non-Neural Cells from the Type-1 Amyotrophic Lateral Sclerosis ratG93A Model Correlated with the Lysosomes' Dysfunction. Biomedicines *9*, 1080. https://doi.org/10.3390/biomedicines9091080.

175. Klickstein, J.A., Johnson, M.A., Antonoudiou, P., Maguire, J., Paulo, J.A., Gygi, S.P., Weihl, C., and Raman, M. (2024). ALS-related p97 R155H mutation disrupts lysophagy in iPSC-derived motor neurons. Stem Cell Rep *19*, 366–382. https://doi.org/10.1016/j.stemcr.2024.01.002.

176. Clarke, B.E., Ziff, O.J., Tyzack, G., Petrić Howe, M., Wang, Y., Klein, P., Smith, C.A., Hall, C.A., Helmy, A., Howell, M., et al. (2024). Human VCP mutant ALS/FTD microglia display immune and lysosomal phenotypes independently of GPNMB. Mol Neurodegeneration *19*, 90. https://doi.org/10.1186/s13024-024-00773-1.

177. Baker, M., Mackenzie, I.R., Pickering-Brown, S.M., Gass, J., Rademakers, R., Lindholm, C., Snowden, J., Adamson, J., Sadovnick, A.D., Rollinson, S., et al. (2006). Mutations in progranulin cause tau-negative frontotemporal dementia linked to chromosome 17. Nature *442*, 916–919. https://doi.org/10.1038/nature05016.

178. Cruts, M., Gijselinck, I., van der Zee, J., Engelborghs, S., Wils, H., Pirici, D., Rademakers, R., Vandenberghe, R., Dermaut, B., Martin, J.-J., et al. (2006). Null mutations in progranulin

cause ubiquitin-positive frontotemporal dementia linked to chromosome 17q21. Nature *442*, 920–924. https://doi.org/10.1038/nature05017.

179. Tanaka, Y., Suzuki, G., Matsuwaki, T., Hosokawa, M., Serrano, G., Beach, T.G., Yamanouchi, K., Hasegawa, M., and Nishihara, M. (2017). Progranulin regulates lysosomal function and biogenesis through acidification of lysosomes. Hum Mol Genet *26*, 969–988. https://doi.org/10.1093/hmg/ddx011.

180. Park, C.B., Lee, C.H., Kang, G.M., Min, S.H., and Kim, M.-S. (2025). Microglial progranulin differently regulates hypothalamic lysosomal function in lean and obese conditions via cleavage-dependent mechanisms. J Neuroinflammation *22*, 68. https://doi.org/10.1186/s12974-025-03370-1.

181. Wang, Z., Chen, Y., He, W., Liu, Y., Jiao, Y., Wang, G., Guan, J., Zhao, K., Zhang, Q., Gao, F., et al. (2025). Progranulin-driven lysosomal acidification facilitates exocytosis of PHEV-hijacked lysosomes for viral release. mBio *17*, e02903-25. https://doi.org/10.1128/mbio.02903-25.

182. Bulfon, D., Breithofer, J., Grabner, G.F., Fawzy, N., Pirchheim, A., Wolinski, H., Kolb, D., Hartig, L., Tischitz, M., Zitta, C., et al. (2024). Functionally overlapping intra- and extralysosomal pathways promote bis(monoacylglycero)phosphate synthesis in mammalian cells. Nat Commun *15*, 9937. https://doi.org/10.1038/s41467-024-54213-1.

183. Replogle, J.M., Marks, J.D., Fernandez, M.G., Yuan, H., Yu, D., Winters, E., Jawahar, V.M., Deshmukh, R., Sutanto, R., Kowal, I., et al. (2026). Neurodegeneration risk variants promote lysosomal TMEM106B fibril accumulation. bioRxiv, 2026.03.26.714634. https://doi.org/10.64898/2026.03.26.714634.

184. Klein, Z.A., Takahashi, H., Ma, M., Stagi, M., Zhou, M., Lam, T.T., and Strittmatter, S.M. (2017). Loss of TMEM106B Ameliorates Lysosomal and Frontotemporal Dementia-Related

Phenotypes in Progranulin-Deficient Mice. Neuron *95*, 281-296.e6. https://doi.org/10.1016/j.neuron.2017.06.026.

185. Ferrari, V., Cristofani, R., Cicardi, M.E., Tedesco, B., Crippa, V., Chierichetti, M., Casarotto, E., Cozzi, M., Mina, F., Galbiati, M., et al. (2022). Pathogenic variants of Valosin-containing protein induce lysosomal damage and transcriptional activation of autophagy regulators in neuronal cells. Neuropathol Appl Neurobiol *48*, e12818. https://doi.org/10.1111/nan.12818.

186. Wang, J., Dai, L., and Zhang, Z. (2025). Protein aggregation in neurodegenerative diseases. Chin Med J (Engl) *138*, 2753–2768. https://doi.org/10.1097/CM9.0000000000003802.

187. Forlenza, O.V., and Barbosa, B.J.A.P. (2025). What are the reasons for the repeated failures of clinical trials with anti-amyloid drugs for AD treatment? Dement Neuropsychol *19*, e2025E001. https://doi.org/10.1590/1980-5764-DN-2025-E001.

188. D, P., C, G., Ml, T., S, D., and C, M. (2017). Inhibitors of protein aggregates as novel drugs in neurodegenerative diseases. Glob Drugs Therap *2*. https://doi.org/10.15761/GDT.1000119.

189. Dhiman, R., and Bhutia, S.K. (2023). Autophagy Processes and Mechanisms (Academic Press).

190. Nixon, R.A., and Rubinsztein, D.C. (2024). Mechanisms of autophagy–lysosome dysfunction in neurodegenerative diseases. Nat Rev Mol Cell Biol *25*, 926–946. https://doi.org/10.1038/s41580-024-00757-5.

191. Sun, Y., Li, M., Zhao, D., Li, X., Yang, C., and Wang, X. (2020). Lysosome activity is modulated by multiple longevity pathways and is important for lifespan extension in C. elegans. eLife. https://doi.org/10.7554/eLife.55745.

192. Zhong, R., and Richardson, C.E. (2025). Expansion of lysosomal capacity in early adult neurons driven by TFEB/HLH-30 protects dendrite maintenance during aging in

Caenorhabditis elegans. PLOS Biology *23*, e3002957. https://doi.org/10.1371/journal.pbio.3002957.

193. Hou, Y., Dan, X., Babbar, M., Wei, Y., Hasselbalch, S.G., Croteau, D.L., and Bohr, V.A. (2019). Ageing as a risk factor for neurodegenerative disease. Nat Rev Neurol *15*, 565–581. https://doi.org/10.1038/s41582-019-0244-7.

194. Marshansky, V., Rubinstein, J.L., and Grüber, G. (2014). Eukaryotic V-ATPase: Novel structural findings and functional insights. Biochim Biophys Acta Bioenerg *1837*, 857–879. https://doi.org/10.1016/j.bbabio.2014.01.018.

195. Song, Q., Meng, B., Xu, H., and Mao, Z. (2020). The emerging roles of vacuolar-type ATPase-dependent Lysosomal acidification in neurodegenerative diseases. Transl Neurodegener *9*, 17. https://doi.org/10.1186/s40035-020-00196-0.

196. Banay-Schwartz, M., Bracco, F., Dahl, D., DeGuzman, T., Turk, V., and Lajtha, A. (1985). The pH dependence of breakdown of various purified brain proteins by cathepsin D preparations. Neurochem Int *7*, 607–614. https://doi.org/10.1016/0197-0186(85)90057-9.

197. Lee, J.-H., Yang, D.-S., Goulbourne, C.N., Im, E., Stavrides, P., Pensalfini, A., Chan, H., Bouchet-Marquis, C., Bleiwas, C., Berg, M.J., et al. (2022). Faulty autolysosome acidification in Alzheimer's disease mouse models induces autophagic build-up of Aβ in neurons, yielding senile plaques. Nat Neurosci *25*, 688–701. https://doi.org/10.1038/s41593-022-01084-8.

198. Chin, M.Y., Patwardhan, A.R., Ang, K.-H., Wang, A.L., Alquezar, C., Welch, M., Nguyen, P.T., Grabe, M., Molofsky, A.V., Arkin, M.R., et al. (2021). Genetically Encoded, pH-Sensitive mTFP1 Biosensor for Probing Lysosomal pH. ACS Sens *6*, 2168–2180. https://doi.org/10.1021/acssensors.0c02318.

199. Xicoy, H., Wieringa, B., and Martens, G.J.M. (2017). The SH-SY5Y cell line in Parkinson's disease research: a systematic review. Mol Neurodegeneration *12*, 10. https://doi.org/10.1186/s13024-017-0149-0.

200. Mauvezin, C., and Neufeld, T.P. (2015). Bafilomycin A1 disrupts autophagic flux by inhibiting both V-ATPase-dependent acidification and Ca-P60A/SERCA-dependent autophagosome-lysosome fusion. Autophagy *11*, 1437–1438. https://doi.org/10.1080/15548627.2015.1066957.

201. Gokhale, P., Bhagwat, S., Crew, A., Cooke, A., Mantis, C., Workman, J., Landfair, D., Bittner, M., Sennello, R., Hart, K., et al. (2009). Abstract #3712: OXA-01, a novel potent mTORC1/TORC2 inhibitor displays improved anti-tumor activity in comparison to rapamycin, an mTORC1 selective inhibitor. Cancer Res *69*, 3712.

202. Yamada, K., Park, H.-M., Rigel, D.F., DiPetrillo, K., Whalen, E.J., Anisowicz, A., Beil, M., Berstler, J., Brocklehurst, C.E., Burdick, D.A., et al. (2016). Small-molecule WNK inhibition regulates cardiovascular and renal function. Nat Chem Biol *12*, 896–898. https://doi.org/10.1038/nchembio.2168.

203. Kim, M.H., Tsuhako, A.L., Co, E.W., Aftab, D.T., Bentzien, F., Chen, J., Cheng, W., Engst, S., Goon, L., Klein, R.R., et al. (2012). The design, synthesis, and biological evaluation of potent receptor tyrosine kinase inhibitors. Bioorg Med Chem Lett *22*, 4979–4985. https://doi.org/10.1016/j.bmcl.2012.06.029.

204. Goyal, L., Shi, L., Liu, L.Y., Fece de la Cruz, F., Lennerz, J.K., Raghavan, S., Leschiner, I., Elagina, L., Siravegna, G., Ng, R.W.S., et al. (2019). TAS-120 Overcomes Resistance to ATP-Competitive FGFR Inhibitors in Patients with FGFR2 Fusion-Positive Intrahepatic Cholangiocarcinoma. Cancer Discov *9*, 1064–1079. https://doi.org/10.1158/2159-8290.CD-19-0182.

205. Cao, W., Liu, Y., Zhang, R., Zhang, B., Wang, T., Zhu, X., Mei, L., Chen, H., Zhang, H., Ming, P., et al. (2015). Homoharringtonine induces apoptosis and inhibits STAT3 via IL-6/JAK1/STAT3 signal pathway in Gefitinib-resistant lung cancer cells. Sci Rep *5*, 8477. https://doi.org/10.1038/srep08477.

206. Huang, H., Song, S., Banerjee, S., Jiang, T., Zhang, J., Kahle, K.T., Sun, D., and Zhang, Z. (2019). The WNK-SPAK/OSR1 Kinases and the Cation-Chloride Cotransporters as Therapeutic Targets for Neurological Diseases. Aging Dis *10*, 626–636. https://doi.org/10.14336/AD.2018.0928.

207. Akella, R., Humphreys, J.M., Sekulski, K., He, H., Durbacz, M., Chakravarthy, S., Liwocha, J., Mohammed, Z.J., Brautigam, C.A., and Goldsmith, E.J. (2021). Osmosensing by WNK Kinases. MBoC *32*, 1614–1623. https://doi.org/10.1091/mbc.E20-01-0089.

208. Rodan, A.R., and Jenny, A. (2017). WNK kinases in development and disease. Curr Top Dev Biol *123*, 1–47. https://doi.org/10.1016/bs.ctdb.2016.08.004.

209. Küry, S., Zhang, J., Besnard, T., Caro-Llopis, A., Zeng, X., Robert, S.M., Josiah, S.S., Kiziltug, E., Denommé-Pichon, A.-S., Cogné, B., et al. (2022). Rare pathogenic variants in *WNK3* cause X-linked intellectual disability. Genet Med *24*, 1941–1951. https://doi.org/10.1016/j.gim.2022.05.009.

210. Peters, E.C., and Gray, N.S. (2007). Chemical Proteomics Identifies Unanticipated Targets of Clinical Kinase Inhibitors. ACS Chem Biol *2*, 661–664. https://doi.org/10.1021/cb700203j.

211. Yamada, K., Levell, J., Yoon, T., Kohls, D., Yowe, D., Rigel, D.F., Imase, H., Yuan, J., Yasoshima, K., DiPetrillo, K., et al. (2017). Optimization of Allosteric With-No-Lysine (WNK) Kinase Inhibitors and Efficacy in Rodent Hypertension Models. J Med Chem *60*, 7099–7107. https://doi.org/10.1021/acs.jmedchem.7b00708.

212. Rodriguez, M., Kannangara, A., Chlebowicz, J., Akella, R., He, H., Tambar, U.K., and Goldsmith, E.J. (2022). Synthesis and Structural Characterization of Novel Trihalo-sulfone Inhibitors of WNK1. ACS Med Chem Lett *13*, 1678–1684. https://doi.org/10.1021/acsmedchemlett.2c00216.

213. McCormick, J.A., and Ellison, D.H. (2011). The WNKs: Atypical Protein Kinases With Pleiotropic Actions. Physiol Rev *91*, 177–219. https://doi.org/https://doi.org/10.1152/physrev.00017.2010.

214. Chou, T.-C., and Talalay, P. (1984). Quantitative analysis of dose-effect relationships: the combined effects of multiple drugs or enzyme inhibitors. Adv Enzyme Regul *22*, 27–55. https://doi.org/10.1016/0065-2571(84)90007-4.

215. Banerjee, S., and Kane, P.M. (2020). Regulation of V-ATPase Activity and Organelle pH by Phosphatidylinositol Phosphate Lipids. Front Cell Dev Biol *8*, 510. https://doi.org/10.3389/fcell.2020.00510.

216. Roy, A., Goodman, J.H., Begum, G., Donnelly, B.F., Pittman, G., Weinman, E.J., Sun, D., and Subramanya, A.R. (2015). Generation of WNK1 knockout cell lines by CRISPR/Cas-mediated genome editing. Am J Physiol Renal Physiol *308*, F366–F376. https://doi.org/10.1152/ajprenal.00612.2014.

217. Hisamoto, N., Moriguchi, T., Urushiyama, S., Mitani, S., Shibuya, H., and Matsumoto, K. (2008). Caenorhabditis elegans WNK–STE20 pathway regulates tube formation by modulating ClC channel activity. EMBO Rep *9*, 70–75. https://doi.org/10.1038/sj.embor.7401128.

218. Gallolu Kankanamalage, S., Lee, A.-Y., Wichaidit, C., Lorente-Rodriguez, A., Shah, A.M., Stippec, S., Whitehurst, A.W., and Cobb, M.H. (2016). Multistep regulation of autophagy by WNK1. Proc Natl Acad Sci U S A *113*, 14342–14347. https://doi.org/10.1073/pnas.1617649113.

219. Zhang, J., Bhuiyan, M.I.H., Zhang, T., Karimy, J.K., Wu, Z., Fiesler, V.M., Zhang, J., Huang, H., Hasan, M.N., Skrzypiec, A.E., et al. (2020). Modulation of brain cation-Cl- cotransport via the SPAK kinase inhibitor ZT-1a. Nat Commun *11*, 78. https://doi.org/10.1038/s41467-019-13851-6.

220. Moniz, S., and Jordan, P. (2010). Emerging roles for WNK kinases in cancer. Cell Mol Life Sci *67*, 1265–1276. https://doi.org/10.1007/s00018-010-0261-6.

221. Duan, S., Agger, K., Messling, J.-E., Nishimura, K., Han, X., Peña-Rømer, I., Shliaha, P., Damhofer, H., Douglas, M., Kohli, M., et al. (2025). WNK1 signalling regulates amino acid transport and mTORC1 activity to sustain acute myeloid leukaemia growth. Nat Commun *16*, 4920. https://doi.org/10.1038/s41467-025-59969-8.

222. Sakurai, H.T., Iwashita, H., Arakawa, S., Yikelamu, A., Kusaba, M., Kofuji, S., Nishina, H., Ishiyama, M., Ueno, Y., and Shimizu, S. (2023). Development of small fluorescent probes for the analysis of autophagy kinetics. iScience *26*, 107218. https://doi.org/10.1016/j.isci.2023.107218.

223. Chiang, G.G., and Abraham, R.T. (2005). Phosphorylation of Mammalian Target of Rapamycin (mTOR) at Ser-2448 IsMediated by p70S6 Kinase . J. Biol. Chem. *280*, 25485–25490. https://doi.org/10.1074/jbc.M501707200.

224. Battaglioni, S., Benjamin, D., Wälchli, M., Maier, T., and Hall, M.N. (2022). mTOR substrate phosphorylation in growth control. Cell *185*, 1814–1836. https://doi.org/10.1016/j.cell.2022.04.013.

225. Chen, X.-G., Liu, F., Song, X.-F., Wang, Z.-H., Dong, Z.-Q., Hu, Z.-Q., Lan, R.-Z., Guan, W., Zhou, T.-G., Xu, X.-M., et al. (2010). Rapamycin regulates Akt and ERK phosphorylation through mTORC1 and mTORC2 signaling pathways. Mol Carcinog *49*, 603–610. https://doi.org/10.1002/mc.20628.

226. Bago, R., Malik, N., Munson, M.J., Prescott, A.R., Davies, P., Sommer, E., Shpiro, N., Ward, R., Cross, D., Ganley, I.G., et al. (2014). Characterization of VPS34-IN1, a selective inhibitor of Vps34, reveals that the phosphatidylinositol 3-phosphate-binding SGK3 protein kinase is a downstream target of class III phosphoinositide 3-kinase. Biochem J *463*, 413–427. https://doi.org/10.1042/BJ20140889.

227. Limpert, A.S., Lambert, L.J., Bakas, N.A., Bata, N., Brun, S.N., Shaw, R.J., and Cosford, N.D.P. (2018). Autophagy in Cancer: Regulation by Small Molecules. Trends Pharmacol Sci *39*, 1021–1032. https://doi.org/10.1016/j.tips.2018.10.004.

228. Abu-Remaileh, M., Wyant, G.A., Kim, C., Laqtom, N.N., Abbasi, M., Chan, S.H., Freinkman, E., and Sabatini, D.M. (2017). Lysosomal metabolomics reveals V-ATPase- and mTOR-dependent regulation of amino acid efflux from lysosomes. Science *358*, 807–813. https://doi.org/10.1126/science.aan6298.

229. Stenmark, H. (2009). Rab GTPases as coordinators of vesicle traffic. Nat Rev Mol Cell Biol *10*, 513–525. https://doi.org/10.1038/nrm2728.

230. Creasy, B.M., Hartmann, C.B., White, F.K.H., and McCoy, K.L. (2007). New assay using fluorogenic substrates and immunofluorescence staining to measure cysteine cathepsin activity in live cell subpopulations. Cytom A *71A*, 114–123. https://doi.org/10.1002/cyto.a.20365.

231. Yadati, T., Houben, T., Bitorina, A., and Shiri-Sverdlov, R. (2020). The Ins and Outs of Cathepsins: Physiological Function and Role in Disease Management. Cells *9*, 1679. https://doi.org/10.3390/cells9071679.

232. Frost, L.S., Dhingra, A., Reyes-Reveles, J., and Boesze-Battaglia, K. (2017). The Use of DQ-BSA to Monitor the Turnover of Autophagy-Associated Cargo. Methods Enzymol *587*, 43–54. https://doi.org/10.1016/bs.mie.2016.09.052.

233. Mahali, S., Martinez, R., King, M., Verbeck, A., Harari, O., Benitez, B.A., Horie, K., Sato, C., Temple, S., and Karch, C.M. (2022). Defective proteostasis in induced pluripotent stem cell models of frontotemporal lobar degeneration. Transl Psychiatry *12*, 508. https://doi.org/10.1038/s41398-022-02274-5.

234. Pradeepkiran, J.A., and Reddy, P.H. (2020). Defective Mitophagy in Alzheimer's Disease. Ageing Res Rev *64*, 101191. https://doi.org/10.1016/j.arr.2020.101191.

235. Iwashita, H., Torii, S., Nagahora, N., Ishiyama, M., Shioji, K., Sasamoto, K., Shimizu, S., and Okuma, K. (2017). Live Cell Imaging of Mitochondrial Autophagy with a Novel Fluorescent Small Molecule. ACS Chem Biol *12*, 2546–2551. https://doi.org/10.1021/acschembio.7b00647.

236. Shchepina, L.A., Pletjushkina, O.Y., Avetisyan, A.V., Bakeeva, L.E., Fetisova, E.K., Izyumov, D.S., Saprunova, V.B., Vyssokikh, M.Y., Chernyak, B.V., and Skulachev, V.P. (2002). Oligomycin, inhibitor of the F0 part of H+-ATP-synthase, suppresses the TNF-induced apoptosis. Oncogene *21*, 8149–8157. https://doi.org/10.1038/sj.onc.1206053.

237. Kondapalli, C., Kazlauskaite, A., Zhang, N., Woodroof, H.I., Campbell, D.G., Gourlay, R., Burchell, L., Walden, H., Macartney, T.J., Deak, M., et al. (2012). PINK1 is activated by mitochondrial membrane potential depolarization and stimulates Parkin E3 ligase activity by phosphorylating Serine 65. Open Biol *2*, 120080. https://doi.org/10.1098/rsob.120080.

238. Jung, J.-U., and Cobb, M.H. (2023). WNK1 controls endosomal trafficking through TRIM27-dependent regulation of actin assembly. Proc Natl Acad Sci U S A *120*, e2300310120. https://doi.org/10.1073/pnas.2300310120.

239. Zagórska, A., Pozo-Guisado, E., Boudeau, J., Vitari, A.C., Rafiqi, F.H., Thastrup, J., Deak, M., Campbell, D.G., Morrice, N.A., Prescott, A.R., et al. (2006). Regulation of activity and localization of the WNK1 protein kinase by hyperosmotic stress. J Cell Biol *176*, 89–100. https://doi.org/10.1083/jcb.200605093.

240. Subramanya, A.R., Liu, J., Ellison, D.H., Wade, J.B., and Welling, P.A. (2009). WNK4 Diverts the Thiazide-sensitive NaCl Cotransporter to the Lysosome and Stimulates AP-3 Interaction. J Biol Chem *284*, 18471–18480. https://doi.org/10.1074/jbc.M109.008185.

241. He, G., Wang, H.-R., Huang, S.-K., and Huang, C.-L. (2007). Intersectin links WNK kinases to endocytosis of ROMK1. J Clin Invest *117*, 1078–1087. https://doi.org/10.1172/JCI30087.

242. Hong-Hermesdorf, A., Brüx, A., Grüber, A., Grüber, G., and Schumacher, K. (2006). A WNK kinase binds and phosphorylates V-ATPase subunit C. FEBS Letters *580*, 932–939. https://doi.org/10.1016/j.febslet.2006.01.018.

243. Lei, Z., Qiang, L., Ge, P., Qiang, Y., Sun, T., Chai, Q., Wang, Y., Lv, S., Qiu, C., Lu, Z., et al. (2026). Rab14 restricts pathogens by promoting V-ATPase lysosomal delivery to drive lysosomal acidification. Nat Commun. https://doi.org/10.1038/s41467-026-70258-w.

244. Lopes, F.M., Bristot, I.J., da Motta, L.L., Parsons, R.B., and Klamt, F. (2017). Mimicking Parkinson's Disease in a Dish: Merits and Pitfalls of the Most Commonly used Dopaminergic In Vitro Models. Neuromolecular Med *19*, 241–255. https://doi.org/10.1007/s12017-017-8454-x.

245. Breuer, H., Bell-Simons, M., and Zempel, H. (2024). Axodendritic targeting of TAU and MAP2 and microtubule polarization in iPSC-derived versus SH-SY5Y-derived human neurons. Open Life Sci *19*. https://doi.org/10.1515/biol-2022-1010.

246. Hodul, M., Lane-Donovan, C., Cheang, E.S., Gao, V., Sampognaro, P.J., Mambou, E.A., Yang, Z., and Kao, A.W. (2026). Prosaposin Is Cleaved Into Saposins by Multiple Cathepsins in a Progranulin-Regulated Fashion. J Neurochem *170*, e70357. https://doi.org/10.1111/jnc.70357.

247. Brenner, S. (1974). The genetics of Caenorhabditis elegans. Genetics *77*, 71–94. https://doi.org/10.1093/genetics/77.1.71.

248. Shih, J.D., and Hunter, C.P. (2011). SID-1 is a dsRNA-selective dsRNA-gated channel. RNA *17*, 1057–1065. https://doi.org/10.1261/rna.2596511.

249. Kamath, R.S., Fraser, A.G., Dong, Y., Poulin, G., Durbin, R., Gotta, M., Kanapin, A., Le Bot, N., Moreno, S., Sohrmann, M., et al. (2003). Systematic functional analysis of the Caenorhabditis elegans genome using RNAi. Nature *421*, 231–237. https://doi.org/10.1038/nature01278.

250. Park, H., V Hundley, F., and Wade Harper, J. (2022). Endosomal and lysosomal immunoprecipitation for proteomics, lipidomics, and TEM v2. Protocols IO. https://doi.org/10.17504/protocols.io.ewov14pjyvr2/v2.

251. Johnston, H.E., Yadav, K., Kirkpatrick, J.M., Biggs, G.S., Oxley, D., Kramer, H.B., and Samant, R.S. (2022). Solvent Precipitation SP3 (SP4) Enhances Recovery for Proteomics Sample Preparation without Magnetic Beads. Anal Chem *94*, 10320–10328. https://doi.org/10.1021/acs.analchem.1c04200.

**Publishing Agreement**

It is the policy of the University to encourage open access and broad distribution of all theses, dissertations, and manuscripts. The Graduate Division will facilitate the distribution of UCSF theses, dissertations, and manuscripts to the UCSF Library for open access and distribution. UCSF will make such theses, dissertations, and manuscripts accessible to the public and will take reasonable steps to preserve these works in perpetuity.

I hereby grant the non-exclusive, perpetual right to The Regents of the University of California to reproduce, publicly display, distribute, preserve, and publish copies of my thesis, dissertation, or manuscript in any form or media, now existing or later derived, including access online for teaching, research, and public service purposes.

DocuSigned by:
Virginia Garda
4C2F5D8E179D432...
Author Signature

08/14/2026
Date